LARGE-SCALE MANUFACTURING AND CHARACTERIZATION OF A SARS-COV-2 VIRUS-LIKE PARTICLE VACCINE ADSORBED ONTO ALHYDROGEL AND ADJUVANTED WITH K3 CPG OLIGODEOXYNUCLEOTIDE FOR PHASE 1/2 CLINICAL TRIALS

A THESIS SUBMITTED TO

THE GRADUATE SCHOOL OF ENGINEERING AND SCIENCE

OF BILKENT UNIVERSITY

IN PARTIAL FULLFILMENT OF THE REQUIREMENTS FOR

THE DEGREE OF

MASTER OF SCIENCE

IN

MOLECULAR BIOLOGY AND GENETICS

By

Artun Bülbül

April 2022

LARGE-SCALE MANUFACTURING AND CHARACTERIZATION OF A SARS-COV-2 VIRUS-LIKE PARTICLE VACCINE ADSORBED ONTO ALHYDROGEL AND ADJUVANTED WITH K3 CPG OLIGODEOXYNUCLEOTIDE FOR PHASE 1/2 CLINICAL TRIALS

By Artun Bülbül

April 2022

We certify that we have read this thesis and that in our opinion it is fully adequate, in scope and in quality, as a thesis for the degree of Master of Science.

İhsan Gürsel (Advisor)

Banu Bayyurt Kocabas

Serkan İsmail Göktuna

Approved for the Graduate School of Engineering and Science

Ezhan Karaşan
Director of the Graduate School of Engineering and Science

ABSTRACT

LARGE-SCALE MANUFACTURING AND CHARACTERIZATION OF A SARS-COV-2 VIRUS-LIKE PARTICLE VACCINE ADSORBED ONTO ALHYDROGEL AND ADJUVANTED WITH K3 CPG OLIGODEOXYNUCLEOTIDE FOR USE IN PHASE 1/2 CLINICAL TRIALS

Artun Bülbül

M.Sc. in Molecular Biology and Genetics

Advisor: Prof. İhsan Gürsel

April 2022

Emergence of COVID-19 pandemic has been met by an exceptionally fast response from vaccine makers around the globe. Vaccines that elicit excellent immunological responses against SARS-CoV-2 are now widely utilized. Existing platforms include mRNA-lipid nanoparticle-based vaccines, adenovirus vectored vaccines, various inactivated virus vaccines and subunit vaccines. We have previously described a novel virus-like particle (VLP) platform expressing the hexaproline prefusion stabilized Spike protein along with the nucleocapsid, membrane and envelope structural proteins. In mice, ferrets and rats, VLPs adjuvanted with K3 CpG Oligodeoxynucleotide (ODN) and adsorbed onto 2% Aluminum Hydroxide (Alum), induced robust humoral and cellular immune response against Spike and Nucleocapsid proteins.

Herein, we have expanded our work to manufacture the virus like particles in a GMP compliant facility intended for testing in phase I/II clinical trials. The technology transfer comprises i) VLP production from suspension adapted HEK293 cells, ii) purification with multimodal fast protein liquid chromatography (FPLC) and iii) concentration and diafiltration using tangential flow filtration (TFF). We have successfully scaled up our production from 50 mL of HEK293 cell culture to 5 L bioreactor, achieving yields reaching up to 40 mg VLPs per L of cell culture. Furthermore, several methods were developed to determine protein identity, purity, functionality, stability and immunopotency of VLP vaccine that was finally formulated with Alum + CpG ODN. Moreover, we investigated the immunogenicity of VLPs decorated either with Wuhan (Hu-1) or with Alpha (B.1.1.7) variant Spike against receptor binding domains (RBD) specific to other variants of concern (VoC).

Although our vaccine platform, could further benefit from process optimization to improve VLP yield, this study presents the first pilot scale production and purification of variant specific hexaproline prefusion stabilized SARS-CoV-2 VLPs. VLP preparations complying with our quality control parameters were released for fill and finish and were used for subsequent Phase 1 (NCT04818281) and Phase 2 clinical trials (NCT04962893).

Keywords: SARS-CoV-2, vaccine, virus like particles, GMP, adjuvant, antibody, COVID-19, pandemic

ÖZET

SARS-COV-2 PANDEMİSİNE KARŞI VİRÜS BENZERİ PARÇACIK TEMELLİ, ALUM ABSORBE VE K3 CPG OLIGODEOKSİNÜKLEOTİD ADJUVANTLI AŞI ADAYININ FAZ 1/2 KLİNİK DENEYLER İÇİN ÜRETİMİ VE İNCELENMESİ

Artun Bülbül

Moleküler Biyoloji ve Genetik, Yüksek Lisans
Tez Danışmanı: Prof. İhsan Gürsel

Nisan 2022

COVID-19 pandemisine, tüm dünyadaki aşı üreticileri tarafından takdire şayan bir hızda yanıt verilmiştir. SARS-CoV-2 virüsünü hedef alan ve oldukça başarılı birçok aşı, tüm dünyada milyonlarca insana uygulanmaya devam edilmektedir. En yaygın aşılar, mRNA-lipid nanopartükülleri, DNA taşıyan adenovirus vektörü, inaktif virus ve rekombinant protein platformlarını kullanmaktadır. Daha önceki çalışmalarımızda, SARS-CoV-2 virüsünün yapısal proteinleri olan Spike, Nucleocapsid, Membrane ve Envelope proteinlerini içeren bir virus benzeri parçacık (VLP) platformu geliştirmiştik. Bu parçacıklardaki Spike proteini, bir prefüzyon öncesi stabilize mutandı olup, HexaPro olarak adlandırılmaktadır. VLP'ler, K3 CpG oligodeoksinükleotid ile adjuvanlanıp 2% Alüminyum Hidroksite absorbe edilip aşılamada kullanıldığında; fare, gelincik ve sıçanlarda Spike ve Nucleocapsid proteinlerine karşı sıvısal ve hücresel immün yanıtı gözlemlenmiştir.

Bu çalışmada, Faz I/II klinik deneylerde kullanılması amacıyla, virus benzeri parçacıkları GMP kurallarına uygun bir tesiste ürettik. Üretim için dizayn ettiğimiz teknoloji transferi üç aşamadan oluşmaktadır. Bunlar; i) süspansiyon adapte HEK293 hücrelerinde virus benzeri parçacıkların ifade ettirilmesi, ii) multimodal sıvı fazlı hızlı protein kromatografisi (FPLC) ile saflaştırma ve iii) çapraz akım filtrasyonu (TFF) yolu ile konsantrasyon ve diafiltrasyon idir. Transfer sırasında üretim ölçeğimizi 50 mL HEK293 kültüründen 5 L biyoreaktöre başarıyla çıkarmış bulunmakta ve 1 L hücre kültürü başına 40 mg VLP gibi bir verim elde etmiş bulunmaktayız. Ayrıca, saf VLP antijeninin ve formüle edilmiş bitmiş ürünün protein karakteri, saflığı, miktarı, fonksiyonelitesi, stabilitesi ve immünojenik kapasitesinin değerlendirilmesi için birçok metot geliştirdik. Bunun yanı sıra, orijinal Wuhan veya Alpha (B.1.1.7) suşunun Spike proteinini içeren VLP'ler kullanılarak hazırlanmış aşıların diğer endişe doğuran suşlara (VoC) karşı oluşturduğu reseptör bağlanma bölgesine (RBD) yönelik antikor seviyelerini belirledik.

Platformumuzun VLP üretim verimini artıracak metot optimizasyonundan fayda göreceği kuşkusuz olmasına rağmen, bu çalışma, suş özelinde prefüzyon stabilize Spike barındıran SARS-CoV-2 VLP'lerinin pilot ölçekte üretiminin ilk örneğidir. Belirlenmiş kalite kontrol parametrelerine uygun

üretilmiş VLP partilerinin dolum ve paketlenme işlemi yapılmış, Faz 1 (NCT04818281) ve Faz 2 (NCT04962893) klinik deneylerde kullanılmıştır.

Anahtar kelimeler: SARS-CoV-2, aşı, virus benzeri parçacık, GMP, adjuvan, antikor, COVID-19, pandemi

To all health care professionals,

true heroes of the pandemic…

Acknowledgements

Firstly, I would like to express my gratitude to my supervisor Prof. İhsan Gürsel for his incredible mentorship. In addition to his great scientific guidance and vision, without him, this project would stay on the laboratory bench and would never ever go into translation for human use. His skill to create opportunities from essentially nothing at all and being able to see a project far beyond from "just a couple of experiments in the laboratory" was truly incredible to witness and learn from. I hope I can apply a fraction of his teachings in the future. I would also like to thank Prof. Mayda Gursel as she was the other creator of this massive effort. Without her, such an innovative vaccine approach would never be materialized. I consider myself very lucky to be exposed to such exceptional mentors. I want to thank my thesis committee members, Dr. Banu Bayyurt Kocabaş and Dr. Serkan Göktuna, for their time, interest and valuable suggestions.

I thank all members from both laboratories as it was a great pleasure to work with them. I am especially greatful for İsmail and Naz for teaching me valuable lessons both inside and outside of the laboratory. I thank Nilsu, Neşe, Emre, Aslı, Tuğçe, İrem, Berfu for all the fun moments we've experienced. I thank Nobel Pharma Biotechnology Research Center Team heads, Mohan Babu Kasa, Mohit Sharma, Naidu Mookala, Vivek Yadav and Tirumal Rao Yannabathina and all their team members for working non-stop for this project with us. I also thank our veterinary physician Gamze Aykut, Ulaş Saçıntı and our laboratory technician Okan Erşahan. I deeply appreciate the encouragement and support from President of TÜBİTAK, Prof Hasan Mandal, and Minister Mustafa Varank towards our team and the project.

I am grateful for having my best buddies Kaan, Engin, Doğa and Kaan with me during this process. Without Engin; it wouldn't be fun, without Kaan; I would have definitely starved, without Doğa; I could say none of my friends thought I was joking for a whole year when I said we were working on a vaccine and without Kaan, I wouldn't have anyone to discuss it with. Thanks Ezgi, for still talking to me after 13 years and Enes, for giving me a break from all this. I also want to acknowledge Arif , Köpük and Arya for being good boys and girls.

Most importantly, I would like to express my deepest gratitude to my family, my mother, Gülsel and my father, Yavuz, without whom, I could have never achieved anything. I am always grateful for their unconditional love and support.

I thank my beloved, Yağmur, who always treats me better than I deserve. Thank you for always listening with intent and making me a better version of myself. I could never know someone like you in all eternity.

Table of Contents

List of Figures

List of Tables

Abbreviations

Antigen presenting cell	APC
Bacillus Calmette–Guérin	BCG
BP	Base pair
BSA	Bovine serum albumin
Cleaning in place	CIP
Deoxyribonucleic acid	DNA
DPBS	Dulbecco’s phosphate buffered saline
Elution	EL
Envelope protein	E
European Medicines Agency	EMA
Fast protein liquid chromatography	FPLC
Flow through	FT
Food and Drug Administration	FDA
FSC	Forward scatter
Good manufacturing practice	GMP
HEPES	4-(2-hydroxyethyl)-1-piperazineethanesulfonic acid
Host cell DNA	HCD
Host cell protein	HCP
Human immunodeficiency virus	HIV
Human papilloma virus	HPV
IFN	Interferon
IL	Interleukin
Lysogeny broth	LB
Membrane protein	M
MHC	Major histocompatibility complex
Neutrophil extracellular traps	NETs
NLR	NOD-like receptor
NOD	Nucleotide-binding oligomerization domain
Nucleocapsid protein	N
ODN	Oligodeoxynucleotide
PBS	Phosphate buffered saline
Polyacrylamide gel electrophoresis	PAGE
Polyethylenimine	PEI

PRR	Pattern recognition receptor
Receptor binding domain	RBD
Retinoic acid-inducible gene 1	RIG-1
RNA	Ribonucleic acid
RT	Room temperature
SA-ALP	Streptavidin - alkaline phosphatase
Spike protein	S
SSC	Side scatter
STING	Stimulator of interferon genes
Tangential flow filtration	TFF
TBS	Tris buffered saline
TBS-T	Tris buffered saline - Tween 20
TLR	Toll-like receptor
TNFα	Tumor necrosis factor alpha
Variant of concern	VoC
Virus like particle	VLP

1. Introduction

1.1 SARS-CoV-2 and the 2019 Pandemic

On December 2019, an outbreak of pneumonia cases was reported in the Wuhan region of China. Causative pathogen was identified to be a novel coronavirus, initially named 2019-nCoV and later designated as Severe Acute Respiratory Syndrome Coronavirus 2 (SARS-CoV-2) [1]. Since then, this virus resulted in a pandemic and at the time of this writing, global number of cumulative cases and deaths reached 450.230.000 and 6.019.085 respectively.

1.1.1 Viral Origin

Debate over the origin of the virus has been going on since the early days of the pandemic and is yet to be resolved. Two popular ideas are "laboratory escape" and natural emergence through "zoonotic transmission" [2]. Emergence of SARS-CoV-2 has a common narrative with the first SARS. Both involved the Wuhan live animal markets, backed by epidemiological data. Earliest cases were reported to involve contact with the Huanan market. It is highly likely that a SARS-CoV-2 progenitor was present in bat population due to its phylogenetic similarity to SARS-CoV-like coronaviruses [3]. Viruses sampled from *Rhinolophus affinis* bat and *Manis javanica* pangolins are ~96% identical to SARS-CoV-2 and possess similar key Receptor Binding Domain (RBD) residues, respectively [4,5]. However, no virus sampled to date has >~96% identity and display the ability to bind to ACE2 receptor by share of these residues. At the time of emergence, Huanan market had immense number of species of live animals and this included SARS-CoV-2 permissive species, including civets and raccoon dogs [6]. It is possible that a progenitor virus from bats jumped to an animal sold in the market and then to humans. However, in what species the evolutionary processes that diversified SARS-CoV-2 Spike underwent, is unclear.

It is likely that SARS-Cov2 had an animal origin similar to the other common coronaviruses, human coronavirus NL63 (HCoV-NL63), human coronavirus-HKU1 (HCoV-HKU1), human coronavirus-229E (HCoV-229E) and human coronavirus-OC43 (HCoV-OC43). Tracing animal origins have proved difficult in the past. HCoV-HKU1 emerged in Guangdong region in China in 2004 and its origin is still unclear [7].

Laboratory escape is also possible as work on bat SARS-CoV-like coronaviruses is routinely done in biosafety level 2/3 (Zeng et al., 2016) laboratories and both SARS-CoV and now SARS-CoV-2 were reported to leak from biosafety level 3 laboratories [8,9]. This theory gained popularity because of somewhat close proximity of Huanan market to the Wuhan Institute of Virology, where work on coronaviruses has been going on for nearly 20 years. Particularly work on sampling wild type viruses [10] and reverse genetics [11] have attracted much attention from public. However, there is no epidemiological or virological data suggesting that SARS-CoV-2 had escaped from a laboratory near the region or whether or not it was engineered or passaged.

Six amino acids in RBD are known to be critical for SARS-like coronavirus Spike binding to hACE2 receptor [12]. Along with general homology, 6 amino acids found in other SARS-like coronavirus RBDs identical to SARS-CoV-2 present a useful strategy to investigate viruses capable of binding to hACE2 through similar interactions. Interestingly, there is evidence that unlike SARS-CoV RBD, SARS-CoV-2 RBD may not be optimal for binding to hACE2 [5]. It is not clear if this alone resulted in less pathogenicity compared to SARS-CoV and whether this is a result of extensive animal to animal and animal to human transmission.

Unique to SARS-CoV-2 and not found in other lineage-B beta coronaviruses, is the presence of a polybasic furin cleavage site between S1 and S2 subunits of the Spike protein. This is also found in another beta coronavirus, common coronavirus HKU1. It is unclear what this site achieves in SARS-CoV-2, but it is known that a variety of host cell derived proteases are able to cut between the two subunits at the furin cleavage site. It is also known from SARS and avian influenza viruses that such cleavage sites impact transmissibility, cell to cell fusion, and pathogenicity [13,14]. It might also allow a suboptimal RBD to bind to ACE2 [15]. Tracing emergence of a polybasic furin cleavage site is also a viable strategy to trace SARS-CoV-2 progenitors.

1.1.2 Genome, Structure and Life Cycle of SARS-CoV-2

Coronaviridae are enveloped viruses harboring a positive single stranded RNA genome. RNA genomes have 5'caps and 3' poly(A) tails [16,17]. This family of viruses are classified under four genera; Alpha, Beta, Gamma and Delta. Beta genus (also called group B) is composed of lineages from A to D. Common cold viruses OC43 and HKU1 are members of Lineage A (Embecovirus). SARS-CoV and SARS-CoV-2 are of lineage-B (Sarbecovirus) and MERS-CoV is a member of lineage-C (Merbecovirus). Beta CoVs have large genomes, spanning from 26 to 32kb. SARS-CoV-2 virions enter cells through interaction with ACE2. Following infection, RNA genome is immediately translated upon cell entry to yield 26 non-structural proteins. These proteins are cleavage products of ORF1ab. Polypeptide pp1a is translated from ORF1a and is cleaved into 11non-structural proteins (nsps) while pp1ab, translated from ORF1b, is cleaved into 15 more nsps. RNA genome (gRNA) is also used to translate structural proteins and other ORFs.

Additionally, transcription of gRNA yields negative sense RNAs, which are then used to generate both positive sense gRNA destined for packaging and a number of subgenomic (sg) RNAs. sgRNAs serve as translation templates to drive synthesis of other proteins. Transcription of (+) RNA occurs from transcription regulatory sites (TRSs). Figure 1.1 summarizes the organization of SARS-Cov-2 genome [18].

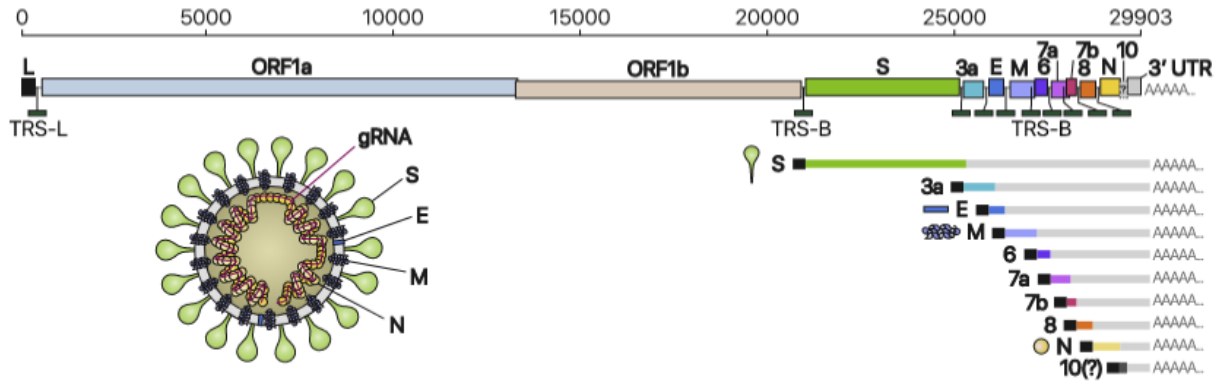

Figure 1.1 Representation of SARS-CoV-2 genes, genomic and sub-genomic RNAs and structure of the virion. Adapted from [18].

There are four structural proteins encoded by the genome. Spike protein (~180kDa) is a so-called type I transmembrane protein. This protein is fusogenic, therefore fascilitates fusion of viral and cell membranes. It functions as a homotrimer where each polypeptide chain is composed of S1 and S2 subunits [19]. Spike binds to ACE2 by its RBD region found in S1 subunit. Fusion of membranes requires cleavage of Spike polypeptide from polybasic furin cleavage site by host proteases like TMPRSS2 [20]. Upon cleavage, S1 and S2 subunits are held by electrostatic interactions and poised to drive membrane fusion. Because of its role in driving membrane fusion, immune responses against Spike are particularly critical. Upon infection or vaccination, some portion of Spike targeting antibodies generated are so called neutralizing antibodies. These specifically block hACE2-Spike interaction and viral entry.

Nucleocapsid protein (~55kDa) is found inside the virions as a ribonucleoprotein complex. Its primary function in virions is to package gRNA. This occurs via a packaging signal found in the gRNA but not the sgRNAs. Exact mechanism of how this occurs is debated, but it is probable that Nucleocapsid-RNA condensates [21] which are driven by liquid-liquid phase separation, function to localize Nucleocapsid and gRNA together and interaction of Nucleocapsid with Membrane protein enables encapsulation of the condensates [22]. Similar to its role in packaging, Nucleocapsid is also important for viral transcription. It acts as a transcription factor, clustering RNA species with viral replication and transcription machineries [23].

Membrane (25-30kDa) and Envelope (8-12 kDa) proteins are small transmembrane proteins with roles in assembly of viral particles [24,25]. Both of these proteins are probably necessary for driving viral assembly. There is conflicting evidence regarding which protein is sufficient, but [24,26,27] it appears that Membrane is the master organizer of viral assembly as it interacts with all 3 other structural proteins and decoration of Spike onto the virions might be directly mediated by the Membrane protein [28]. Figure 1.2. summarizes the life cycle of SARS-CoV-2 virus [29].

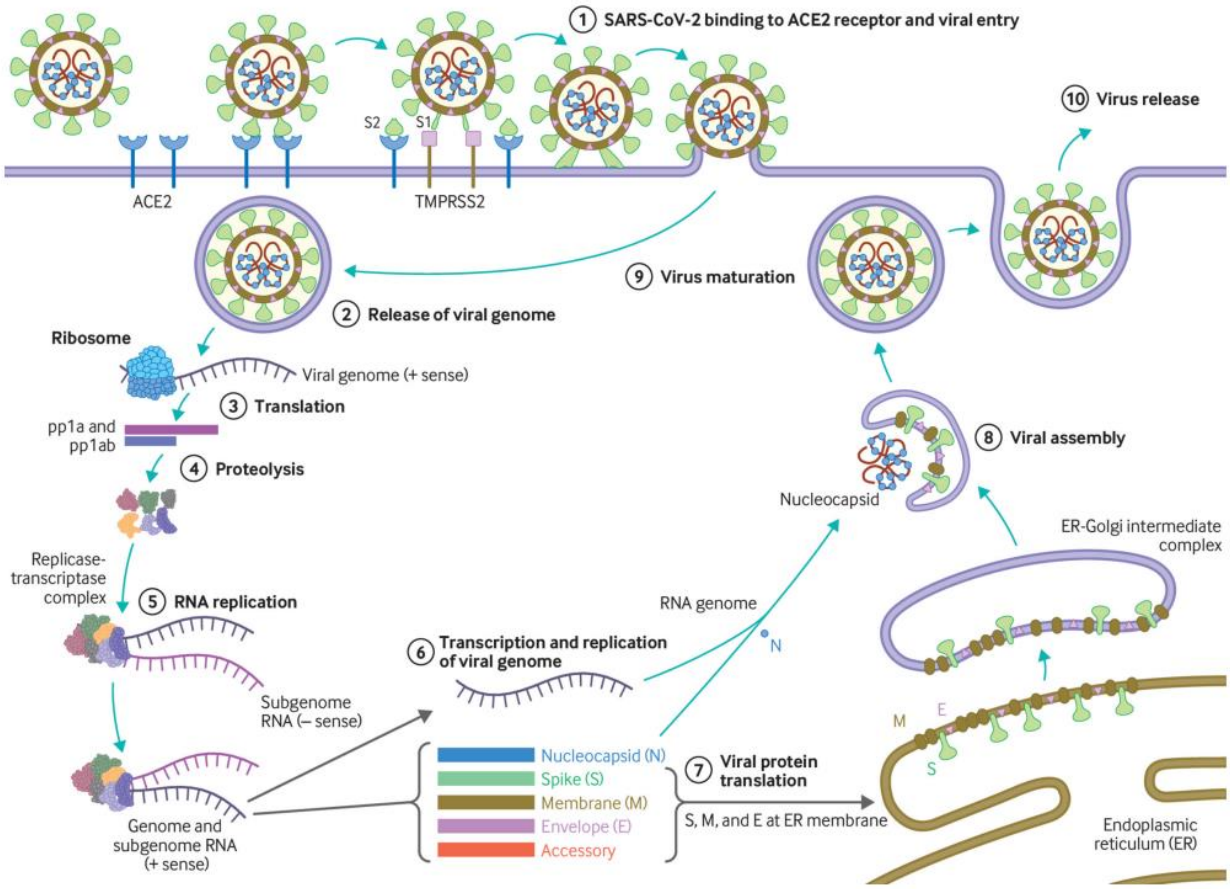

Figure 1.2 Life cycle of SARS-CoV2. Circle of life for the virus starts with the interaction of Spike with the ACE2 receptor. Target cell proteases like TMPRSS2 cleave Spike into its fusogenic form and viral membrane fuses with the cell membrane. As explained in detail above, a variety of translation and transcription events occur, resulting in newly formed virions. Assembly occurs in the ER-Golgi intermediate complex (ERGIC) and virions are then released from the cell via exocytosis. Adapted from [29].

The viral genome also encodes a variety of nonstructural ORFs and nsps. Nsp3 is a papain-like cysteine protease [30] and Nsp5 is a 3-Chymotrypsin-like protease respectively [31]. Nsp3 governs proteolytic cleavage of Nsp1 to Nsp3 while Nsp5, which is also called the main protease, governs from Nsp4 to Nsp16. RNA dependent RNA polymerase is composed of Nsp12, Nsp7 and Nsp8. Other nsps and ORFs antagonize the host immune reactions by interfering with interferon signaling, viral sensing and antigen presentation [32]. Figure 1.3 depicts the nsps derived from polyproteins pp1A and pp1ab [33].

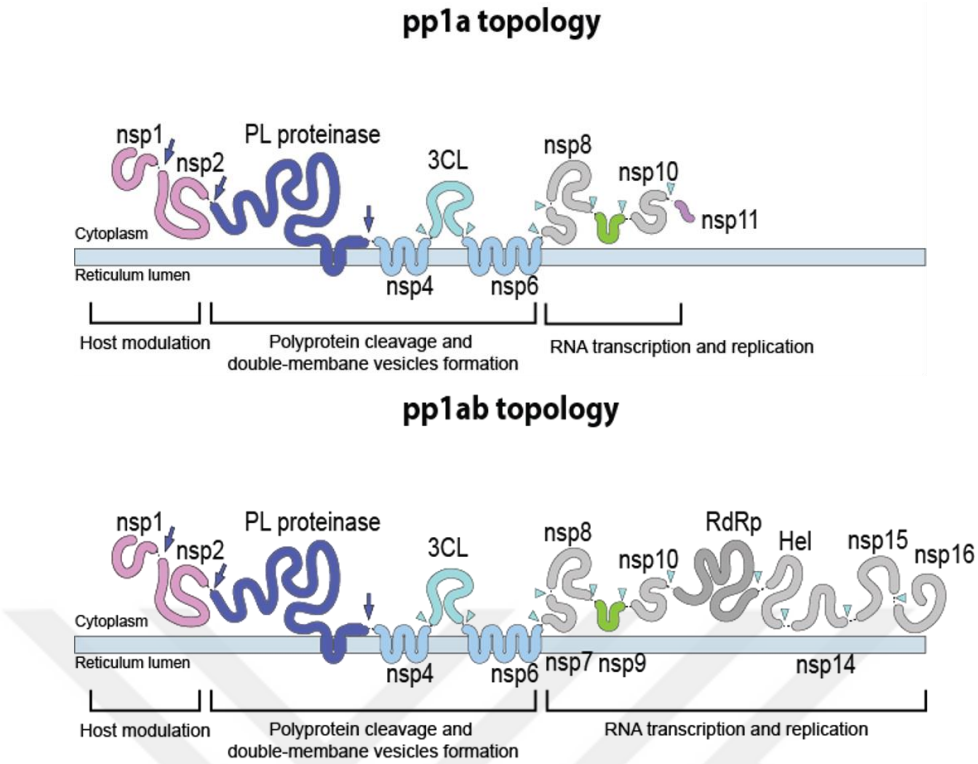

Figure 1.3 Polyprotein coded non-structural proteins of SARS-CoV-2. Unlike structural proteins and other ORFs, nsps are generated through cleavage from pp1a and pp1ab, encoded by ORF1ab. Adapted from [33].

1.1.3 Transmission and Pathogenesis of SARS-CoV-2

Coronaviridae that infect humans do so by respiratory droplets, aerosols, contact and fecal-oral route. SARS-CoV-2 replicates in upper and lower respiratory tract and particles of virus containing droplets can be transmitted from individual to individual by coughing. Initially this was thought to be the main route the virus spreads. However, there is now plenty of evidence to suggest that especially later evolved variants with higher transmissibility can infect individuals as an aerosol. Although contact transmission was also considered a main route, it was later stated as not a primary route by CDC [34]. This view is supported by lack of evidence regarding correlation of viral RNA detection in medium of transmission and potential pathogenicity and intact virion presence.

Upon infection, average incubation period is ~5-6 days [35]. Disease presents with initially "flu-like" symptoms. In some individuals, infection is resolved with few systemic symptoms like fatigue and fever. Some however, present with severe symptoms that include pneumonia, acute respiratory distress syndrome, myocardial inflammation and arrhythmias, diarrhea and extended fever. Additionally depending on the severity, patients may present with ground-glass opacities in lung X-rays, lymphocytopenia (decrease in lymphocyte numbers in blood), thrombocytopenia (low platelet count), neutrophilia (increased neutrophil count in blood) and increase in chronic inflammation markers such as C-reactive protein and D-dimer [36]. Severity is correlated with a "cytokine storm" like condition where there is increased IL-6 and IL-8 in serum and BALF together with influx of inflammatory monocytes

and neutrophils to lungs and other organs [37]. Hyperinflammation not only causes irreversible lung damage but can also cause multi-system organ failure through vascular leakage [38]. Interestingly, there also is evidence regarding direct infection of endothelial cells [39]. There might be a causative correlation between myocarditis induced by severe disease and in some cases by mRNA vaccination [40]. Most obvious and probable mechanism would be via molecular mimicry and autoantibody production. Spike targeting antibodies can target self-antigens to a degree. Notably, one of these self-antigens is α-myosin, a cardiac specific myosin heavy protein. However, role of this phenomenon in rare symptoms to infection and vaccination remains highly speculative as of now.

1.1.4 Variants of Concern

A variant of concern (VoC) is a variant of SARS-CoV-2 that has a potential to be more transmissible, pathogenic or immune evading and therefore, is "of interest". VoCs are declared by World Health Organization (WHO). As of now, five VoCs exits and these are named Alpha (B.1.1.7), Beta (B.1.351), Gamma (B.1.1.248 P.1), Delta (B.1.617.2), and Omicron (B.1.1.529). Mutations in Spike protein are particularly important in terms of immune evasion and transmissibility. It is important to note that not all mutations lead to VoCs. Most of other variants remained local thereby did not merit for a declaration of VoC.

Alpha variant emerged probably in United Kingdom and was identified in September of 2020. Sequencing studies revealed; i) N501Y substitution in RBD, which might increase affinity to hACE2; ii) Δ69-70 deletion, which can confer substantial evasion from neutralizing antibodies and iii) D614G substitution which improves Spike stability and decoration frequency on the surface of the variant [41,42].

Beta variant emerged in Eastern Cape of South Africa in October 2020. Similar to Alpha variant, it contains N501Y and D614G substitutions. It also harbors two additional mutations (K417N and E454K) which are associated with reduced neutralization activity [43]. Identified in January of 2021, Gamma variant possesses earlier E484K, D614G and N501Y mutations while having novel mutations K417T and D138Y [44,45].

Delta variant was identified in India as early as October of 2020. By the summer of 2021, it had become the globally dominant variant. Delta possesses D614G mutation detected in earlier variants, lacks the E484K substitution and also bears unique substitutions L452R and P681R, which enhances RBD-ACE2 interaction and increase infectivity through increase in fusogenic capacity respectively [46]. A secondary variant named Delta plus was later identified. Delta plus gained a K417N substation identified originally in Beta.

During the writing of this thesis, a fifth VoC was identified in South Africa in November of 2021. Omicron Spike harbors staggering number of 30 mutations in Spike. Some mutations like Δ69-70, K417N, E484A, N501Y, D614G were also seen in other VoCs and were associated with increased infectivity and immune evasion. Omicron is incredibly infective and must be considered an aerosol pathogen [47]. It is also extremely immune evasive. Omicron virtually made effectiveness against

symptomatic disease of all approved 2-dose vaccines go down below 10% after 25 weeks and only ~60% effectiveness is achieved with a 3rd booster dose [48]. However, it is apparently less pathogenic in terms of causing severe disease [49]. Figure 1.4. explains the phylogeny and global frequency of cases for each variant [50].

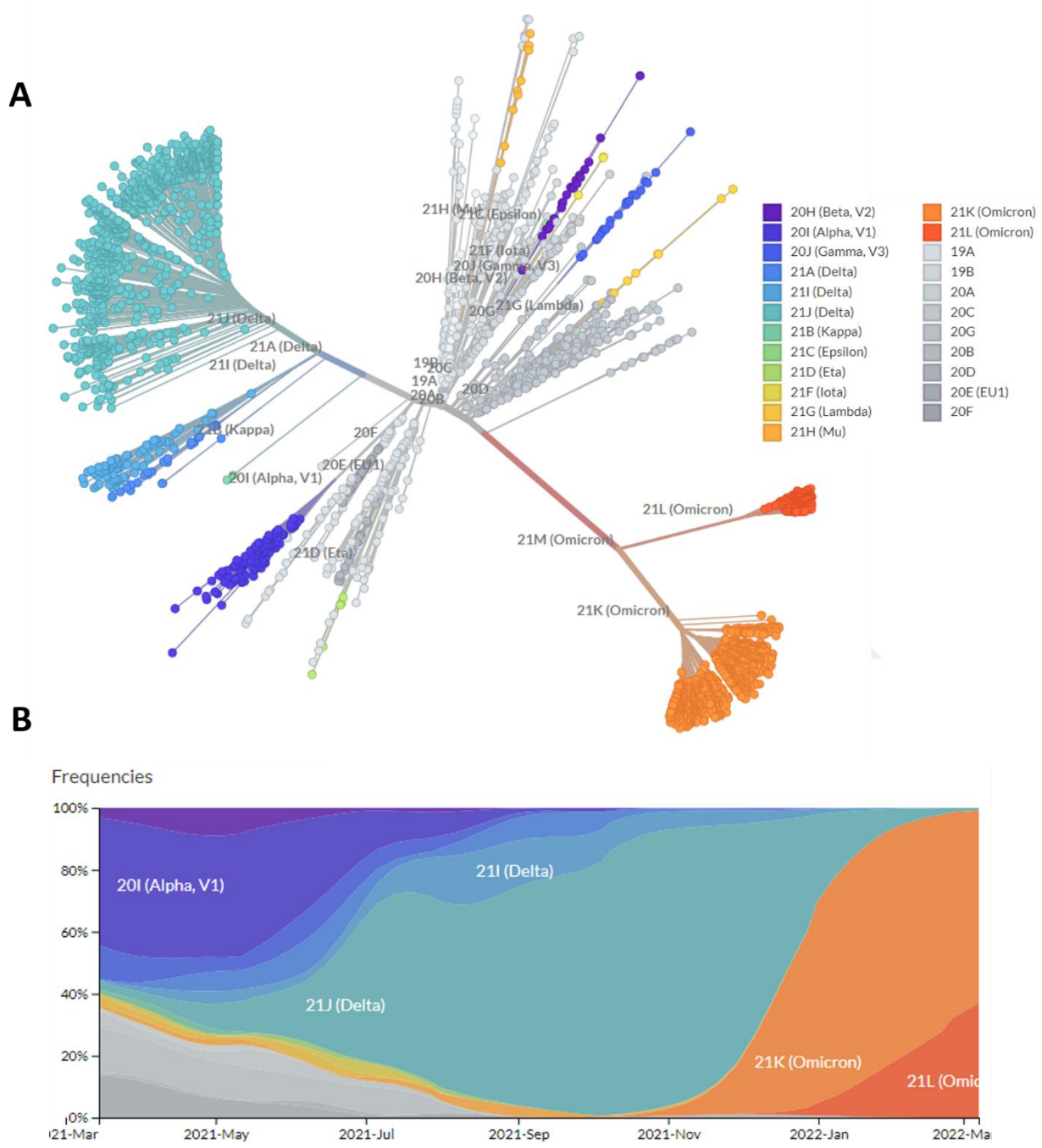

Figure 1.4 Phylogeny and frequency of cases for each variant worldwide. A. All strains of SARS-CoV-2 identified and sequenced are plotted in an unrooted phylogenetic tree. Colored strains are variants being monitored or of concern. **B.** Worldwide strain frequencies shows that Delta dominated the case number in Summer and Fall of 2021.Remarkably, Omicron dominated all cases in just 3 months after it has been identified. Adapted from [50].

1.2 Immune System

The mammalian immune system is an interrelated network composed of cells, tissues, organs, and humorous substances that respond to foreign insult. The initiation of these responses rely on a very simple principle; immediate discrimination of self from non-self [51]. Pathogens of four main type; viruses, bacteria and archaea, parasites and fungi constantly assault a mammalian immune system and this multifaceted network has evolved three main actions to counteract; avoidance, resistance and tolerance [52].

Barriers of the body across skin, gut, lungs, eyes, nose and oral cavity represent the avoidance strategy. These surfaces do not only employ mechanical avoidance via tight junctions of the epithelia, they also employ chemical barriers [53]. Defensins, cathelicidin, histatins are antimicrobial peptides that function at those barriers together with lysozyme and mucus. Oral cavity and lungs are actively washed with mucus via movement of the cilia layer. Pulmonary surfactant secreted by alveolar cells opsonize pathogens [54,55]. Microbiota composed of nonpathogenic bacteria is also a form of avoidance mechanism. These organisms live in an equilibrium with the immune system, producing bacteriocins and also outcompeting possible pathogenic bacteria [56].

Breaching of barriers induces inflammation via activation of cells with specific pattern recognition receptors (PRRs). PRRs include Toll-like receptors (TLRs), retinoic acid-inducible gene 1 (RIG-1)-like receptors (RLRs), nucleotide binding oligomerization domain (NOD)-like receptors (NLRs), C-type lectin receptors and absent in melanoma 2 (AIM2)-like receptors [57]. These germ line encoded receptors are found in variety of immune and other somatic cells. Cells in immediate proximity to the breach get activated and secrete cytokines. Chemokines, a collection of secreted proteins within the cytokine classification, act as chemoattractants for circulating immune cells. Immediate arrivers of the innate arm of the immune system include circulating monocytes, neutrophiles and dendritic cells [58]. These cells not only phagocytose the pathogen and deploy extracellular effector mechanisms, they also present antigens to cells of the adaptive immune system.

Antigen presenting cells (APCs) are the link between innate and adaptive arm of the immunity. Antigens ride to the lymphoid tissues on mainly dendritic cells— cells specialized for migration upon activation to lymphoid organs [59]. Lymphoid organs are home to so-called lymphocytes. T- and B-lymphocytes are central to the adaptive immunity as they not only learn to cope with specific antigens but also remember them [60]. Antigen specific cells can efficiently eliminate pathogens in an epitope specific manner. A reinfection with the same or similar pathogen activates the memory lymphocytes and adaptive immune response is equipped faster.

1.2.1 Innate Immune System and Reaction to SARS-CoV-2

Innate immune system functions through recognizing pathogenic molecular patterns through PRRs [57]. It limits viral molecular processes and also eliminates infected cells. Innate cells also present antigens to the adaptive immune cells to instruct and prime for long lasting antigen specific immunity.

Inflammatory reaction caused by activation of PRRs can also create a microenvironment in the site of infection that allows proper immune reaction [58,61]. Cells of the innate arm include macrophages, monocytes, NK cells, dendritic cells, neutrophils, basophils, eosinophils, and mast cells [62]. Macrophages are specialized for phagocytosis with the purpose of pathogenic clearance. Dendritic cells on the other hand do phagocytosis to alarm the adaptive immune cells. Monocytes supply a stock of undifferentiated macrophages to the site of infection via blood. NK cells are invariant lymphoid cells that can recognize and kill infected/malignant cells. Neutrophils are short lived blood cells that can do phagocytosis, degranulation and release their genomic DNA (NETs) to extracellular space to kill and trap pathogens [62,63]. Below, Figure 1.5 summarizes types of receptors and effector mechanisms employed by the innate immune system [64].

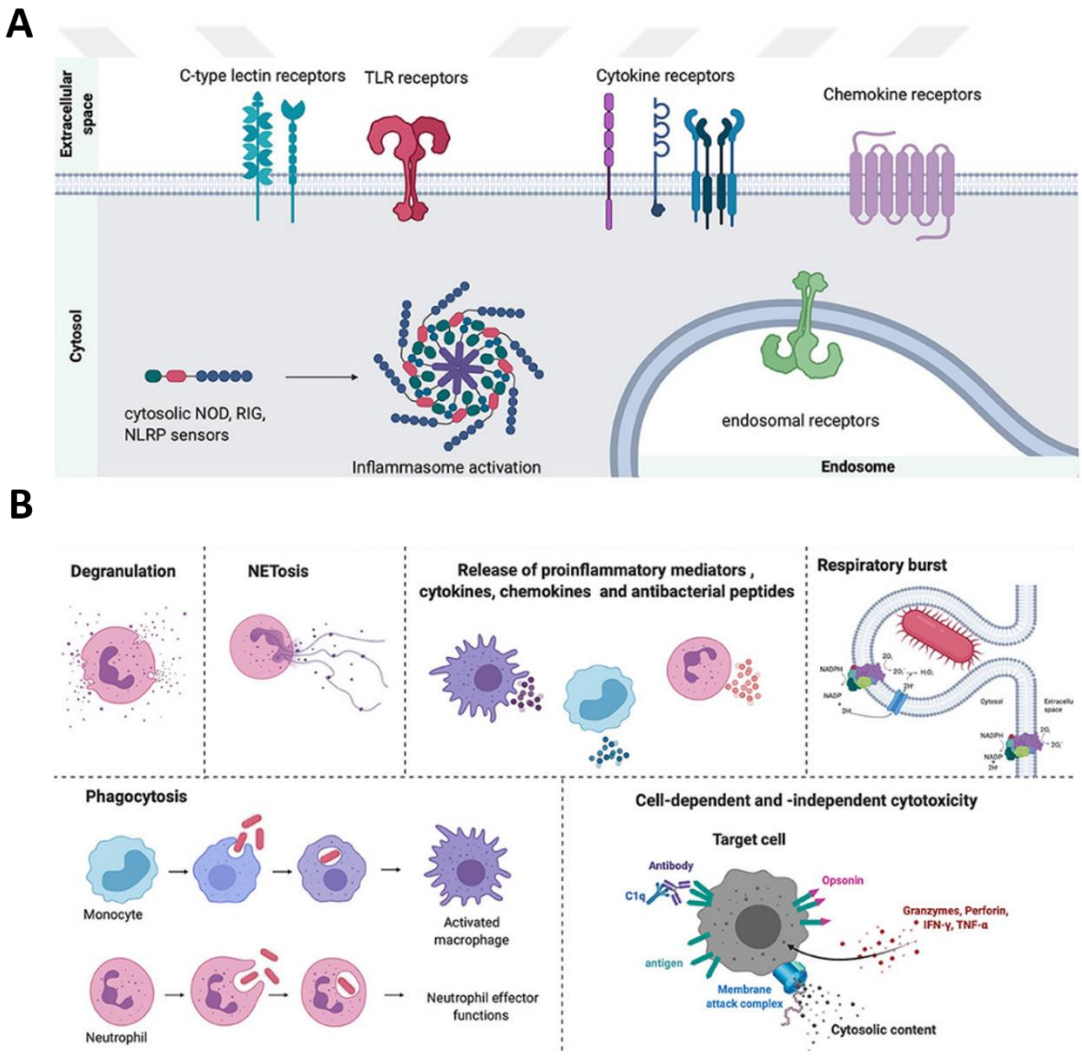

Figure 1.5 Different classes of receptors and effector mechanisms of the innate immune system. A. Wide range of PRRs recognize pathogen and danger associated molecular patterns encountered in different cellular compartments. Cytokine/chemokine receptors allow amplification or resolution of immune responses and also *direct* trafficking of immune cells. **B.** Activation of PRRs and subsequent cytokine production causes inflammation. Inflammatory microenvironment allows effector mechanisms including degranulation of granulocytes, uptake of pathogens through phagocytosis and

subsequent elimination through respiratory bursting. It also results in increased production of antimicrobial compounds. Adapted from [64].

SARS-CoV-2 components thought to trigger numerous of these mentioned PRRs. Envelope protein can activate TLR2 signaling both in vitro and during in vivo infection [65]. There is also evidence, albeit computational, regarding binding of Spike to TLR1, TLR4 and TLR6 [66]. However, validation of these possible interactions remains missing. Interestingly, TLR3 can limit SARS-like coronavirus infection in mice [67]. Upon possible recognition, TLR1, 2, 4 and 6 activates transcription factors NFκB and AP-1 via MyD88- NFκB/ERK adaptor interaction. NFκB and AP1 then drives expression of inflammatory cytokines/sensors like TNFα, IL-6, NLRP3 and IL-1β. TLR4 and TLR3 can activate transcription factor IRF3 through TRIF adaptor [68].

Viral RNA species are also recognized by variety of RLRs. Infection causes activation of MDA5, LGP2 [69] and RIG-1 through a non-canonical mechanism [70]. Upon activation, RLRs activate transcription factor IRF3 via MAVS adaptor complex. IRF3 activates expression of Type I and III interferons.

Nucleocapsid and ORF3a activates NLRP3 inflammasome which in turn, causes release of mature forms of IL-1β/IL-18 and host cell destruction through pyroptosis [71,72]. It is unclear if recognition by the NLRP3 inflammasome is benefiting the virus or the host immune system.

Putative recognition mechanism of SARS-CoV-2 through PRRs is outlined in Figure 1.6 [68].

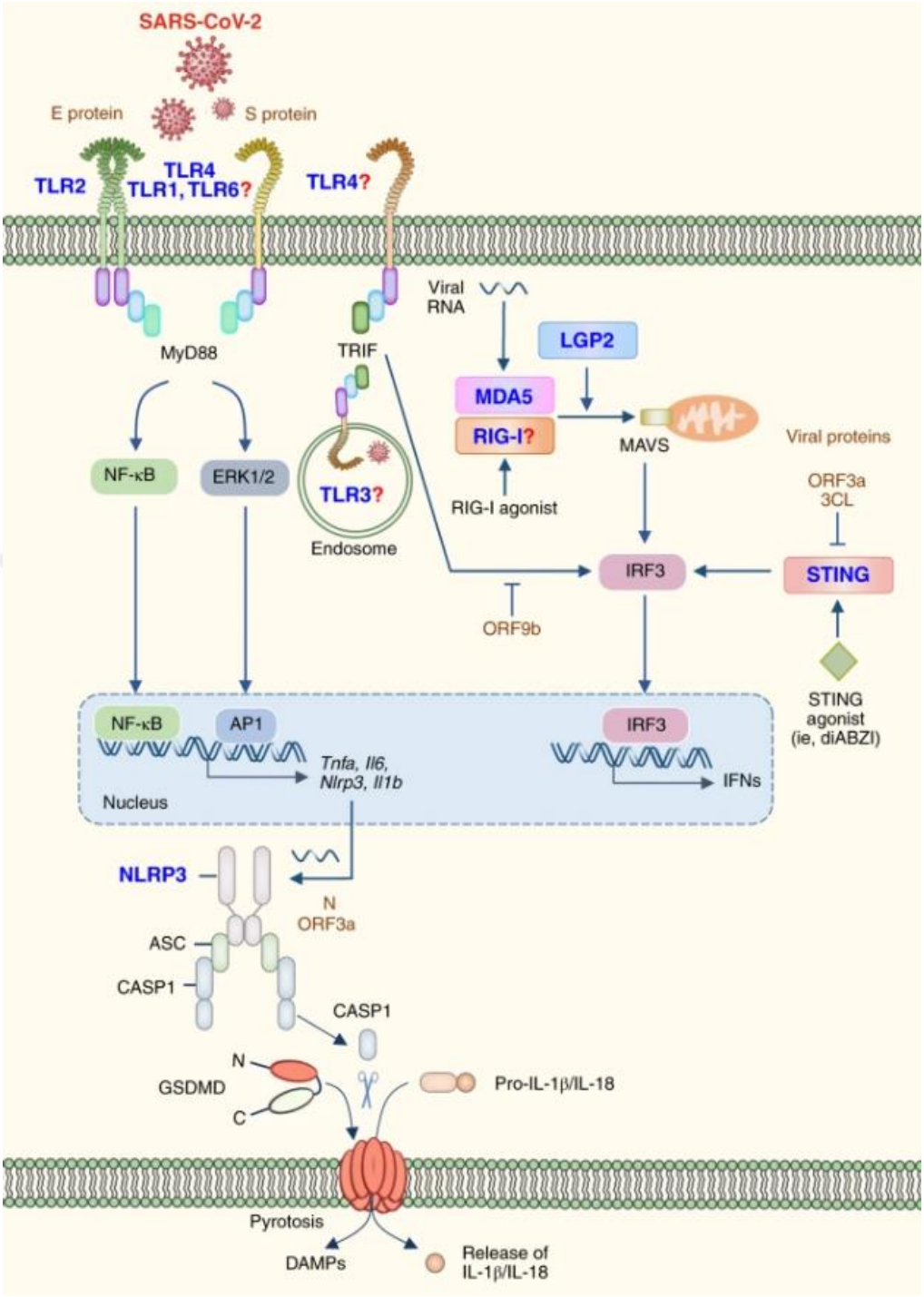

Figure 1.6 Putative recognition of SARS-CoV-2 through PRR signaling cascades. Constituents of SARS-CoV-2 are hypothesized to activate variety of PRRs. Viral proteins *might* activate TLR1, TLR2, TLR4 and TLR6 to drive expression of inflammatory mediators including IL-1β and IL-6. Viral RNA *would* activate cytosolic nucleic acid sensors MDA5 and RIG-1 to drive expression of Type I and III interferons. Nucleocapsid and ORF3a activates NLRP3 inflammasome to drive release of active IL-1β/IL-18. Adapted from [68].

1.2.2 Adaptive Immune System and Reaction to SARS-CoV-2

Major histocompatibility complex (MHC) proteins link the innate arm of the immune system to adaptive arm. Two classes of MHC proteins, MHC I and MHC II are instrumental to harbor and present processed endogenous antigens arising either from malignancy or from viral infections and exogenous antigens arising from intracellular pathogens, respectively [59]. Of important note, only professional antigen presenting cells express MHC II molecules on their surface and these are dendritic cells, macrophages and B cells. All nucleated cells express MHC I molecule.

Naïve T cells — T cells that have not been differentiated following exposure to an epitope/MHC complex, reside mainly in secondary lymphoid tissues. An antigen can arrive to lymph node carried via the lymphatics or on an APC, as an epitope loaded to MHC. Lymph nodes also have their own APCs for antigens carried by lymphatics. These include subcapsular sinus macrophages, medullary macrophage, interfollicular macrophages, interdigitating dendritic cells and B cells [73]. Instruction and triggering of naive T cells to differentiate into effector T cells requires at least three signals. The MHC complexed peptide epitope, APC-associated co stimulatory molecule engagement of CD28 and a specific cytokine milieu to induce T cell differentiation.

There are two main types of T cells, CD4+ T helper cells and CD8+ cytotoxic T cells. MHC-peptide complex on an APC is a ligand for T cell receptor (TCR) of a T cell. CD4+ T cells bind to the MHC II – peptide complexes and CD8+ T cells bind to the MHC I – peptide complexes. CD4+ T helper cells are potent cytokine secreters and induce differentiation of antigen specific B cells. CD4+ T helper cells can influence the type of immune reaction in a phenomenon called Th programs. CD8+ cytotoxic T cells can kill cells that express the epitope the naïve T cell first responded to, prior to becoming an effector [74].

In line with these mechanisms, dendritic cells are equipped with unusual antigen processing and presentation functions. Exogenous antigens from endocytosed material can be loaded onto MHC I molecules in a process called cross-presentation. (Joffre et al., 2012) Cross presentation is the only way some vaccines induce CD8+ T cell responses. For example, an inactivated vaccine adjuvanted with an aluminum salt is a typical example for a vaccine that is thought not to induce cytotoxic T cell responses. [75] However, extracellular antigens coupled with adjuvants that promote cross presentation can induce robust cytotoxic T cell responses. One such adjuvant is CpG oligodeoxynucleotides [76,77].

Effector helper T cells can be of Th1, Th2, Th17, Treg or Tfh sub-types [74]. Th1 cells induce an environment where immune system is dealing with an intracellular pathogen, such as a virus. These cells secrete mainly IFNγ and IL2. IFNγ indices expression of about 200 genes that can halt viral or bacterial infections [78]. IL2 is crucial for the generation of CD8+ memory and effector cytotoxic T cells [79]. Th1 response also skews macrophages to an M1-like phenotype via secretion of IFNγ and CD40L expression. M1-like macrophages have heightened microbial effector functions having increased MHC II expression, producing nitric oxide and superoxide radicals in phagolysosomes, increased TNFα

production and upregulation of CD80/86 co-receptor ligands. Th1 cytokine milieu also promotes B cell class switching to IgG2a in BALB/c mice (IgG1 in humans). IgG2a antibodies are potent complement activators [80] and also drive antibody dependent cell-mediated toxicity [81]. Th2 responses are driven by IL4 and Th2 CD4+ T helper cells secrete IL4, IL5 and IL13 [82]. This program of immunity is designed for fighting extracellular parasites—helminths. Th2 cytokines mediate basophil, eosinophil and mast cell responses and support class switching of B cells to IgG1(Balb/c) and IgE. Th2 response is unwanted in vaccines against viruses as this can cause vaccine-associated enhanced disease (VAED) by antibody dependent enhancement and aberrant recruitment of Th2 associated cells like eosinophils [83]. Th17 cells produce IL17 and IL22 in response to fungi and extracellular bacteria. These cytokines activate epithelial cells and neutrophils.

B cells can encounter antigen in the periphery and home to a lymphoid tissue to proliferate and differentiate or they can also encounter the antigen in the lymphoid tissue. Naive B cells can be activated with two types of antigens. Most antigen require T cell help from Tfh cells. Such an antigen is first endocytosed by the B cell, processed and then displayed on MHC II molecules to Tfh cells via MHC II/peptide/TCR interaction. Upon activation, the Tfh secrete cytokines and express other costimulatory molecules, allowing the B cell to proliferate and differentiate. Initial endocytosis occurs when this antigen is recognized by B cell receptor (BCR). Therefore, B cell epitopes are in general not linear but conformational. Some antigens are so called thymus independent, meaning they can induce antibodies without T cell involvement. These antigens crosslink BCRs via their highly repetitive nature or with secondary signaling occurring via activation of a B cell PRR, like TLR4 activation by LPS. This way, B cells can be activated without T cell help. Figure 1.7 summarizes effector mechanisms of the adaptive immune system.

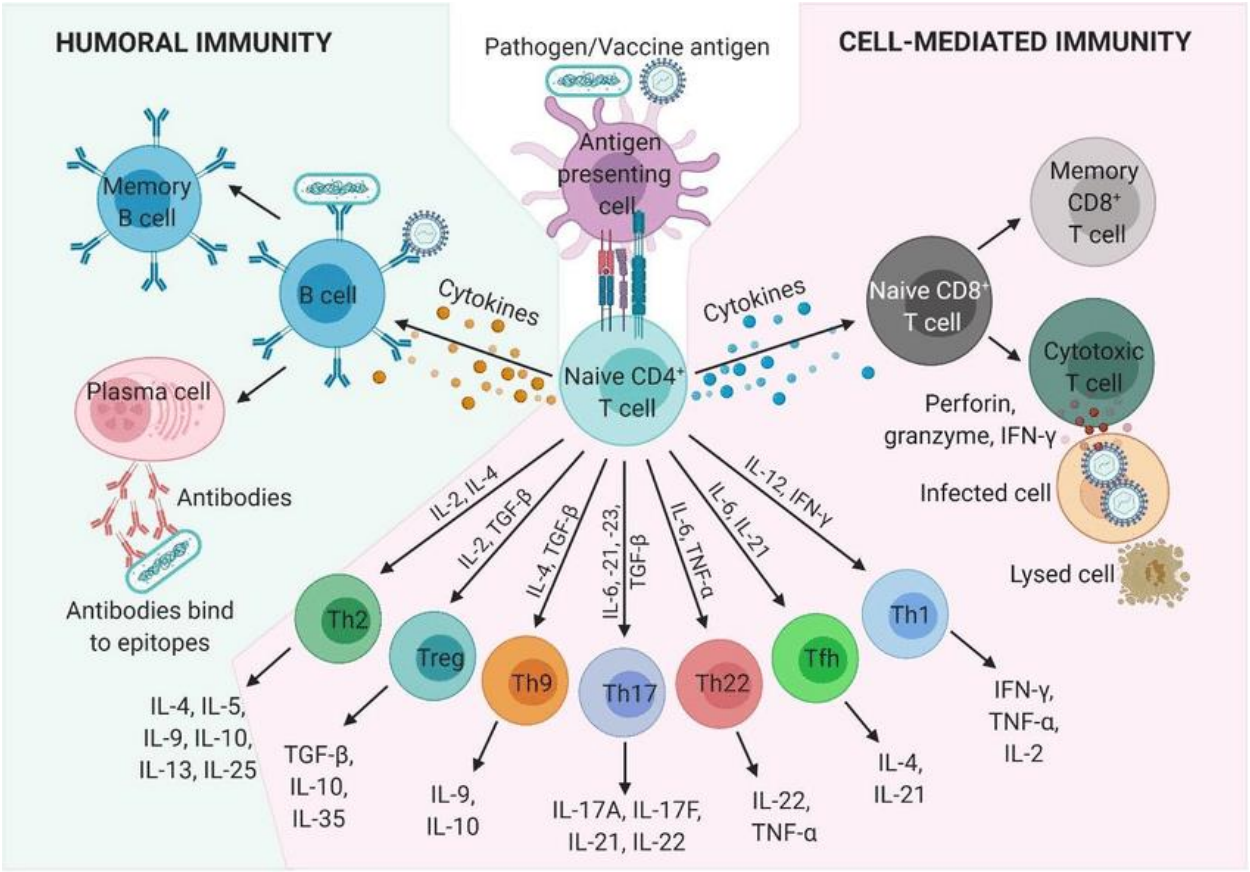

Figure 1.7 Cellular and humoral effector mechanisms of the adaptive immune system. Adaptive immunity is *alerted* through antigen presentation to naïve lymphocytes. Upon activation with an antigen *and costimulatory signals* and in the presence of correct cytokine milieu, antigen specific differentiation and proliferation of T and B lymphocytes occur. Humoral effector mechanisms include antibody dependent neutralization and opsonization of antigens. Antibodies are produced by plasma cells, which are differentiated from naïve B cells upon antigen exposure and T cell interaction. Subset of antigen exposed B cells differentiate into long lived memory B cells to protect host from future insult. Cellular effector mechanisms include cytotoxic T cells, which kill infected or malignant cells and also wide range of helper T cells, which are important for orchestrating the overall immune response against a specific type of pathogen. Helper T cells secrete different cocktails of cytokines which influence *the* type of immune cell recruitment and also function *of the recruited cells*. Adapted from [84].

SARS-CoV-2 has some tricks up its sleeve to evade the immune system, particularly to evade the early interferon signaling, but it is in general, processed like any other human viral pathogen [85]. CD4+ T cell responses to Spike, Membrane and Nucleocapsid, ORF3a and Nsp3 are detected in a large majority of convalescent individuals [86]. Envelope is thought to be too small to harbor any T cell epitopes. Although found less consistently among individuals, CD8+ T cells against Spike, Membrane, Nucleocapsid and ORF3a are also detected [87]. Interestingly, even though Membrane is quite small, it still induces T cell responses with high proportions compared to other proteins. How and why exactly this occurs is unclear. CD4+ T cells are detectable 2 to 4 days after symptom onset and CD8+ T cell are sometimes detectable even after a day [88,89]. Antibody responses against Spike, RBD, S2, Nucleocapsid are apparent in most individuals and correlate with disease severity [90]. Although heterogeneous and decreasing around 10 folds, even 6 months after the infection, IgG titers against Spike, RBD and Nucleocapsid are measurable

[91]. This is also the case for memory CD4+ T cells, CD8+ T cells against Spike, Membrane, Nucleocapsid, ORF3a, Nsp3 and memory B cells against Spike, RBD and Nucleocapsid. It is interesting that T cell compartment is dominated by cells targeting Membrane and Nucleocapsid epitopes [91].

1.3 Vaccines

The goal of vaccination is to generate long-lasting, protective immunity against a target pathogen. Many types of vaccines exist and will be briefly discussed. Classically, vaccines can be separated into two categories, live and non-live. Live vaccines are attenuated versions of pathogens that are still viable. Examples include *Mycobacterium bovis* bacillus Calmette–Guérin (BCG) vaccine against tuberculosis and vaccines against polio and measles. Non-live vaccines are either inactivated whole pathogens, purified antigens or toxins from the pathogen or their recombinantly produced counterparts. Non-live vaccines in general require adjuvants to create a durable immune response.

Next generation vaccines include viral vectored and plasmid DNA vaccines and in vitro transcribed mRNA vaccines [92]. Both strategies are nucleic acid driven where genetic information of the target antigen is delivered to cells. These cells then produce the antigen and invoke an immune response. These vaccines so far do not use adjuvants in a classical sense as their components possess an intrinsic adjuvant effect.

Summarized in Table 1.1, Center for Disease Control (CDC) recommends vaccines with distinct technologies in its Birth to 18-Year-old vaccination program. These include recombinant protein and toxoid vaccines, inactivated vaccines, conjugate vaccines, polysaccharide vaccines and live attenuated vaccines. No single type of vaccine technology is superior to another in all aspects. There remains substantial lack of knowledge on what induces a robust immune response and what makes another approach intrinsically better than another depending on the disease its targeting.

Table 1.1 Birth-18 years old immunizations recommended by the CDC. Exemplary commercial choice of vaccine and summary of vaccine ingredients are presented [93].

Vaccines	Trade Names	Type
Diphtheria, tetanus, and acellular pertussis vaccine	Daptacel	Toxoid, recombinant, absorbed *Diphtheria toxoid, tetanus toxoid, and acellular pertussis antigens absorbed onto aluminum phosphate*
Haemophilus influenzae type B vaccine	Hiberix	Conjugate *Influenzae type b polysaccharide conjugated to tetanus toxoid*
Hepatitis A vaccine	Havrix	Inactivated, absorbed *Inactivated Hepatitis A adsorbed onto Alum*
Hepatitis B vaccine	Engerix-B	Recombinant, absorbed *Hepatitis B surface antigen absorbed onto aluminum hydroxide*
Human papillomavirus vaccine	Gardasil 9	*Recombinant VLP, absorbed* *Multivalent L1 VLPs absorbed onto aluminum hydroxyphosphate sulfate*
Influenza vaccine (live, attenuated)	FluMist Quadrivalent	Live, attenuated
Measles, mumps, and rubella vaccine	M-M-R II	Live, attenuated
Meningococcal serogroups A, C, W, Y vaccine	Menactra	Conjugate *Polysaccharide from serogroup A, C, Y and W-135 conjugated to diphtheria toxoid*
Meningococcal serogroup B vaccine	Bexsero	Recombinant, absorbed *Recombinant proteins Neisserial adhesin A, Neisserial Heparin Binding Antigen and factor H binding protein, 25 micrograms of Outer Membrane Vesicles (OMV) absorbed on 1.5mg Alum*
Pneumococcal 13-valent conjugate vaccine	Prevnar 13	Conjugate, absorbed *Streptococcus pneumoniae serotypes 1, 3, 4, 5, 6AB, 7F, 9V, 14, 18C, 19A, 19F, 23F saccharides, diphtheria toxin and aluminum phosphate*
Pneumococcal 23-valent polysaccharide vaccine	Pneumovax 23	Polysaccharide *Pneumococcal polysaccharides from types 1, 2, 3, 4, 5, 6B, 7F, 8, 9N, 9V, 10A, 11A, 12F, 14, 15B, 17F, 18C, 19F, 19A, 20, 22F, 23F and 33F*
Poliovirus vaccine (inactivated)	IPOL	Inactivated *Type 1, Type 2, and Type 3 inactivated poliovirus*
Rotavirus vaccine	Rotarix	Live attenuated
Varicella vaccine	Varivax	Live attenuated *Oka/Merck varicella virus*

1.3.1 History of Vaccines

While Europe met with the concept of vaccination through British Doctor Edward Jenner in 1796, history of such practices is as old as the history of infectious diseases. Inoculation of orthopox material, termed variolation, was practiced in China, India and Ottoman Empire around 1000 AD [94]. Janner

inoculated a boy with cowpox and then challenged the primed boy with a live smallpox. Luckily the boy survived [95]. The term "Vaccination" is derived from the latin word '***vacca'*** as it means 'cow'. Although development of smallpox vaccine is credited to Jenner, several others have done what Jenner has done before him. Benjamin Jesty, a farmer in England, practiced variolation on his wife and two eldest sons in 1774 [96].

In 1880, Louis Pasteur developed a chicken cholera vaccine by realizing the attenuation of the bacteria by oxidation did not disturb its immunogenicity [97].

In 1880, Jean Joseph Henri Toussaint developed an Anthrax vaccine by taking blood from a sheep dying from Anthrax, filtering and treating it with 1.5% phenol. Pasteur applied this oxidation process to chicken cholera. Since Anthrax spores are resistant to oxidative inactivation, in 1881, Pasteur conducted the famous sheep experiment in Pouilly-le-Fort with his potassium dichromate killed vaccine [97] which he, perhaps dishonestly, marketed as a live vaccine [98].

In 1885, a nine-year-old boy, bitten by a rabid dog two days earlier, was brought to Pasteur's laboratory. For ten days, the boy was given increasingly less dried spinal fluid from a rabid rabbit and was eventually healed from the disease. This was perhaps Pasteur's greatest achievement. It was later understood that continuous culturing of rabies virus from rabid dogs— not the drying process that Pasteur was using, was the attenuation factor [97].

In early 20th century, a killed salmonella vaccine, killed bubonic plague vaccine, killed cholera vaccine was developed and used as antitoxins, what we now call antibodies, against diphtheria and cholera toxins were in common use.

In 1921, Guerin and Calmette started the experiments for a tuberculosis vaccine. They have isolated a mycobacterium species of bovine origin and after 13 years of passaging on beef bile, potatoes and glycerol, *Mycobacterium bovis* was attenuated. Original vaccine "bacille calmette-guérin" (BCG), was sent to numerous countries and today there are dozens of strains derived from the original strain.

In 1935, Sir Frank Macfarlane Burnet and Wilson Smith discovered that the causative agent of flu, a virus that was isolated from nasal secretions of infected patients 2 years before, could be grown on embryonated chicken's eggs. Formalin inactivated virus was used as a vaccine in clinical trials in late 1930s.

Second half of the 20th century was dominated by advancements in cell culture techniques and more recently, recombinant and nucleic acid vaccines.

1.3.2 Adjuvants

Adjuvants are immune-activators that enhance antibody production as well as cell mediated immunity. In mid 1920s, Gaston Ramon experimented with injection of starch to drive sterile inflammation at the injection site of the horses that he inoculated with diphtheria toxin [99]. Immune enhancing effects of aluminum salts were shortly discovered by Alexander Glenny [99].

Aluminum salts are most widely used adjuvants even today. Function of aluminum salts as adjuvants arise from two main effects—absorption of antigen and action of it as a PAMP. Aluminum salts are Th2 skewing adjuvants [100]. Immune enhancing effects of absorption is believed to be caused by slowing the diffusion of the antigen from the injection site, giving time for antigen presenting cells (APCs) for phagocytosis. Alum causes both self-associated and pathogen associated patterns to arise as it's a NLRP3 inflammasome agonist [101]. Resulting cell death releases self-associated danger signals, mainly urea and ATP. This further enhances the proinflammatory environment. There are also however, conflicting findings regarding this theory [102]. Aluminum salts also enhance stability of antigens in vaccines, particularly those with aggregation tendencies.

Knowledge of PAMPs and their receptors further moved the adjuvant research forward. Current adjuvants in licensed vaccines include Aluminum salts, AS04— Monophosphoryl Lipid A adsorbed onto an aluminum hydroxide or phosphate, AS03—oil in water emulsion composed of alpha-tocopherol, squalene, polysorbate 80, MF59—oil in water emulsion containing squalene and CpG 1018—a TLR9 agonist oligodeoxynucleotide [103].

CpG ODNs are synthetic oligodeoxynucleotides with unmethylated cytosine guanine dinucleotide motifs. They are potent inducers of TLR9 signaling pathway. Effect of a CpG ODN is determined by its backbone chemistry and sequence, influencing the ODN's folding. K type ODNs (B class) harboring multiple CpG motifs, stimulate B cells, resulting in IL6 and IL10 secretion and plasma cell differentiation [104]. K ODNs also activate monocyte/dendritic cell lineages in PBMC. Activation of this APC lineage, together with B cells, creates a Th1 dominant heightened antibody response [105]. K type ODNs have a phosphorothioate backbone and exist as single stranded DNA molecules.

D type ODNs (A class), unlike K ODNs, have multiple guanosine repeats surrounding the core CpG motif, found in a palindromic sequence. Duplex formation caused by the palindromic region drives Hoogsteen base pairing of the guanosine repeats, organizing them into a G-tetrad structure [106]. D ODNs are optimally immunogenic as phosphorothioate/phosphodiester chimeras. They drive substantial amounts of type I Interferon release from plasmacytoid dendritic cells (pDCs) and activate NK cells. Unlike K ODN, they do not cause proliferation of B cells. D ODNs are mild inducers of B cell activation and differentiation [104].

Notably, K type CpG ODN 1018 is used in HEPLISAV-B, an FDA approved hepatitis B vaccine composed of rHBsAG combined with CpG adjuvant [107].

1.3.3 Current SARS-CoV-2 Vaccines and Global Vaccination Status

COIV-19 pandemic resulted in perhaps the most impressive "arms race" in vaccine development to date. Various vaccine types are now approved for use around the world with strategies ranging from mRNA, adenoviral vectors, inactivated whole virions to recombinant vaccines. Figure 1.8 summarizes technologies utilized for vaccine making during the pandemic.

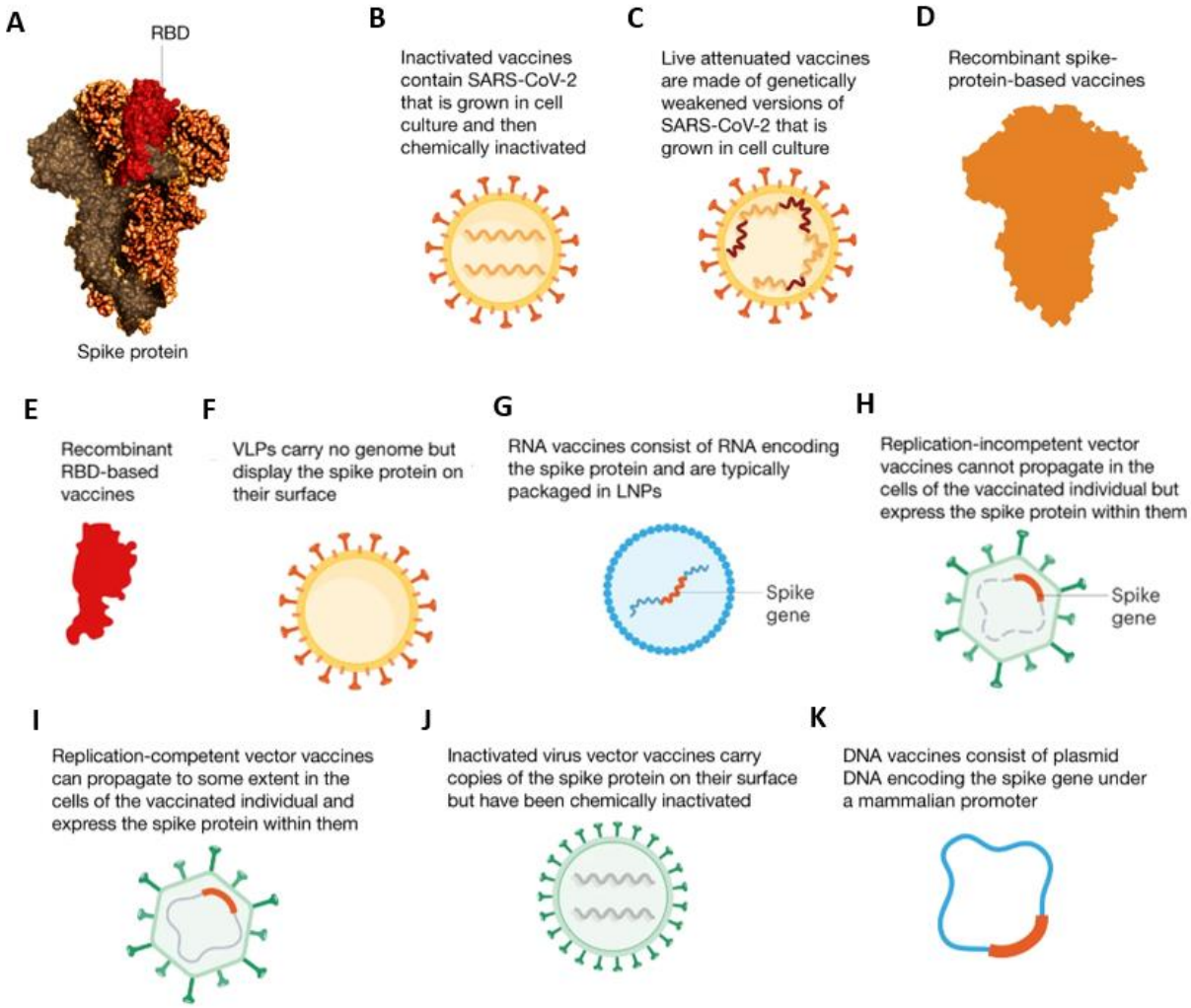

Figure 1.8 Strategies used by variety of manufacturers for vaccine development during SARS-CoV-2 pandemic. A. Spike and RBD are the main targets of most next generation vaccines. **B.** Inactivated virion vaccines require culturing of the pathogenic live virus and subsequent inactivation by irradiation or chemical substances like formalin. **C.** Live attenuated vaccines are composed of live virus that has lost its pathogenicity through genetic modifications or continuous passaging. Unlike nucleic acid vaccines that are on the market, inactivated and live attenuated vaccines confer immunity towards all antigens found in the virus. Recombinant protein vaccines use purified **D.** Spike or **E.** RBD to induce immune responses. Similarly, **F.** Virus like particles (VLPs) are recombinantly produced structures that mimic the original virus. These may either only display Spike/RBD or all structural proteins. **G.** RNA vaccines utilize RNA encoding Spike/RBD packaged in lipid nanoparticles (LNPs) to drive expression of the antigen in host. Similarly, in viral vectored DNA vaccines, **H.** replication incompetent and **I.** replication competent viruses carry Spike/RBD encoding DNA. Other strategies include **J.** recombinantly produced Spike expressing inactivated vaccines and **K.** plasmid DNA vaccines encoding Spike/RBD. Adapted from [108].

In addition, Table 1.1 summarizes the types and efficacies of some of the major authorized/approved SARS-CoV-2-specific vaccines.

Table 1.2 Major authorized/approved vaccines against SARS-CoV-2 Adapted from [109].

Name	Type	Developers	Reported Effectiveness
Comirnaty (BNT162b2)	mRNA vaccine (Spike encoding mRNA)	Pfizer, BioNTech (Multinational)	95% efficacy in Phase 3 clinical trial (NCT04368728)
Moderna COVID-19 Vaccine (mRNA-1273)	mRNA vaccine (Spike encoding mRNA)	Moderna, NIH (USA)	94.1% efficacy in Phase 3 clinical trial (NCT04470427)
COVID-19 Vaccine Janssen (Ad26. COV2.S)	Adenovirus vaccine (Spike encoding DNA)	Johnsons & Johnsons (The Netherlands, US)	85% efficacy in Phase 3 trial (NCT04505722).
COVID-19 Vaccine AstraZeneca (Covishield)	Adenovirus vaccine (Spike encoding DNA)	AstraZeneca, University of Oxford (UK)	79% efficacy in Phase 3 clinical trial (NCT04516746).
Sputnik V (Gam-COVID-Vac)	Adenovirus vaccine	Gamaleya Research Institute (Russia)	94.1% efficacy in Phase 3 clinical trial (NCT04530396)
NVX-CoV2373	Recombinant Spike Protein Vaccine	Novavax (USA)	90.4% efficacy in Phase 3 clinical trial (NCT04611802)
CoronaVac (PiCoVacc)	Inactivated vaccine	Sinovac (China)	50% efficacy in Phase 3 clinical trial (NCT04456595)
Convidicea (Ad5-nCoV)	Adenovirus vaccine	CanSino Biologics (China)	65.7% efficiency in Phase 3 clinical trial (NCT04526990).
Covaxin	Inactivated vaccine	Bharat Biotech (India)	81% efficiency in Interim phase 3 trial

During the pandemic the speed of vaccine development was truly remarkable. Particularly, the mRNA vaccine candidates had the upper hand in speed owing to not only their easy to scale up procedure and experience but also to the nature of mRNA platform itself. As soon as the virus was sequenced on 10th of January, 2020, both Moderna and BioNTech were essentially ready to produce pilot products. On 11th of December, 2020, Pfizer/BioNTech vaccine became the first vaccine authorized for emergency use by FDA.

As of now, 63% of the world population has received at least one dose of a COVID-19 vaccine. (Figure 1.4) Pfizer/BioNTech vaccine has dominated the market with approximately 600 million doses being used so far. Next closest candidate, from Moderna, has been used for approximately 100 million doses so far [110]. Despite these numbers, vaccine inequality is still a persistent problem. Only 19% of people

have received partial vaccination in Africa. Below, Figure 1.5 shows percentage of completely/partially vaccinated of individuals in each continent and in worldwide.

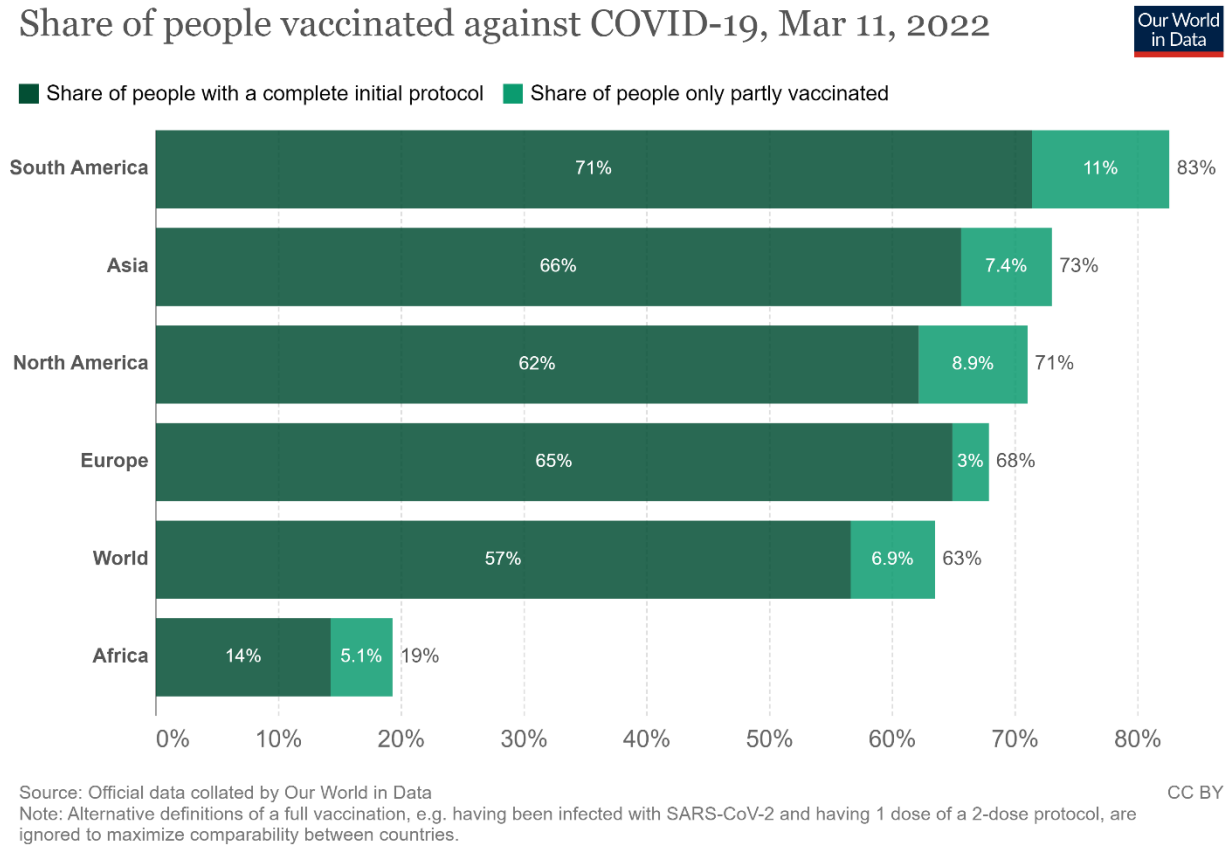

Figure 1.9 Proportion of people that have received at least one dose of a COVID-19 vaccine in the world and in individual continents. Adapted from [110].

1.4 Virus Like Particles

Virus like particles encompass a variety of kinds of virus mimicking structures that lack genetic information and thus, not viable. There are two main types of VLPs, native enveloped structures that self-assemble in producer cells and are secreted to extracellular space or capsid-like structures that can be assembled in vitro with purified capsid proteins. Wide range of VLPs from viruses including Influenza, Human immunodeficiency virus (HIV), coronavirus, Human papilloma virus, Hepatitis virus and Ebola virus have been produced by others and us [111,112]. As of now, there are five FDA approved VLP vaccines on the market. These are Gardasil, Gardasil-9 and Cervarix targeting HPV, Sci-B-Vac targeting Hepatitis B and Mosquirix targeting malaria [111].

In February of 2022, a plant VLP based SARS-CoV-2 vaccine produced by Medicago and GlaxoSmithKline was approved for use in Canada by authorities [113]. VLPs harbor the SARS-CoV-2 spike and are adjuvanted with GlaxoSmithKline's adjuvant AS03. AS03 proved to be a better adjuvant in terms of antibody production but CpG ODN 1018 was determined to be more Th1 skewing [114].

1.5 Good Manufacturing Practice

GMP stands for several guidelines and standards to ensure a given quality standard is achieved during manufacturing. Guidelines aim to not only reduce but also monitor mix ups, equipment failures and experimenter errors. They also aim to make sure what is produced in a facility is what was aimed to be produced. These guidelines can be for variety of products like pharmaceuticals, cosmetics, food and beverages. In 1967, first international GMP guidelines for pharmaceuticals were submitted to World Health Organization. In Europe, GMP guidelines are enforced by European Medicines Agency (EMA). In USA, FDA oversees the implementation these regulations.

GMP regulations encompass quality control measures of a product, actions of the personnel, standardization of all facility instruments and the experiments being run. Perhaps most importantly, it also regulates cleanliness of the facility. Not all areas of a GMP laboratory are equal. Areas are graded from A (cleanest) to D (dirtiest). During operation, these areas are ranked amongst their maximum permitted number of particles smaller than 500 nm. During operation, Grade A area allow 3520 particles per m^3 while Grade B and Grade C allows for 352000 m^3 and 3520000 m^3 respectively.

1.6 Aim of the Study

Previously, our group has developed a virus like particle production strategy to recombinantly produce enveloped SARS-CoV-2 VLPs. Usage of prefusion stabilized Spike mutants enabled us to enhance decoration of Spike onto VLPs and also increase its immunogenicity by several orders of magnitude [112]. Developed process for VLP production was fully scalable, composed of transient transfection of suspension mammalian cells, fast protein liquid chromatography and tangential flow filtration.

Herein, we have aimed to implement a large-scale production scheme to produce a GMP-grade, SARS-CoV-2 VLP vaccine adjuvanted with Alum and K3 CpG ODN for use in planned clinical trials. Possibilities and also the limitations of the proposed production process were to be determined. Along with this, further experiments on both purified VLPs and fill and finished vials were planned to better understand the properties of the antigen and the vaccine. Along with VLPs that are decorated with Spike from the original Wuhan strain which was to be used in Phase 1 clinical trial, we have also aimed to produce VLPs that harbor Alpha variant Spike to be used in Phase 2 clinical trial. Finally, immunogenicity of several lots of the above mentioned GMP grade VLP vaccine was tested.

2. Materials and Methods

2.1 Materials

2.1.1 Suspension HEK293 Cell Line

Suspension adapted HEK293 cell line was obtained from Florabio, Turkey together with GMP grade Orchid293 CD production medium and Orchid293 CD transfection medium. Details regarding the usage of these media are explained in further sections.

2.1.2 Bacterial Strain for Plasmid Manufacturing

NEB Stable (C3040) was obtained from New England Biolabs, U.S.A. This strain was used to create a transformed bacterial master cell bank and purify endotoxin free plasmids for GMP grade VLP production.

2.1.3 Fast Protein Liquid Chromatography System

FPLC was performed using ÄKTA avant chromatography system. Chromatographic media Capto Core 400 was obtained from Cytiva, U.S.A, along with Hiscale 26/20, XK 50/30 and Axichrom 70 columns.

2.1.4 Tangential Flow Filtration System

SARTOFLOW Smart TFF system along with Sartocon Slice 200 Hydrosart 100kDA cassettes were obtained from Sartorius, Germany.

2.1.5 Antibodies

Tables 2.1, 2.2 and 2.3 outline antibodies used in ELISA experiments, antibodies used in immunoblotting and recombinant proteins used for various purposes respectively.

Table 2.1 IgG specific ALP conjugated antibodies used throughout ELISA experiments.

Product	Catalog No.	Company	Working Concentration
anti-mouse IgG ALP	1030-04	Southern BioTech	1:1000
anti-mouse IgG1 ALP	1070-04	Southern BioTech	1:1000
anti-mouse IgG2a ALP	1080-04	Southern BioTech	1:1000

Table 2.2 SARS-CoV-2 antigen specific primary antibodies and HRP conjugated secondary antibodies used throughout immunoblotting experiments.

Product	Catalog No.	Company	Working Concentration
anti-S1	9083	ProSci	1:1000
anti-Nucleocapsid	9103	ProSci	1:1000
anti-Histag	HRP-66005	ProteinTech	1:10000
anti-mouse HRP	7076	CST	1:10000

anti-rabbit HRP	7074	CST	1:10000

Table 2.3 Recombinant proteins used throughout the study.

Product	Catalog No.	Company	Working Concentration
recS1	9083	ProSci	5 ug/ml
Spike (HexaPro)	-	In-house	3 ug/ml
Nucleocapsid	-	In-house	20 ug/ml
RBD (Wuhan)	-	In-house	3 ug/ml
RBD (Wuhan)	PX-COV-P046-10	ProteoGenix	2 ug/ml
RBD (Alpha)	PX-COV-P052-10	ProteoGenix	2 ug/ml
RBD (Beta)	PX-COV-P053-10	ProteoGenix	2 ug/ml
RBD (Gamma)	PX-COV-P054-10	ProteoGenix	2 ug/ml

2.1.6 Inactivated Virus

β-Propiolactone inactivated SARS-CoV-2 was obtained through collaboration with Prof. Osman Erganiş from Selçuk University. Upon arrival, inactivated virus was sterile filtered through 0.22 um microfiltration and total protein was determined with Micro-BCA.

2.2 Methods

2.2.1 Expression Plasmids

HexaPro stabilized [115] version of Wuhan strain Spike (S), HexaPro stabilized version of British strain (alpha variant), membrane glycoprotein (M) (NCBI Refseq: YP_009724393.1), envelope (E) (NCBI Refseq: YP_009724392.1) and nucleocapsid (N) (NCBI Refseq: YP_009724397.2) proteins of SARS-CoV-2 were synthesized by Integrated DNA Technologies, Inc. (California, USA). All sequences were flanked by BamHI sites and all except Nucleocapsid had a C' terminus 6xHistidine tag.

S and E genes were cloned into pVitro2 (Invivogen, France) backbone by BamHI and BglII digestion respectively. S was cloned under human ferritin heavy chain promoter and E was cloned under human ferritin light chain promoter. Similarly, M and N genes were cloned into pVitro1 (Invivogen, France) backbone by BamHI and BglII digestion respectively. N was cloned under mouse elongation factor 1 alpha promoter and M was cloned under rat elongation factor 1 alpha promoter. Further details on these plasmids were published previously by our group. [112]

2.2.2 Plasmid Manufacturing

pVitro1 and pVitro2 transformed bacterial master cell (NEB Stable E. coli, New England Biolabs, U.S.A.) bank were grown in Low-salt LB medium supplemented with 100ug/ml Hygromycin B gold (Invivogen, France) in a shaking incubator (200rpm, 37°C). Cells we+re harvested after 20 hours of culture by centrifugation at 3000g for 20 minutes. Plasmids were extracted from bacterial biomass by

NucleoBond Xtra Endogen free Maxiprep kit (Macherey-Nagel, France) according to the manufacturer's instructions. All plasmids that were to be used in GMP production were digested with BamHI to ensure correct band patterning. BamHI digestion of pVitro2 S_E results in a Spike fragment of size 4kb and E+Backbone fragment of 6kb. BamHI digestion of pVitro1 M_N results in a Membrane fragment of 770bp and N+Backbone fragment of 7.8 kb. Plasmids were also analyzed for endotoxin levels using LAL Chromogenic Endotoxin Quantitation Kit (Thermo Scientific, U.S.A.), according to manufacturer's instructions.

2.2.3 Growth and Transfection of HEK293 Suspension Cells

HEK293 suspension cells were purchased from Florabio, Turkey. Cells were thawed and passaged in Orchid293 CD production medium. (Florabio, Turkey) Cells were passaged every two to three days or when cell densities reached $3x10^6$/ml. Prior to transfection, cells were passaged in Orchid293 CD transfection medium (Florabio, Turkey) for at least 2 passages. All media were supplemented with 400mg/L L-Glutamine (Sigma,Canada), were serum and animal product free, complying with GMP regulations. No antibiotics were used in cell culture. For freezing, cells were resuspended in 10% (v/v) DMSO (Sigma, USA) supplemented Orchid293 CD production medium.

Viability and density of the cultures were measured via Novocyte 3000 flow cytometer (Agilent, U.S.A.). From the culture, 500ul of cells were sampled and 1ul of Propidium Iodide (0.025mg/ml). (Thermo Scientific, U.S.A) was added.

Cells were grown at 36.5°C, 8% CO_2 with reciprocal shaking at 130rpm in shake flasks (SPL Life Sciences, Korea). Culture volume was never more than $1/5^{th}$ of the flask volume. Cells were grown in polycarbonate flaks with filtered caps. Glass flasks with solid caps were found to be not appropriate for growth. For 1L and 5L cultures, cells were also grown in BioStat B Bioreactor (Sartorius, Germany) Cells were reciprocatively shaken at 140 rpms. pH was set to 7.15 with acceptable range at 6.75 to 7.35. Glucose was maintained at 2.5 to 3 mg/L. Cell culture for producing GMP grade VLPs were maintained in GMP facility of Nobel Pharmaceuticals in Istanbul.

Transfection was done at $1.5x10^6$ cells/ml cell density. Plasmids were transfected at equimolar ratio and total DNA amount was adjusted to 1ug (0.45ug pVitro1 and 0.54ug pVitro2) of plasmid per 1 million of cells. Transfection was performed using the PEIpro (Polyplus, France) reagent. Transfection mix was always 10% of original culture volume. Volumetrically, exactly half of the mix were plasmids diluted in transfection medium and other half was 1:2(w/w, DNA to PEI) PEI diluted in transfection media. Both PEI and DNA solutions were sterile filtered with 0.22um microfilter. (Sartorious, Germany) PEI solution was added to the DNA solution all at once. Solution was vortexed immediately and was incubated at room temperature for 15 minutes exactly. After the incubation, transfection mix was added to the suspension culture.

VLP producing cells were cultured in shake flasks or in a Bioreactor for 5 days. Depending on the batch, medium was replenished with either transfection medium or 1:1 mixture of transfection medium and production medium 48 hours after transfection.

2.2.4 Denarase Treatment and Supernatant Clarification

Cell supernatant was harvested by centrifugation at 1000g for 20 minutes. Supernatant was then filtered through a 0.22um capsule filter (Sartopore, Sartorious, Germany). Depending on the Denarase (c-LEcta, Germany) scheme used, Denarase was either added to cell culture 12-16 hours before harvest at 400U/ml concentration and at 50U/ml concentration after harvesting and incubated for 2 hours at room temperature. Alternatively, 200U/ml or 400U/ml Denarase treatment was conducted for 2 or 4 hours at room temperature, respectively. All Denarase treatments were performed with constant shaking. After treatment, supernatant was filtered again through a 0.22um microfilter. At this point, clarified and Denarase treated supernatant was considered ready for chromatography.

2.2.5 Chromatography

All chromatography experiments were run on ÄKTA Avant fast protein liquid chromatography system (Cytiva, U.S.A.). Capto Core 400 (Cytiva, U.S.A.) resin was packed into HiScale 26/20 (Cytiva, USA), XK50 (Cytiva, USA) and AxiChrome 70/300 columns according to the manufacturer's instructions. Capto Core 400 medium has a compression factor of ~1.1. Slurry was washed with %20 EtOH 0.4M NaCl (Packing Buffer) for 5 times and used at a 50% concentration in said buffer. Required slurry amount was calculated considering the bed height, cross section of the column and the compression factor. Bed supports of the column and the tubing was primed to avoid introducing air bubbles. Slurry was poured into the column and the packing tube. Packing buffer was passed from the column at a velocity of 300cm/h. After media was consolidated under buffer flow, if the bed height was still higher than what was calculated via compression factor, axial compression was used to get to the desired bed height.

Packing quality was checked with a column performance test. This is discussed further in the results section. During upscaling residence time of 6 minutes was kept constant. For purification, Denarase treated clarified cell supernatant was loaded onto the column previously equilibrated with 5 column volumes (CV) of DPBS (Biological Industries, U.S.A.). After sample application, column was washed with 5 CV of DPBS and later, 5 CV of 50 mM HEPES buffer supplemented with 2M NaCl. VLP containing flowthrough fractions were pooled for diafiltration and concentration. All chromatographic experiments for purifying GMP grade VLPs were performed in GMP facility of Nobel Pharmaceuticals in Istanbul.

After each chromatography run, columns were cleaned according to the advised cleaning in place (CIP) method the manufacturer suggests. 2 CV of 1M NaOH in 30% isopropanol (IPA) was applied to the column. NaOH in IPA solution was incubated on the column further for 30 minutes. Following this,

column was washed from NaOH in IPA with 5 CV of water for injection (WFI). Columns were stored, together with the ÄKTA Avant system, in 20% ethanol.

2.2.6 Tangential Flow Filtration (TFF)

SARTOFLOW Smart (Sartorious, Germany) device was used in all TFF runs. Sartocon Slice 200 Holder (Sartorious, Germany) was used with Sartocon Slice 200 Hydrosart 100kDA (Sartorius, Germany) cassette. One cassette was used for 1L batches and two cassettes were used in parallel for 5L batches. Cassettes and the tubings were washed with 2Ls of WFI before each run and permeate line was checked for pH and conductivity against WFI. When device was equilibrated, sample was loaded and concentrated 5 times the initial starting culture volume, regardless of the flowthrough volume. Concentrated supernatant was then diafiltrated against DPBS with 10 times the volume of concentrated supernatant. Diafiltration was only stopped when A205 reading of permeate was same as the DPBS. In all filtration steps, sample was circulated such that inlet pressure was 1bar, with no pressure applied to retentate and permeate lines.

2.2.7 SDS-PAGE and Western Blot

For SDS-PAGE, samples were mixed with 4X Laemmli Buffer and boiled at 95C for 5 minutes. In all experiments 4–20% Mini-PROTEAN TGX Stain-Free Protein Gels (Bio-Rad,USA) were used. PageRuler Plus Prestained 10 to 250 kDa or 10 to 180kDa Protein Ladder (Thermo Scientific, USA), was used as the ladder. Gels were run at 100Vs for an hour and a half in 1X Running Buffer using Mini-PROTEAN® Tetra cell system (Bio-Rad,USA).

SDS-PAGE separated proteins were transferred to PVDF 0.2 µm Transfer Membrane (Thermo Scientific, USA) using Mini Trans-Blot® Cell System (Bio-Rad,USA). Wet-transfer was done at 100Vs for an hour. PVDF membrane was blocked in either %5 non-fat dried milk (Bio-Rad, U.S.A) or %5 bovine serum albumin (BSA) (Capricorn, U.S.A.) in PBST for 2 hours at room temperature. Membrane was washed in PBST three times for 5 minutes. HRP-conjugated 6xHis, His-Tag antibody (Proteintech, USA), Spike-S1 and Nucleocapsid antibody (ProSci, USA) were used as primary antibodies at a dilution of 1:10000, 1:1000 and 1:1000 respectively and incubated at room temperature for 1 hour. Membrane was washed after primary and secondary antibody incubation as before. Anti-rabbit and anti-mouse secondary antibodies were used for anti-spike S1 and anti-N immunoblots at dilution of 1:10000 respectively. Horseradish Peroxidase (HRP) signal was detected with ECL™ Prime HRP Reagent (Cytiva, U.S.A.) and blot was imaged by Amersham Imager 600 (Cytiva, U.S.A.) or ChemiDoc MP (Bio-Rad, U.S.A). Densitometric analysis was done using Image Lab Software (Bio-Rad, U.S.A).

2.2.8 Dot Blot

5 µl dots were placed on 0.45um nitrocellulose membrane (Thermo Scientific, USA) with a micropipette. Back paper cover of the membrane was not taken out during this procedure and acted as an absorbent. After dots were thoroughly dried, blocking, antibody incubations and imaging was done by the same method as western blot methodology.

2.2.9 Silver Staining

SDS-PAGE separated proteins were detected with silver stain by using Pierce™ Silver Stain for Mass Spectrometry (Thermo Scientific, USA). Kit was used according to the manufacturer's instructions. During development, time course photos were taken.

2.2.10 Total Protein Measurement of VLPs

Total protein was measured with Pierce Micro BCA protein assay kit (Thermo Fisher Scientific, USA) according to manufacturer's instructions.

2.2.11 Bead Based Binding Assay

50µl of carboxyl modified latex beads (4% (w/v), Thermo Fisher Scientific, USA) were washed with 1ml PBS. To the washed pellet, 5µg of recombinant hACE2 (ProSci, USA) was added and mixture was adjusted to 150µl with PBS. Beads were incubated for 30 minutes at room temperature and then adjusted further to 500µl with PBS. Beads were incubated on a rotator overnight at room temperature. Beads were washed once and blocked with 5% BSA in PBS for 4 hours on a rotator. Beads were washed once again and finally resuspended in 500µl FACS Buffer (1% BSA, 0.1% Na-Azide in PBS). As negative control bead, IL1B antibody was also coated following the same protocol.

VLPs were stained with 75 µM 5-(and-6)-Carboxyfluorescein diacetate, succinimidyl ester (CFDA-SE) or Cell Tracer Violet for 30 mins at 37°C and free dye was removed using HiTrap Sephadex G-25 desalting column (Cytiva, U.S.A.).

1µl of hACE2 and IL1B coated beads were resuspended in 50µl FACS Buffer per test. Serially diluted CFSE-loaded VLPs and recombinant S1 (Prosci, USA) conjugated to PE/Cy7 were prepared according to the experiment detailed in Results Section 3.3.4. 50µl bead and 50µl VLP-CFSE and/or S1 was mixed for all dilutions prepared. Mixture was incubated overnight at 4C with shaking. Beads were washed 3 times with FACS Buffer and analyzed via Novocyte 3000 flow cytometer. FITC channel was used for CFSE detection. Pacific Blue channel was used for Cell Tracer Violet detection.

2.2.12 Determination of Host Cell DNA Amount and Size

dsDNA content was measured by Quant-iT PicoGreen dsDNA Assay Kit (Thermo Fisher Scientific, USA) according to the manufacturer's instructions. Size of contaminating dsDNA was determined by agarose gel electrophoresis. SYBER-Safe dye was used at a dilution of 1:30000, meaning for a 150ml %2 agarose gel, 5ul 10000X stock dye solution was used. To avoid shadowing, a colorless 10X loading dye was prepared by mixing 3.9ml Glycerol, 500ul 10% SDS and 200ul 0.5M EDTA and bringing the volume to 10ml. 100bp ladder (New England Biolabs, USA) was used in these experiments. Gel was run at 100V and imaged via Amersham Imager 600 (Cytiva, U.S.A.).

2.2.13 Host-cell Protein Determination

Host cell protein content was determined via HEK293T host cell protein ELISA kit (ENZO Life Sciences, USA) according to the manufacturer's instructions.

2.2.14 Desorption

Antigen content of the final product was desorbed from Alhydrogel adjuvant via treatment with desorption buffer (SCP) for 2.5 hours at 60ºC. Desorption buffer contains 0.60 M sodium citrate dihydrate, 0.55 M sodium phosphate dibasic and %0.8 SDS dissolved in ultrapure water. [116] Buffer was stirred at 40ºC until it was clear and filtered through a 0.45um filter. If any precipitation were to be observed during storage at room temperature, buffer was heated to 40ºC and mixed thoroughly before use. For analysis, 1mL vaccine was centrifuged at 5000g for 10 minutes. 933ul supernatant was removed from the tube without disturbing the pellet and stored as vaccine supernatant for later analysis. Alhydrogel pellet was resuspended in the remaining volume. To this, 133uls of desorption buffer was added. Final volume of this mix was approximately 200uls, representing 5 times concentration of the antigenic content. During incubation, tube was mixed gently every 20-30 minutes. After the incubation period was over, samples were centrifuged at 3000g for 10 minutes. Supernatant was taken to a new tube and stored as desorbed vaccine.

2.2.15 Nanoparticle Tracking Analysis

VLPs were analyzed with qNano Gold (IZON S/N 601A) and accompanied IZON Control Suite 3.4.2.48 software. NP150 pore was coated and CPC100 calibration particles (1:1000 diluted) were used to calibrate the run before VLP samples. 35uls of sample is loaded to the upper fluid cell and measured. Following the manufacturer's recommendations, all reading were gathered from >500 events with a rate higher than 100/min. All materials from Izon Science LTD, New Zealand.

2.2.16 Animal Housing and Maintenance

BALB/c and C57BL/6 mice were housed in the Bilkent University Animal Facility. Mice were exposed to 12-hour light/dark cycles at 22°C and were provided with food and water ad libitum All experimental procedures were approved by the Bilkent University Animal Ethics Committee.

2.2.17 Fill and Finish of VLP Vaccine

GMP-grade Alum from Croda Health Care, Denmark and GMP-grade K3 CpG ODN from Hanugen, India was used to adjuvant VLP vaccine. Bulk VLP antigen was mixed with 600 μg/dose of Alum (10 mg/mL) and 300 μg/dose of K3 CpG ODN (2.5 mg/mL). This mixture was then topped to 1 mL with DPBS. Vials were filled with 1.2 mL of finished vaccine to account for dead volume.

2.2.18 Immunization for 90 Day Stability

6-10 weeks old BALB/c mice (12mice) were vaccinated with fill and finished GMP grade vials prepared for Phase 1 clinical trials. Vials were injected as 1 vial per 5 mice, which corresponds to 8 ug GMP3 VLP + 60ug K3-CpG ODN + 120ug Alum per mice. Mice were vaccinated twice (on Day 0 and Day 14) subcutaneously with two weeks between injections. On Day 28, blood samples were collected from tail veins of the animals. Blood was centrifuged at 2500g for 10 minutes in BD Microtainer (BD Biosciences, U.S.A.) and serum layer was collected and stored at -20ºC. One group of mice were

vaccinated with freshly formulated vaccine and another group was vaccinated 3 months later with now 3-month-old vials.

2.2.19 Immunization for Potency and Variant RBD Study

6-10 weeks old C55BL/6 mice (10mice) were vaccinated with 7.5ug GMP3 (Wuhan) or Exp18 (Alpha) VLP + 60ug K3-CpG ODN + 30ug Alum formulation. Mice were vaccinated twice (on Day 0 and Day 14) subcutaneously with two weeks between injections. On Day 28, blood samples were collected from tail veins of the animals. Blood was centrifuged at 2500g for 10 minutes in BD Microtainer (BD Biosciences, U.S.A.) and serum layer was collected and stored at -20ºC.

2.2.20 Determination of vaccine specific IgG Titers with Enzyme Linked Immunosorbent Assay (ELISA)

50ul/well of recombinant Spike (1ug/ml), recombinant S1 (2ug/ml), recombinant Nucleocapsid (20ug/ml), recombinant RBD (3ug/ml) or β-propiolactone inactivated whole SARS-CoV-2 (10ug/ml) were used to coat 2HB ELISA plates (SPL Life Sciences, Korea) overnight at 4°C. Coating concentrations for variant RBDs are shown in Table 2.3. Plates were then blocked with 200ul/well blocking buffer at room temperature for 4 hours. Plates were washed 3 times with wash buffer, then 2 times with dH_2O and then excess liquid was rinsed. Serum from each animal was diluted first 1/50 and then 5-fold serially diluted. 50ul of diluted sera was transferred to ELISA plate and incubated overnight at 4°C. Plates were washed again and this time 50ul/well of 1/1000 diluted ALP conjugated anti-mouse IgG, anti-mouse IgG1, or anti-mouse IgG2a (all Southern Biotech, U.S.A.) antibodies were added and plates were incubated at room temperature for 2 hours. Plates were washed and rinsed. 50ul/well of PNPP substrate solution (Thermo Scientific, U.S.A.) was added and optical density at 405nm was measured using a microwell plate reader (Molecular Devices, U.S.A.) Final log10 titers were calculated in Graph Pad 9 software.

3. Results

Processes related to VLP manufacturing, quality testing and immunogenicity determinations are summarized in the flowchart below (Figure 3.1.), together with the corresponding Results Section numbers.

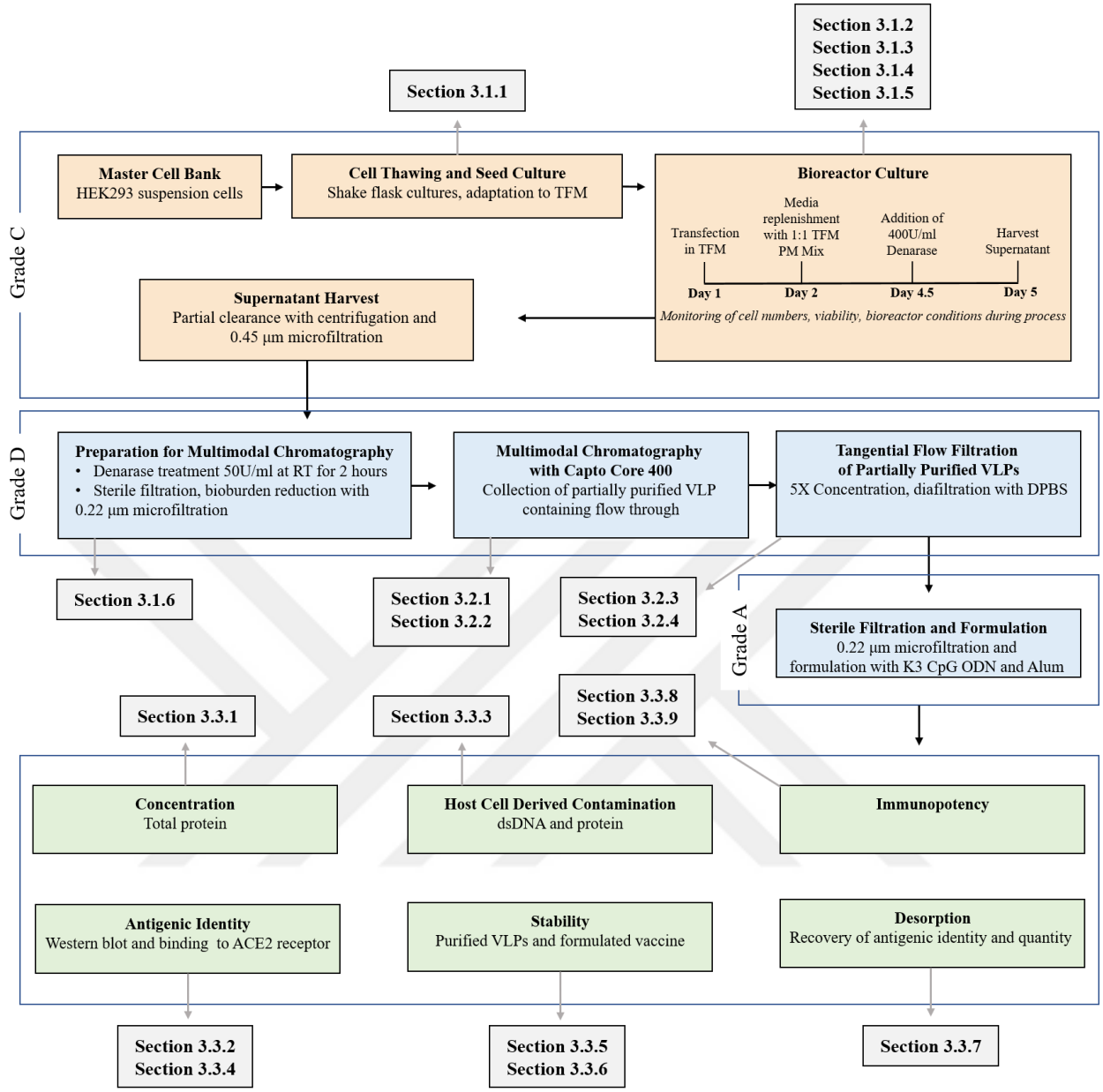

Figure 3.1. ***Flowchart for u*pstream and downstream processing, formulation, analytical testing and immunopotency**. Topics discussed in this thesis are shown in color coded boxes. Orange, blue and green boxes encompass upstream processing, downstream processing and bio-analytics, respectively. Each respective chapter is indicated by gray arrowheads and boxes. Grade D, C and A correspond to GMP areas explained in Section 1.5.

3.1 Upstream Processing

3.1.1 Suspension Adapted HEK 293 Cell Growth in Different Commercial Media

The HEK293 cell line has been preferentially utilized in biotechnological processes due to its straightforward culture conditions and high yield in protein production. HEK293 cells adapted for suspension growth were used throughout this study for VLP production. For growth and transfection of HEK293 cells, two commercial media were used. Cells and media were produced by a Turkish biotechnology company, Florabio, located in İzmir. These media — Orchid293 CD growth media (PM hereafter) and Orchid293 CD transfection media (TFM hereafter) were advertised to be suitable for growth and transfection of these cells, respectively. Growth dynamics of HEK293 suspension cultures in shake flask format was explored and reported in Figure 3.1.

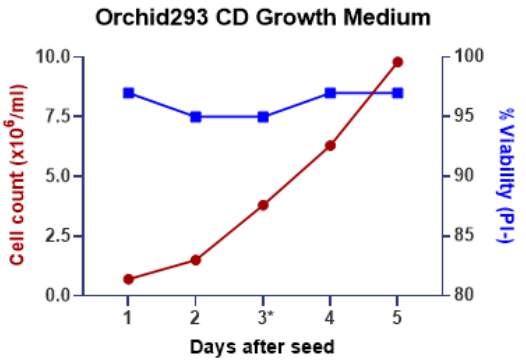

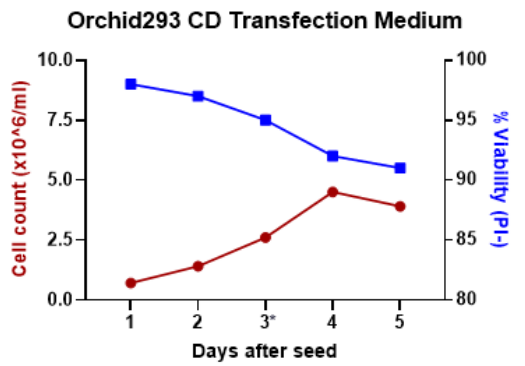

Days after seed	1	2	3*	4	5
Cell count (x10^6/ml)	0.7	1.5	3.8	6.3	9.8
% Viability	97	95	95	97	97

Days after seed	1	2	3*	4	5
Cell count (x10^6/ml)	0.7	1.4	2.6	4.5	3.9
% Viability	98	97	95	92	91

Figure 3.2 Growth curve and viability of HEK 293 suspension adapted cells. Cells were cultured in PM and TFM over the course of 5 days. 50ml cultures were grown in 250ml polycarbonate shake flasks. On day 3, cell media was replenished for both flasks.

After two passages for recovery from thawing, cells were seeded to fresh PM or TFM at $7.5x10^5$/ml density in separate flasks to record growth and viability dynamics. PM sustains cell densities upwards of 10^7/ml with no observed significant reduction in viability (Figure 3.1). TFM is not suitable for long term culturing as even though near 7-fold increase in cell density was achieved, percent viability decreased continuously following initiation of the culture.

Shown in Figure 3.2, gross appearance of cells grown in TFM showed increased aggregates sticking to the flask wall and smaller aggregates in the culture itself. It is apparent that although PM supported cell growth at densities around 10^7 cells/ml, TFM wasn't suitable for growth above densities $5x10^6$/ml without extended adaptation.

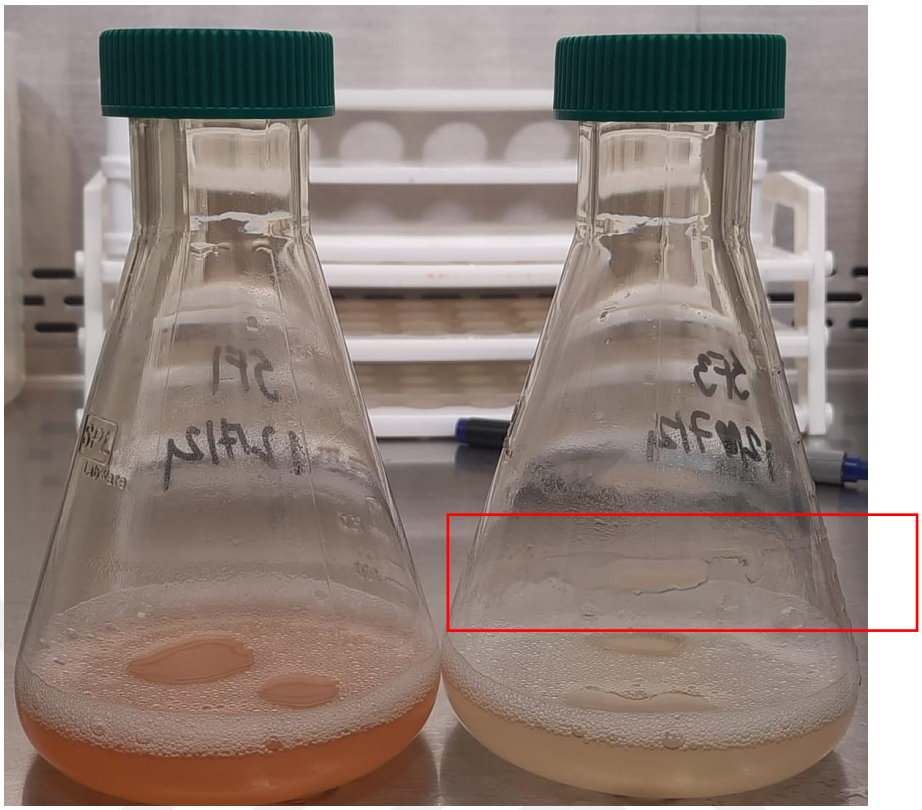

Figure 3.3 Gross appearance of shake flasks upon extending culturing. Drop in cell count of flasks cultured in TFM (flask shown on the right) was marked by aggregation and adherence to the flask edges. (Red rectangle). CD media supported cell growth at much higher confluency without showing any aggregation (flask shown on the left).

These results suggest that the PM was optimal for routine maintenance of HEK 293 cells, while TFM was only to be used for transfection experiments. Of note, the cells were passaged at least once in TFM prior to transfection in order to prevent decrease in cell count and viability, possibly due to the additive stress induced by the change in media type and exposure to the transfection reagent PEI.

3.1.2 Optimization of PEIpro/DNA Ratio

Optimization of the PEI/DNA ratio is particularly important for transient transfection of cells because inadequate complexation results in lower transfection efficiency, while high PEI concentrations cause toxicity to cells impacting overall culture viability.

In order to determine the most favorable PEI/DNA ratio for efficient complexation and low toxicity, cells were transfected according to the protocol outlined in Methods Section 2.2.3. In these experiments, cells were transfected in 6-well plates. Firstly, in the context of transfection, orbital shaking at 140rpm was explored. Orbital shaking resulted in decreased cell growth 48 hours after transfection and therefore was abandoned in favor of reciprocal shaking in subsequent experiments. (Figure 3.3A)

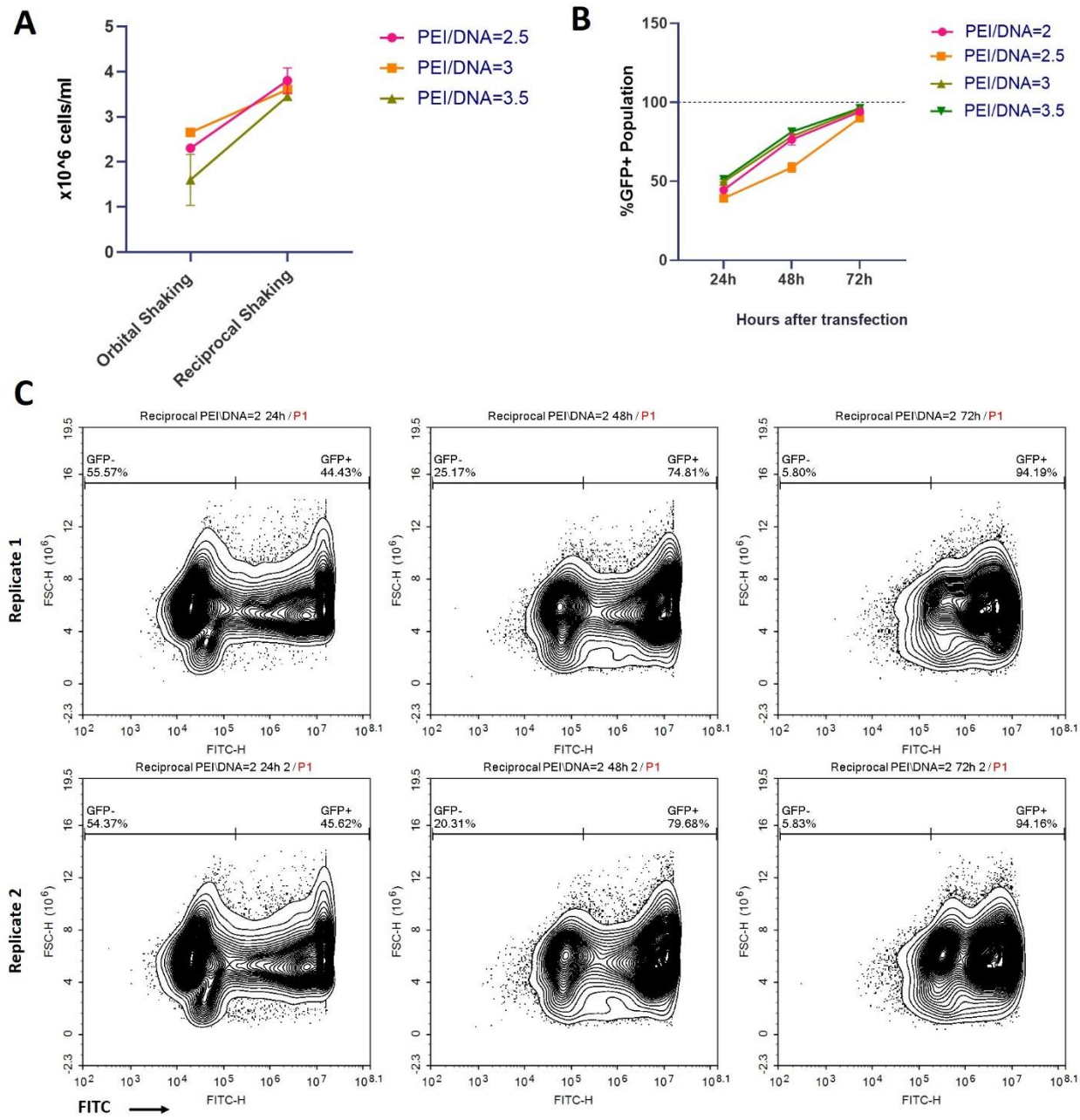

Figure 3.4 Optimization of PEI/DNA ratio for transient transfection of cells growing in GMP-grade Transfection Media. A. Cell densities of transfected 6-well plates using several PEI/DNA ratios after 48 hours. Additionally, cells were grown in reciprocal shaking or orbital shaking**. B.** Transfection efficiency of 6-well plates transfected with PEI/DNA ratios ranging from 2 to 3.5 with an eGFP encoding plasmid. **C.** Daily flow cytometric analysis of PEI/DNA = 2 group from panel B. x: FITC-H y: FSC-H (Daily flow cytometric readings available in Appendix Figure 5.1)

Increasing PEI/DNA ratios from 2 to 3.5 were explored using a GFP encoding plasmid. (pcDNA3.1(+)_eGFP) Flow cytometry analysis revealed that even at PEI/DNA=2, by the next day, three fourths of all cells were GFP positive and by 72 hours, nearly all cells (>94%) were GFP positive. (Figure 3.3B and C) These results indicate that transfection of TFM adapted HEK293 suspension cells is optimal at a ratio of 2 µg of PEI per 1 µg of plasmid DNA.

3.1.3 Production of VLP Plasmids

As detailed in Methods Section 2.2.2, two plasmids were used for transient transfection of suspension HEK 293 cells to produce the virus like particle antigen. Plasmids pVitro2-S/E and pVitro1-M/N were stored as glycerol stocks of *E. coli* NEB Stable cells. As described previously [112], two plasmids encode 4 structural proteins of SARS-CoV-2 under constitutive promoters. Spike protein encoded is a thermostable prefusion stabilized mutant called HexaPro [115]. As a Type I fusogen, Spike can undergo spontaneous conformational change to its post-fusion form, without any interaction with its receptor. This tendency results in lower yields and also thermosensitivity for recombinant proteins. Notably, prefusion structure is desirable for vaccines to induce optimum levels of neutralizing antibodies. Proline mutations coded by HexaPro stabilizes the Spike protein into its prefusion confirmation and confer increased immunogenicity [112]. These plasmids were analyzed for their integrity and validated for their identity (Fig3.4A). Moreover, the plasmid production yields were determined from a liter of *E. coli* culture grown overnight (Fig 3.4B).

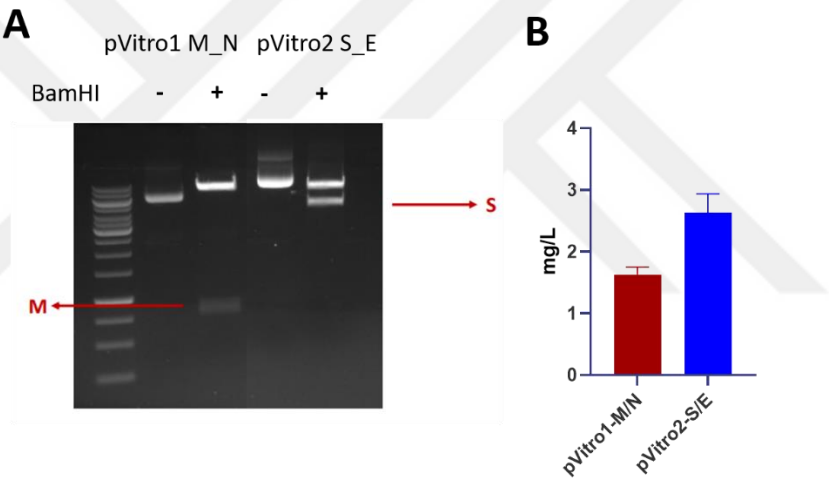

Figure 3.5 BamHI diagnostic digest of VLP encoding plasmids and average production yields. A. Plasmids pVitro1 M/N and pVitro2 S/E were cut with BamHI for each isolate to ensure correct band patterning. BamHI digestion of pVitro2 S/E results in a Spike fragment of size 4kb and E+Backbone fragment of 6kb. BamHI digestion of pVitro1 M/N results in a Membrane fragment of 770bp and N+Backbone fragment of 7.8 kb. **B.** Average yield per liter of E. coli culture grown overnight in low-salt LB media supplemented with 100 µg/ml Hygromycin. Results are represented as mean ± SD.

3.1.4 Batch Master Table

Multiple batches of VLP production were carried out under GMP settings for method optimization and the eventual use of VLPs in clinical trials. Table 3.1. summarizes "Batch" specific features for each GMP lot.

Table 3.1 Batch Master Table. Cell cultures for these batches were grown and VLPs were isolated under GMP conditions. GMP3 antigen was used in Phase 1 Clinical Trial (NCT04818281) which explored dose escalation, safety and immunogenicity. Exp19 and Exp20 were used in Phase 2 Clinical Trial (NCT04962893). The primary end-point was to determine humoral and cellular responses elicited by Wuhan and Alpha (British) variant VLP vaccines as well as safety and efficacy.

Batch Name	Volume	Cell Culture Type	Denarase Scheme	Chromatography	TFF	Purpose	dsDNA Content (ng/ml)	BCA Conc. (µg/ml)
GMP1 (Wuhan)	1 L	Shake flask	200 U/mL, RT, 2 hours	CaptoCore 400 (HiScale 26/20)	100kD, Hydrosart (0.02 m^2)	R&D	NA	NA
GMP2 (Wuhan)	1 L	Shake flask	400 U/mL, RT, 4 hours	CaptoCore 400 (HiScale 26/20)	100kD, Hydrosart (0.02 m^2)	R&D	244	41.89
GMP3 (Wuhan)	1 L	Shake flask	400 U/mL, 37 °C, o/n + 50 U/ml, RT, 2 hours	CaptoCore 400 (XK50/30)	100kD, Hydrosart (0.02 m^2)	**Phase I**	6	39.75
GMP4 (Wuhan)	1 L	Shake flask	Same as GMP3	CaptoCore 400 (HiScale 26/20)	100kD, Hydrosart (0.02 m^2)	R&D	6	36.1
Exp15 (Wuhan)	1 L	Bioreactor	Same as GMP3	CaptoCore 400 (XK50/30)	100kD, Hydrosart (0.02 m^2)	R&D	10	54.2
Exp18 (Alpha)	5 L	Bioreactor	Same as GMP3	CaptoCore 400 (AxiChrom 70/300)	100kD, Hydrosart (0.04 m^2)	R&D	14	132.1
Exp19 (Alpha)	5 L	Bioreactor	Same as GMP3	CaptoCore 400 (AxiChrom 70/300)	100kD, Hydrosart (0.04 m^2)	**Phase II**	16	133.8
Exp20 (Wuhan)	5 L	Bioreactor	Same as GMP3	CaptoCore 400 (AxiChrom 70/300)	100kD, Hydrosart (0.04 m^2)	**Phase II**	53.4	201.4

Shortly, GMP1, GMP2, GMP3 and GMP4 were grown with five 200 mL shake flasks, adding up to 1 L of culture volume for each lot. This period was used to optimize process development. From Exp15 onwards cells were grown in 1 L or 5 L bioreactors. Downstream processing was upscaled accordingly with increasing cell culture volume. R&D batches were used for developing analytical methods to analyze bulk antigen and finished product.

3.1.5 Cell Culture of Transiently Transfected HEK293 Cells

Suspension HEK293 cells were cultured as described in Methods Section 2.2.3. In all batches, cells were seeded at a density of $1.5x10^6$/ml and transfected as described in Methods Section 2.2.3. Starting from the day of transfection until the isolation, cultures were sampled daily and analyzed for cell density and viability using flow cytometry. Reduced viability and decreased cell numbers were observed in the course of cell culturing of GMP1 and GMP2. (Figure 3.5A) This was hypothesized to be caused by nutrient depletion. To solve this problem, cell media were replenished 2 days after transfection with fresh TFM for batches beginning with GMP3 up until Exp15. Later, fresh media replenishment was done with 1:1 mixture of TFM and PM for Exp18 and onwards as this was observed to enable higher cell densities and viability.

The use of the bioreactors instead of the shake flask plus CO_2 incubator setting was a necessity for optimizing the upstream processing. Shake flasks are limited in terms of their volumetric capacity because they require at least 4 times the volume of the actual culture to allow for proper oxygenation. They also require external incubators and shakers, elements that can cause additional malfunction. On the other hand, bioreactors allow live monitoring of vital culture parameters such as pH, glucose concentration and dissolved O_2. As shown in the batch master Table above (Table 3.1), onwards from Exp15, cells were grown in bioreactors. Progressive improvement in cell densities was also the result of continuous improvement in utilized cell media. The exact nature of these improvements is beyond the scope of this thesis.

Earlier work from our group indicates that Spike protein is first detected by immunoblotting at 48 hours. Furthermore, flow cytometry analysis of HEK293 cells transiently transfected with a GFP reporter indicates, amount of time necessary to have a culture with ~%100 GFP+ expression was approximately 72 hours. (Figure 3.3B) Considering these, Day 5 after transfection was determined to be ideal for harvesting the cell supernatant for VLP purification, as it would be prior to the major decline in cell viability while allowing enough time for proper protein expression and assembly of particles. Figure 3.5. summarizes findings related to cell densities, viabilities of various HEK293 cell cultures grown for a period of 5 days and daily VLP immunoblots of culture supernatants.

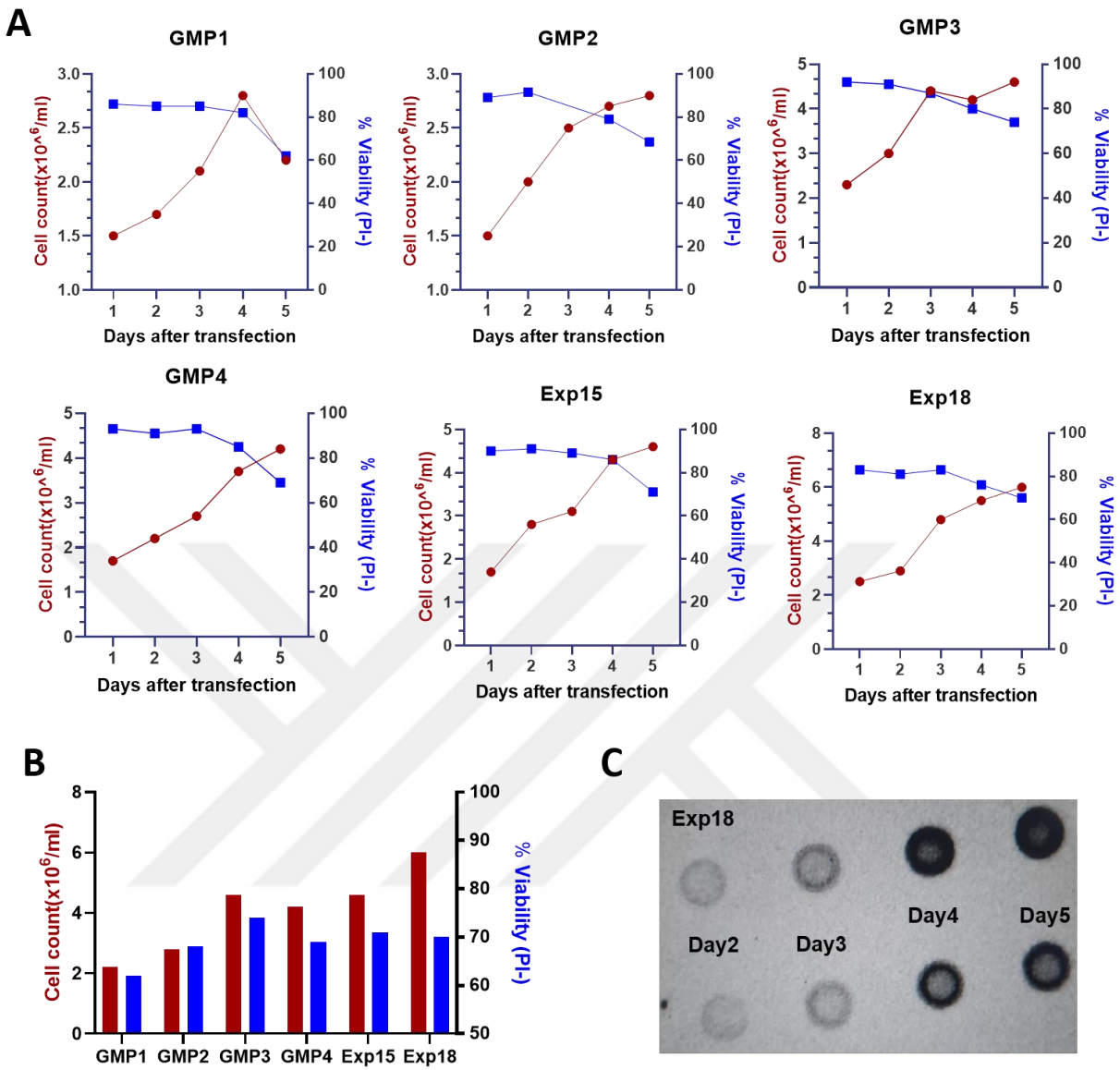

Figure 3.6 Daily cell densities, percent viability of VLP producing cells and antigenic content of the supernatant. A. Daily cell densities and viabilities were determined by flow cytometry for indicated batches. (Daily flow cytometric readings available in Appendix Figure 5.2) **B.** Comparison of culture densities and viabilities for different VLP production lots at the end of day 5 culture. **C.** Daily anti-his specific immunoblot of cell supernatant sampled from Exp18 culture. Immunoblotting was done using anti-Histag antibody and therefore, signal represents mixture of Spike, Membrane and Envelope proteins.

3.1.6 Optimization of Denarase Treatment

In bioprocessing, reducing host cell DNA contamination is a major issue. In 1997, host cell DNA was defined as a contaminant to be removed from purified biologicals by European Medicines Agency (EMEA) [117]. Although a 10ng/dose limit was determined by WHO Expert Committee on Biological Standardization (ECBS), it was noted that size and state of this host cell DNA was also of significance. Particularly, very small fragments (~100bp) are considered less dangerous than longer fragments as the

latter have more potential to harbor “potentially infectious or oncogenic sequences” [117] This limit is naturally not enforced for live vaccines.

The removal of nucleic acids from biotechnological products such as recombinant vaccines is commonly achieved via endonuclease treatment. Denarase is a trade name for *Serratia marcescens* endonuclease produced by c-LEcta, Germany. This enzyme is extremely versatile, having the ability to hydrolyze virtually all forms of DNA and RNA. The end products are generally 2-5 bases in size. We postulated that cleavage products along with Denarase itself will be removed from the purified antigen by subsequent multimodal chromatography and tangential flow filtration (TFF).

Denarase optimally functions at 37°C, between pH:8.0 and 9.0 and requires Mg^{2+} as a cofactor at a minimal 1mM concentration. 3 different application schemes were tested aiming to reduce DNA contamination in final bulk antigen.

To evaluate the Denarase schemes, highly sensitive fluorescent dsDNA staining reagent PicoGreen was used. In untreated cell supernatant, the dsDNA concentration was around 3 µg/ml and subsequent treatment reduced this to 475 ng/ml, 368 ng/ml and 3 ng/ml as seen in Figure 3.6B, C and D. respectively. Based on these results, Scheme C was opted for further purifications. Secondary treatment was retained as a safety precaution. It is also interesting to note that the “removability” of dsDNA is corelated with its decrease of signal in PicoGreen assay. Scheme C already reduces dsDNA concentration in the cell supernatant to near undetectable levels when assayed with PicoGreen Assay.

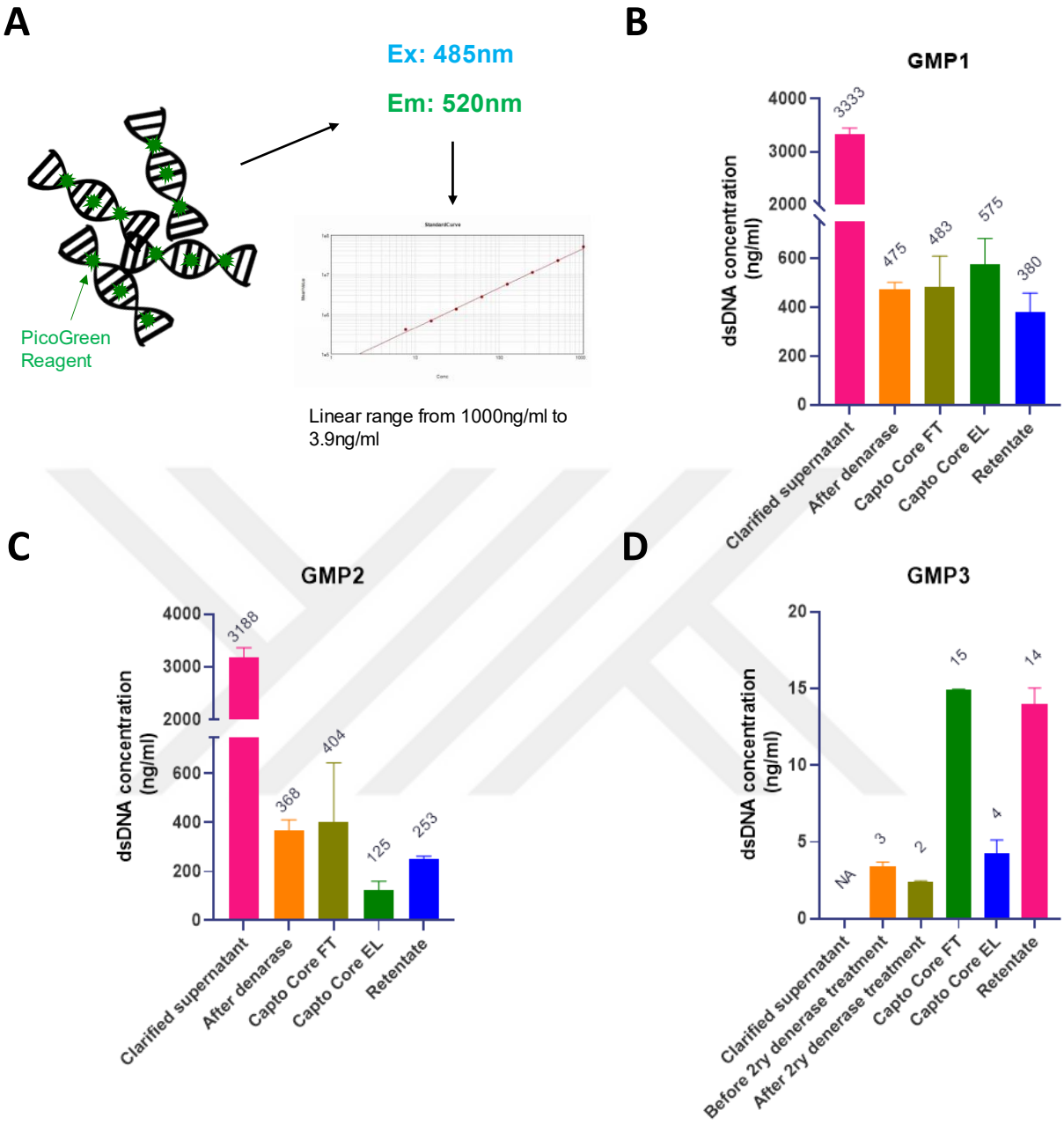

Figure 3.7 Optimization of Denarase treatment in large scale production. A. Working principle for PicoGreen assay. **B.C.D.** Optimum Denarase treatment was determined using three batches. dsDNA concentration of in process samples treated with Denarase of concentration of 200 U/ml for 2 hours at room temperature **(B.),** 400 U/ml for 4 hours at room temperature **(C.)** and 400 U/ml for 12-16 hours added directly onto cell culture prior to harvest and a secondary treatment at 50 U/ml for 2 hours at room temperature. **(D.)** Bar head represent mean and error bars represents ± SD. Capto Core FT and Capto Core EL refers to flow through and elution from Capto Core chromatography respectively. Retentate is the concentrated and diafiltrated VLPs from TFF process.

3.2 Downstream Processing

Fast protein liquid chromatography (FPLC) was done using Capto Core 400 resin. This is a multimodal system that combines properties of size exclusion and ion exchange chromatography. Beads in the media have inactive pores that allow molecules smaller than ~400kDa to interact with them. Larger molecules, like VLPs, do not interact with the column and are collected in flowthrough. The core of each bead is functionalized with an Octylamine ligand, which is hydrophobic and positively charged. Relative to VLPs, various small-sized contaminants are then captured by the ligand-activated core.

3.2.1 Performance of HiScale, XK and AxiChrom Columns Packed with Capto Core 400 Resin

The Capto Core 400 resin was packed into HiScale 26/20, XK 50/30 and AxiChrom 70. Procedure for packing these columns is explained in Methods Section 2.2.5. The performance of these columns was assessed using the so-called Pulse Test. The principle is to apply a small amount, generally $1/10^{th}$ of the column volume, of a tracer substance. Depending on the tracer used, this is then visualized by either through UV absorbance or conductivity. The flow of the tracer substance gives a quantitative measurement on how even and tight the column is packed. In Figure 3.7, terminology and parameters related to column performance are presented.

Peak broadening, representing how tight the column is packed, it is represented by reduced plate height *(h)*. It is dimensionless and corrected for both the bed height and particle diameter of the resin. [118] For porous media, so-called optimal column efficiency is achieved when $h \leq 3$. [119] This number is also dependent on test parameters and therefore the hardware capabilities of the chromatographic apparatus. A^s is the second parameter describing column packing quality and stands for asymmetry factor. It is the ratio of peak widths measured from the center at a peak height of %10 of maximum height. It is dimensionless and $A^s=1$ represent an ideal Gaussian peak with perfect symmetry while $0.8<As<1.8$ is generally acceptable. It is again important that although A^s is used for measuring peak asymmetry caused by medium irregularities, it can also be influenced by hardware irregularities. Both $h \leq 3$ and $0.8<As<1.8$ are a rule of thumb and do not represent all chromatographic systems (Fig 3.7).

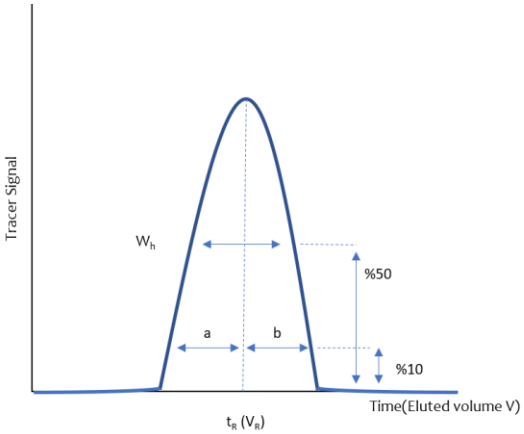

$$N = 5.54\left(\frac{V_R}{W_h}\right)^2$$

$$HETP = L/N$$

$$h = HETP/d_p$$

$$A^s = b/a$$

N	*Plate number*
V_R	*Retention Volume*
W_h	*Peak width at half peak height*
L	*Bed height*
d_p	*Particle diameter of the medium*
h	*Reduced plate height*
$HETP$	*Height equivalent of a theoretical plate*
A^s	*Asymmetry factor*

Figure 3.8 Pulse test terminology. Terms related to Pulse Test are equated in relation to an exemplary peak of a tracer substance. Adapted from Cytiva Booklet on "Column efficiency testing" [119].

For testing, columns were equilibrated with 0.4M NaCl (Buffer A). Next, %1 of total column volume was applied as tracer (0.8M NaCl) which equals to approximately 10 mL for HiScale 26/20, 45 mL for XK 50/30 and 100 mL for AxiChrom 70. The application speed of the tracer was 20cm/h as recommended by GE Healthcare for Capto medium. UNICORN software comes with a performance test method where it calculates column specific values such as retention volume, asymmetry factor, HETP and h.

Example in Figure 3.8, represents an actual scenario where A^s is similar for two columns but h differs greatly. Reduced efficiency of the column, parameterized by higher reduced plate height, causes a broader peak for the tracer substance. Interestingly, even though retention, defined as the volume of liquid that passes through the detector from the beginning to the end of the peak is nearly the same, the peak shapes are different.

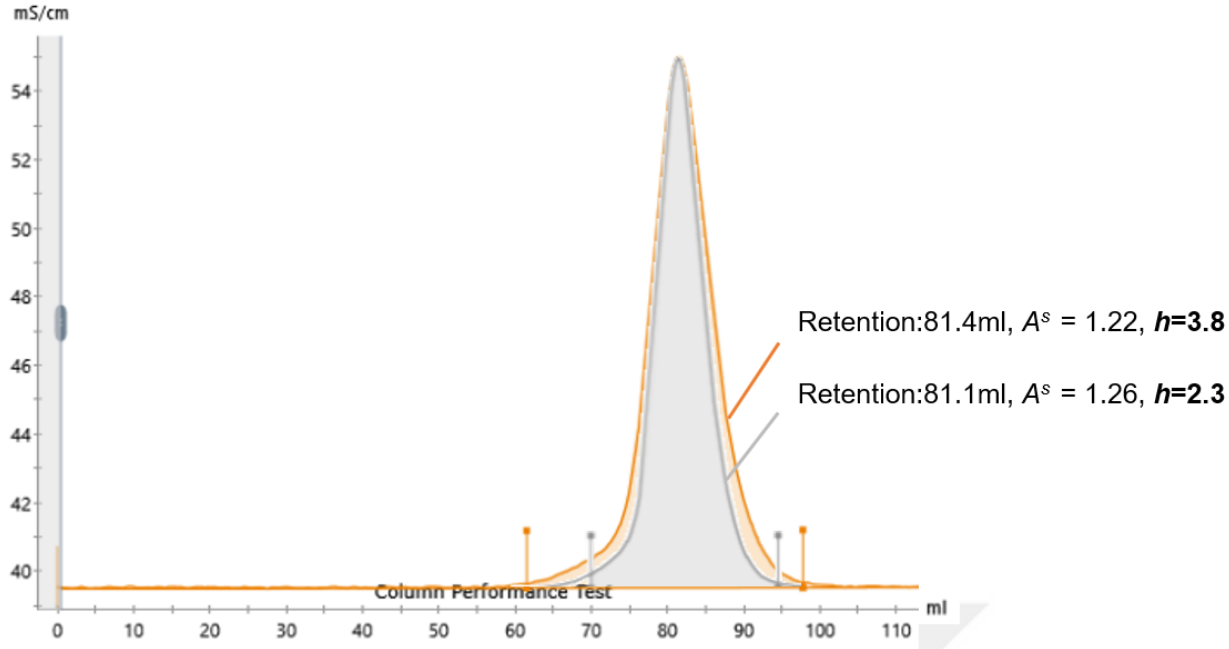

Figure 3.9 Example of reduced plate height and its relation to peak shape. HiScale 26/20 was packed with Capto Core medium twice. Pulse test of these columns reveals an example for independence of h and A^s.

Capto Core 400 packed HiScale 26/20, XK 50/30 and AxiChrom 70 columns were examined with the above explained Pulse Test. Pulse peaks and column specific values of retention, *HETP*, *h*, and asymmetry factor are shown in Figure 3.9. Both *h* and A^s were in acceptable limits, enabling the use of these columns for batch purifications. It should be noted that the *h* value of AxiChrom 70 was slightly above 3. However, this column was similar in performance to others and no problems were encountered during its operation.

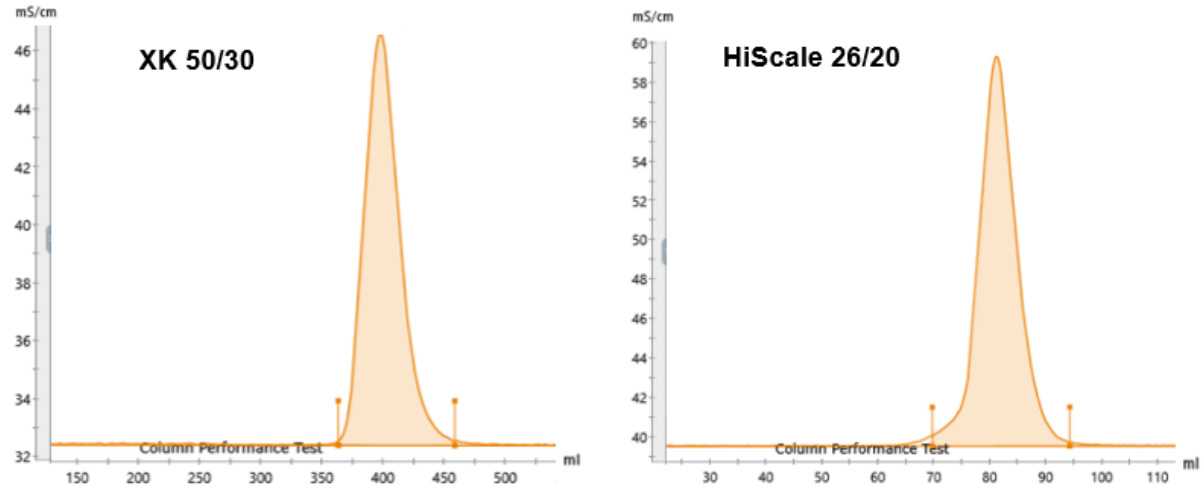

	AxiChrom 70	XK 50/30	HiScale 26/20
Retention (ml)	822	397	81
A^s	1.09	1.38	1.26
HETP (cm)	0.03	0.02	0.02
h	3.74	2.88	2.37

Figure 3.10 Performance test results of columns packed with Capto Core 400 media. Column specific values of retention, A^s, HETP and h were calculated for packed columns by using UNICORN column performance test method [119].

3.2.2 Multimodal Chromatography of Virus Like Particle Antigen

Following the production of four structural proteins and their intracellular assembly, the virus like particle antigen is secreted to extracellular space. After Denarase treatment, the culture supernatant containing the unpurified VLP antigen is clarified, through a series of centrifugation and filtration steps. The clarified supernatant is then, depending on the scale, applied to Capto Core 400 resin via different columns described previously. Basis of the Capto Core 400 method is described in Methods Section 2.2.5. Here, details regarding scale-up and corresponding chromatograms will be discussed. Figure 3.10 shows representative chromatograms from different runs on AxiChrom 70, HiScale 26/20 and XK 50/30 columns.

The Capto Core is a type of flow through chromatography. A major advantage of this type of purification is its speed. In Figure 3.10A, different stages of the purification are shown using a representative chromatogram of an AxiChrom 70 run. Stage I is equilibration with Buffer A (DPBS) followed by Stage II in which clarified supernatant is applied to the column. Note that shortly after

application, appearing peak represents the semi-purified VLP solution. The Capto Core flow through can be then collected immediately and downstream processing commences with tangential flow filtration.

At Stage III, column is washed with Buffer A followed by elution of impurities with a high salt buffer in Stage IV. As detailed in Methods Section 2.2.5, a cleaning in place method involving isopropanol (IPA) and NaOH is performed (Stage V). NaOH removes impurities that are resistant to high salt elution and held by the resin. Note that these processes are actually much longer than the time required to have the Capto Core flow through.

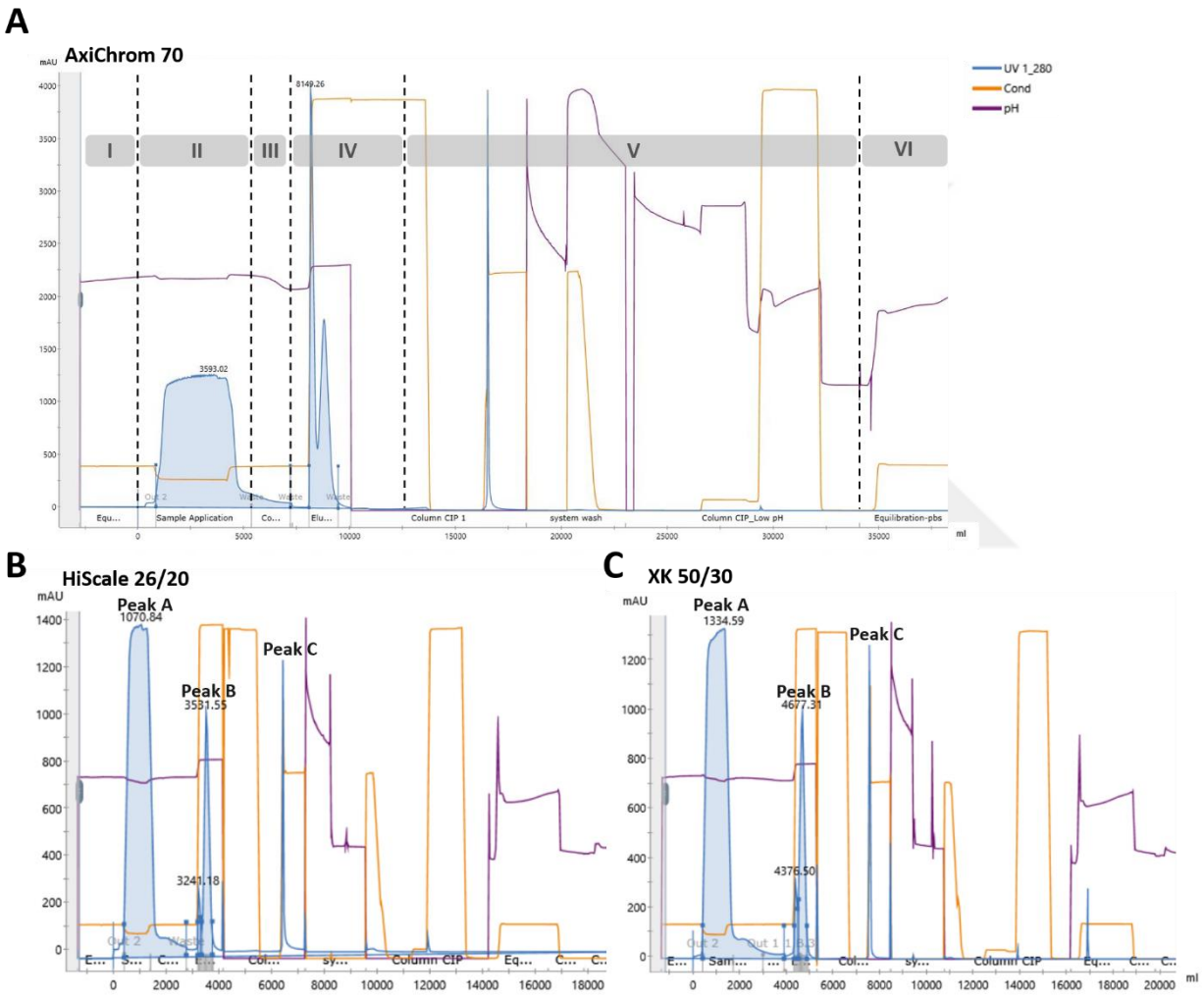

Figure 3.11 Representative chromatograms from different isolation runs on AxiChrom 70, HiScale 26/20 and XK 50/30 columns. Columns were packed with approximately 1 L, 100 mL and 450 mL of Capto Core 400 resin respectively.

As expected, different column sizes did not influence the chromatograms. Capto Core is relatively simple as the only variable in upscaling is the flow speed, which can be described in different ways. Flow rate is the amount of liquid (mL) that passes through the column per unit time (minutes). Flow velocity (cm/h) or linear flow velocity is flow rate normalized for cross section (cm^2) difference [118]. Use of flow velocity is more meaningful in cases where the bed height is the same but the column diameter

is increased during scale up. In this particular case, scale up from HiScreen to HiScale to XK and then to AxiChrom meant changes in both bed height and cross section. A second variable called residence time describes the amount of time needed for a sample with particular velocity to pass through the column. Therefore, while flow velocity is informative for technical aspect such as keeping the column pressure stable, residence time gives a better estimate for keeping the efficacy of the chromatography constant during scale up.

Initial chromatography experiments were done with lab-scale column HiScreen with 6 minutes of residence time corresponding to a flow rate of 0.75ml/min and a flow velocity of 100cm/h. The residence time was kept constant during scale up. Naturally, flow rate increased with increasing column radius and bed height. Column dimensions and upscaling calculations are presented in Figure 3.11.

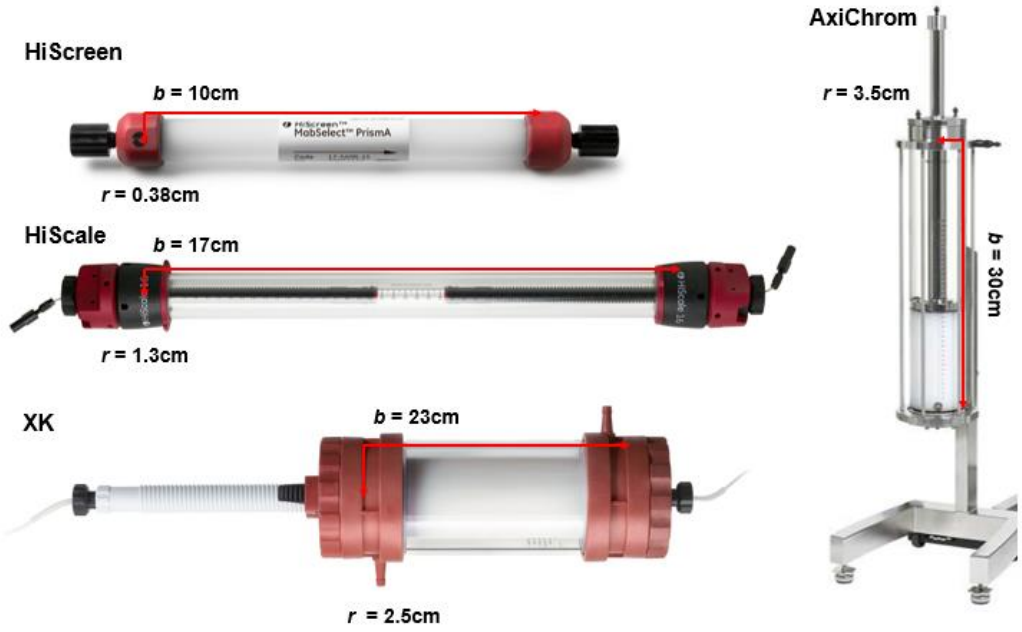

b	*Bed height*
r	*Column inner radius*
A_c	*Cross section area*
V_c	*Column volume*
R_F	*Flow rate (ml/min)*
V_F	*Flow velocity (cm/h)*
T_R	*Residence time (min)*

$V_F = A_c / R_F x\, 60$

$T_R = b / V_F$

	HiScreen	HiScale 26/17	XK 50/23	AxiChrom 70/300
R_F	0.75	15	75	190
V_F	100	170	230	300
T_R	6	6	6	6

Figure 3.12 Upscaling calculations for multimodal chromatography. Terms related to upscaling of fast protein liquid chromatography are equated [118]. Residence time of the sample was kept constant at 6 minutes and resulting flow speeds and velocities were calculated. Indicated column dimensions of pre-packed HiScreen, packed HiScale, XK and AxiChrom columns were used for calculations.

3.2.3 Tangential Flow Filtration of Capto Core Flow Through

The tangential flow filtration (TFF hereafter) is the next key step during the extraction of the bulk VLP antigen from the multimodal chromatography flow through. The details of the tangential flow filtration

process are explained in Methods Section 2.2.6. Here, rational for the chosen parameters and in process data will be discussed. After Capto Core chromatography, semi-purified flow through is filtered by TFF using a 100kDA MWCO regenerated cellulose cassette. In the case of viruses, the most common process issue with TFF is the occurrence of a concentration gradient along the cassette. This gradient can cause precipitation and irreversible decrease in filtration capacity. This phenomenon, called gel layer formation, can be prevented by increasing filtration speed as faster fluid circulation decrease the probability of material accumulation on the cassette. However, elevated filtration speed creates higher shear forces, which are detrimental to some biologics like enveloped viruses, hence to virus like particles as well.

Through a literature review, inlet pressure of 1 bar and no restriction on retentate line was found to be an ideal starting point [120]. This initial setting was found to be quite a fit as from scales of 50mls to 5Ls, it caused no problems in process development.

In Figure 3.12A, exemplary data from a TFF run (GMP3) is shown. During filtration, TMP is kept constant at 0.5 bar. Since no restriction in retentate line is applied, this equals to a constant inlet pressure of 1 bar. Permeate rate decreases logarithmically during filtration. This initial decrease is considered normal as the surface of the membrane is equilibrated. Importantly, this decrease was always reversible. Conductivity increases gradually to around 15 mS/cm which indicates buffer exchange to DPBS is taking place. Diafiltration volume was calculated to have an initial contaminant present in the starting semi-purified solution diluted 2^{10} times after diafiltration. The analysis of in-process retentate and permeate samples reveal that absorbance at 205nm steadily declines. Filtration is stopped when A@205nm of permeate is indistinguishable from DPBS, meaning that material leaving the filtration apparatus has undetectable protein levels (smaller than 3ug/ml for A@205nm method). Substantial decrease in A@205nm of permeate and very high A@205nm of semi-purified flow through likely reflects the fact that the cell media itself contains some substance(s) that interferes with this reading.

In Figure 3.12C and 3.12D, silver staining for in process retentate and permeate samples reveal that although there is some general decrease in band species (red arrows) in the retentate during filtration, protein removal does not seem to be the main outcome of TFF. This is further supported by absence of detectable levels of protein in permeate samples. Interestingly, these early permeate samples have a very high A@205nm reading, suggesting that TFF mainly removes small contaminants, such as biological small molecules, media components and others.

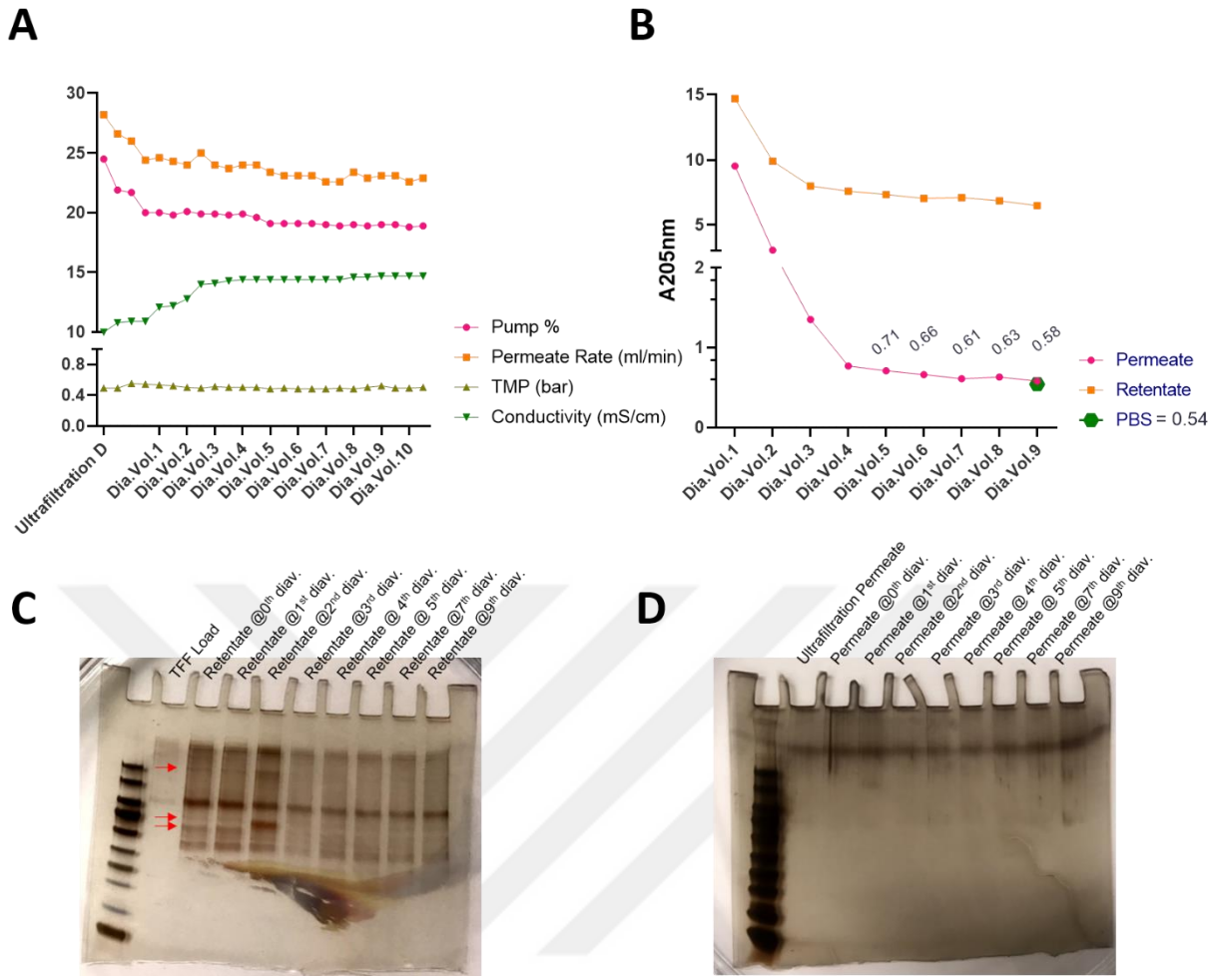

Figure 3.13 Tangential flow filtration of partially purified VLP solution. A. Pump %, which corresponds to inlet speed, permeate rate, TMP and conductivity were recorded and plotted against diafiltration volumes. **B.** Absorbance at 205nm were recorded similarly. In process samples from TFF were taken with a syringe from the liquid line while the filtration is running. Retentate **(C.)** and permeate **(D.)** samples were analyzed by Silver Staining.

3.2.4 High Pressure Liquid Chromatography – Size Exclusion Analysis of In-Process Samples

As discussed previously, evidence suggests that TFF mainly removes non-protein contaminants. The analysis of Capto Core in-process samples with immunoblotting or silver staining was found to be impractical as protein levels were too diluted for these assays. Particularly, the elution sample was not compatible because of its high salt concentration.

In order to analyze the downstream processing efficacy, analytical size exclusion high pressure liquid chromatography (HPLC-SEC) was used (Figure 3.13). HPLC was run on the Waters Arc system with Tosoh tskgel g3000swxl column. This silica-based size exclusion column is capable of separating molecules up to 500 kDa. VLPs are estimated to be larger than 1000 kDa due to their multi-protein structure, therefore lie outside of the separation range of the column. Nevertheless, this analysis still allows a broad image to be drawn. It should be kept in mind that the peak that is attributed to be VLPs

can have additional larger constituents (possibly cell derived exosomes) as this column is unable to distinguish size differences at that range.

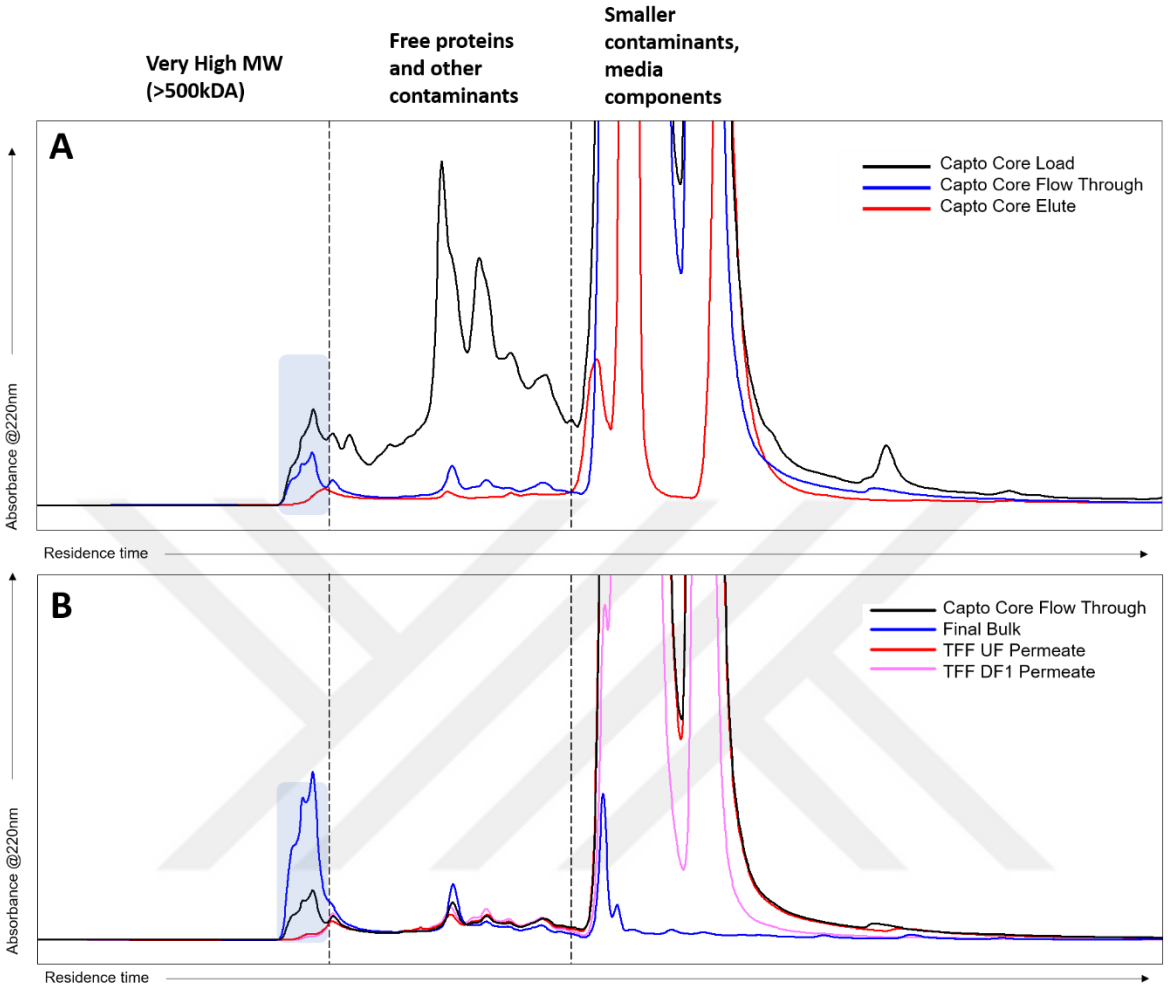

Figure 3.14 HPLC-SEC analysis of in process samples during VLP purification. Analysis of in process samples from Capto Core **(A.)** and TFF **(B.)** x-axis corresponds to residence time, y-axis corresponds to absorbance at 220nm. Blue rectangle is the peak attributed to be enriched in VLPs. (Image is kindly provided by Dr Naidu Mokala)

Figure 3.13A shows that Capto Core load (black line) can be very broadly separated via three segments using residence time (represented via dashed lines). The first high MW segment (>500 kDa) contains the VLP antigen, while the second segment designates smaller proteins that are separated by the column and a third segment with smallest of contaminants originating from the media (vitamins, pigments etc.) and other cell derived molecules.

Chromatography allows for nearly complete removal of contaminants in segment 2, while segment 3 components still remain in the flow through. Traces of segment 3 contaminants are detectable in the Capto Core elution, suggesting that partial but incomplete removal takes place. The segment 2 contaminants are almost completely separated from the solution but are undetectable in elution, indicating that they are removed from the column during CIP. Unfortunately, CIP flow through is not compatible with any employable assays due to its significant NaOH content.

The complete removal of residual segment 3 contaminants is achieved with TFF. The area of the VLP peak (blue highlight) increases as the solution is 5 times concentrated during filtration. It should be kept in mind that the A220 reading of segment 3 contaminants likely do not correspond to concentration in a regular sense as these are not actually proteins. The identification of the final product composition with mass spectrometry is planned to be performed in future experiments.

3.3 Analytical Experiments on the VLP Vaccine and Its Constituents

3.3.1 Correlation of Bulk Concentration and Cell State on Harvest Day

Determining protein concentration of the purified bulk antigen is important for being able to distinguish between batches and determining correct antigen dosage. Protein concentration of VLP preparations were determined by Micro BCA assay (Methods Section 2.2.10). Below, Figure 3.14 shows increased yield during process optimization and correlation of this increase with improvement in cell culture conditions.

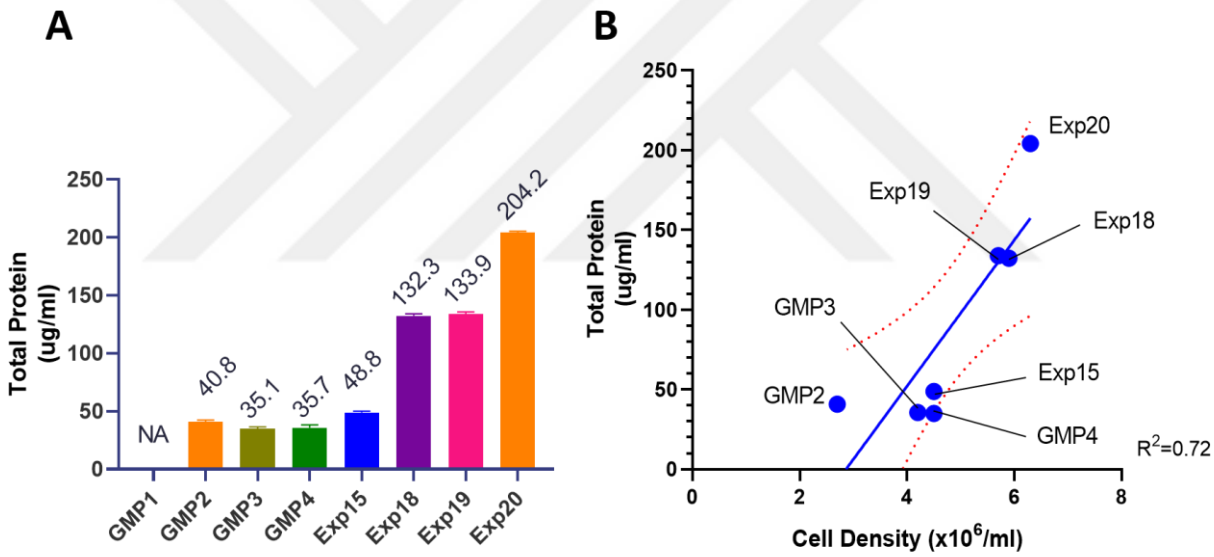

Figure 3.15 Total protein of purified VLP preparations. A. Total protein of each isolate was measured with Micro BCA and reported. **B.** Total protein and cell density on the day of harvest was plotted against each other. Linear regression was done in Graph Pad 7. Red dashed lines indicate 95 percent confidence interval of the regression.

During the process development, yield significantly increased. This was due to improvements in cell culture conditions mainly driven by introduction of media replenishment in the second day of culture. Effect of this was amplified when cells were replenished with 1:1 mixture of TFM and PM from Exp18 and onwards. Clear increase in cell density in final day of culture also effected the total protein content of purified VLP preparations. Although there is 1.5x increase (from $4x10^6$/ml to $6x10^6$/ml) in cell number from GMP3 to Exp20 batch, yield was increased ~6 fold (from 35.2 µg/ml to 204.2 µg/ml). This argues for a situation where media depletion affects cells even when it does not necessarily cause cell death.

3.3.2 Western Blot Analysis of the Bulk Antigen

While quantity of antigen was detected via total protein quantification with Micro BCA, quality of antigen was determined with immunoblotting using antibodies against Histag and Nucleocapsid. The details of the western blot procedure are explained in Methods Section 2.2.7.

Below, Figure 3.15 shows western blot images that compare several VLP batches. In Figure 3.15A, there are 3 GMP batches with similar total protein levels and western blot images showed comparable band densities of Spike, Membrane and Envelope proteins (Figure 3.15A, left panel). As clearly seen and strikingly, GMP3 has very low amounts of Nucleocapsid protein compared to GMP1 and GMP2 (Figure 3.15A right panel). Coincidently, GMP3 marked the optimization of the Denarase treatment where HCD was significantly eliminated during purification. It is tempting to speculate that since nucleocapsid is an RNA/DNA interacting protein, rich in intrinsically disordered domains, its presence in extracellular space from secretion or cell death might cause formation of nucleic acid containing phase separated droplets. These droplets are documented to be nearing ~1um in size [21] and therefore, would directly be isolated via our isolation protocol. Proper reduction in HCD by Denarase treatment might dissolve such droplets as they require nucleic acids to form. These dissolved droplets could then be removed by our downstream processing like any other protein contaminant. Decreased Nucleocapsid presence was observed for latter batches where this Denarase scheme was applied with modifications to original procedure. (Figure 3.15C)

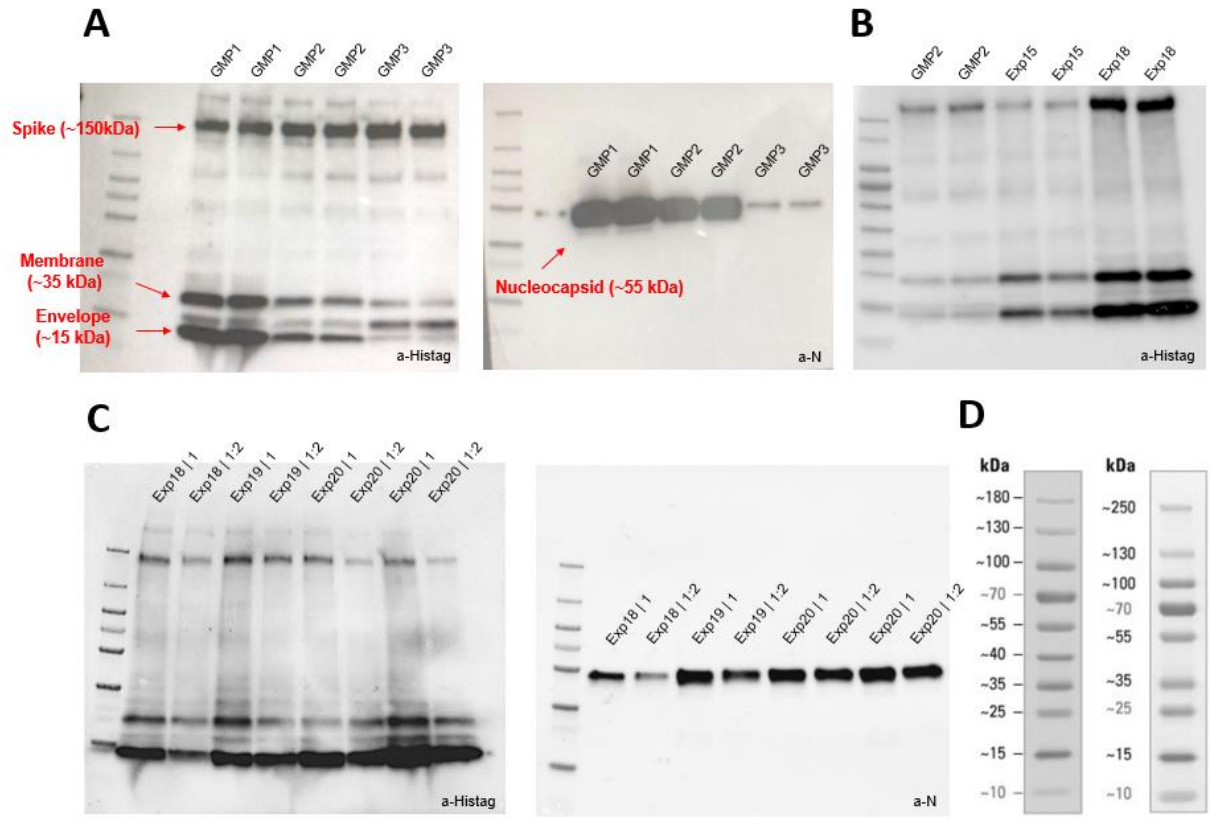

Figure 3.16 Western blot analysis of various purified bulk VLPs. **A.** Blots analyzing GMP1, GMP2 and GMP3 were probed with anti-Histag (left panel) and anti-Nucleocapsid (right panel). **B.** Blots

analyzing GMP2, Exp15 and Exp18 were probed with anti-Histag. **C.** Blots analyzing Exp18, Exp19 and Exp20 were probed with anti-Histag (left panel) and anti-Nucleocapsid (right panel). **D.** 180kDa ladder was used in blots shown in panels B. and C. while 250kDa ladder was used in panel A. Identified band identities are shown by red text and arrow head.

The immunoblot in Figure 3.15B demonstrates that the intensities of the Spike, Membrane, and Envelope proteins of Exp18 are considerably higher compared to GMP2 and Exp15, supporting the ~3fold increase in total protein concentration. Exp18 to 20 were isolated from a 5L bioreactor with the same upstream and downstream processes. Figure 3.15C shows that these preparations are again similar in band intensities and therefore should provide similar antigenicity. Difference between these batches however, were in Spike encoding gene fragment. pVitro2-S/E plasmid used in Exp18 and Exp19 encodes the Alpha variant (B.1.1.7) spike, while pVitro2-S/E plasmid used in Exp20 encodes the original Wuhan spike.

Work from our group showed that Delta and Alpha variant Spikes have enhanced decoration onto VLPs. [121] This is speculated to be occurring in a similar fashion as it occurs for the native virus, where mutations such as D614G increase stability and decoration of the protein. (Yang et al., 2021, Zhou et al., 2021)

3.3.3 Determination of Host Cell Derived Factors in Purified Bulk Antigen

As mentioned previously, Denarase optimization experiments revealed that the ideal treatment that efficiently eliminates contaminating nucleic acid excipients such as dsDNA. From the regulatory stand-point any vaccine product (excluding live attenuated vaccines) should not contain >10ng/dose host cell derived DNA in the final formulation. In our devised scheme, we've added 200 U/ml Denarase to the bioreactor and sustained the cell culture at 37°C overnight, then supernatant was harvested next day. Interestingly, even before Capto Core and TFF, dsDNA levels were undetectable. To investigate this process, culture supernatant and its Denarase treated counterpart were run on an agarose gel stained with SYBR Green I, which is a highly sensitive dsDNA specific dye (Methods Section 2.2.12). Figure 3.16A shows that after treatment, virtually all large fragments are degraded and indiscernible by agarose gel electrophoresis.

To ensure that the presence of remaining DNA elements do not create a safety concern, the Exp20 bulk antigen was run on an agarose gel stained with SYBR Safe (Figure 3.16A). The visible faint band at the bottom of the gel corresponds to a <100bp fragment, which is not associated with any possible open reading frames of which can harbor oncogenes and therefore is acceptable from the safety stand-point (Shin et al., 2007).

dsDNA contamination shows a linear relation with bulk antigen concentration. (Figure 3.16C) This suggests that either some dsDNA is carried over during purification and its initial amount is actually corelated with VLP amount and therefore the health of the cell culture; or that it is physically associated with VLPs so that increased VLP concentration is inevitably linked to more dsDNA presence.

Host cell protein was determined using HEK293T host cell protein ELISA kit (Enzo Life Sciences). Amount of host cell protein (HCP hereafter) was around ~5 ug/ml for all reported batches (Figure 3.16D) and because these batches have total protein amounts ranging from ~40ug/ml to ~200ug/ml, it is suggested that some small amounts of HCP contamination is carried away during purification and it's not correlated with total protein amount of final isolate.

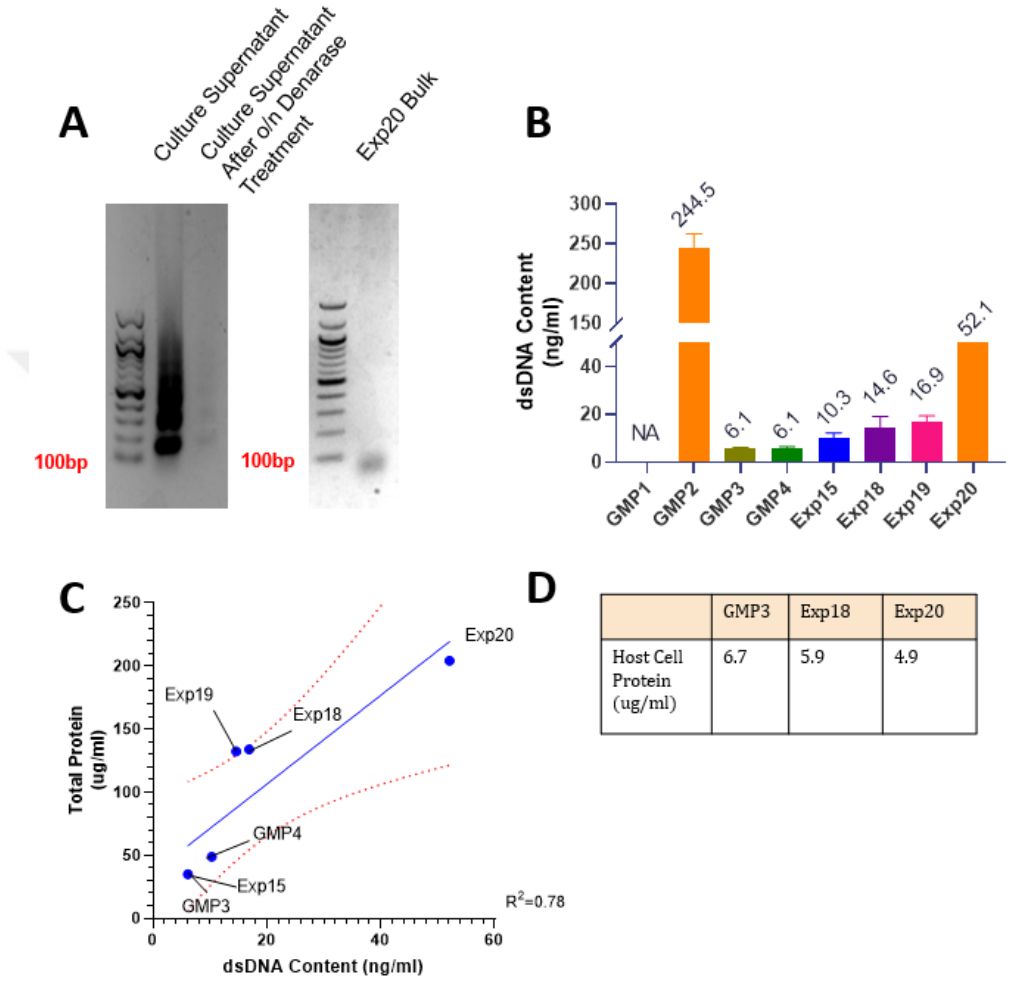

	GMP3	Exp18	Exp20
Host Cell Protein (ug/ml)	6.7	5.9	4.9

Figure 3.17 Amount and size of host cell derived DNA and amount of host cell derived protein in purified VLP bulk preparations. A. Culture supernatant with or without Denarase treatment and a purified VLP preparation was run on an agarose gel stained with SYBR Safe. (Ladder: 100np DNA Ladder, NEB) **B.** dsDNA content of purified VLPs measured by PicoGreen assay. **C.** Total protein and dsDNA content of indicated VLPs were plotted against each other. Linear regression was done in Graph Pad 7. Red dashed lines indicate 95 percent confidence interval of the regression. ***D.*** *Host cell protein content was measured with a HEK293T HCP ELISA kit. Measured host cell protein contamination was reported for indicated batches.*

Although the HCD and HCP amounts are satisfactory for vaccine manufacturing purposes, they bring interesting questions to mind. VLPs are not simple recombinant proteins, and are, by definition, cell derived vesicles that mimic the virus both in terms of their protein composition and secretion pathway. It is known that many host cell proteins can be decorated onto virions (Burnie & Guzzo, 2019).

To investigate the extend of this, purified VLPs were analyzed with antibodies against Alix and Tsg101. These proteins are part of the endosomal sorting complex and found inside exosomes. Hence, they can be used as markers of exosomes. [124] Figure 3.17 shows that both Alix and Tsg101 are present in purified VLPs. This is perhaps expected as like exosomes, VLPs are also secreted through the ERGIC. Alix and Tsg101 amounts in VLPs are not however correlated as Alix is differentially expressed in these three batches. Remaining questions are what is the percentage of exosomes in VLP preparations or which exosome markers are also present in VLPs. Structural proteins that drive VLP formation hijack the secretion machinery so cells might only secrete VLPs and negligible amounts of exosomes. Another view would be that difference between exosomes and VLPs becomes blurry upon expression of these proteins as exosomal proteins are loaded to VLPs and vice versa.

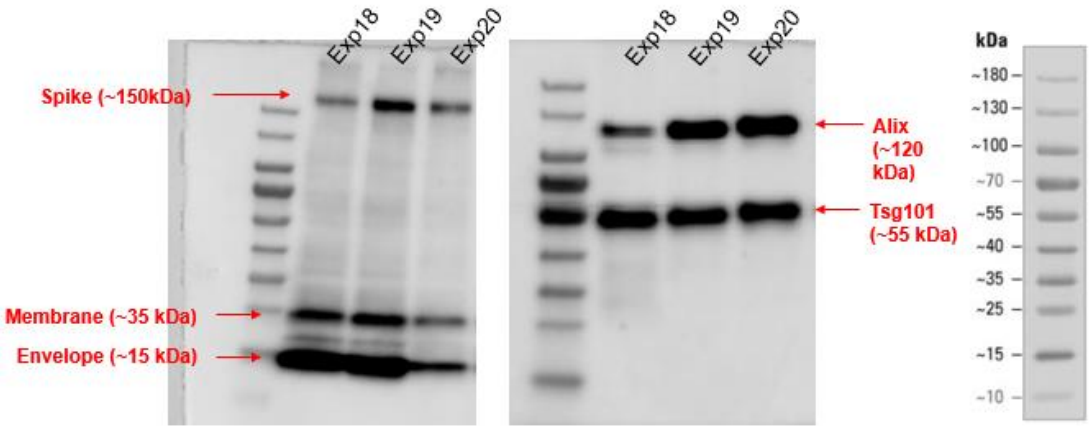

Figure 3.18 Exosomal markers present in purified VLP preparations. Indicated VLP preparations were analyzed with Western Blot using antibodies against Alix and Tsg101. Red text and arrows indicate the identity of the protein band.

Although interesting, presence of these host proteins in VLP preparations should not cause any problems regarding their immunopotency. These proteins are also found in inactivated virus preparations. (Unpublished results.) Inactivated virus vaccines have proved to be extremely reliable over the decades.

3.3.4 Binding of Virus Like Particles to hACE2 Receptor

If VLPs are truly mock viruses, these membranous vesicles should be capable of binding to hACE2 receptor. To investigate this, several binding experiments were conducted. These experiments were done using carboxy latex beads, which have an activated surface and allows for coating of recombinant protein of choice. Here, we've prepared hACE2 coated beads that would resemble to a hACE2 expressing cell.

To ensure hACE2 coated beads were functional in terms of binding, its interaction with S1 alone was determined. Recombinant S1 conjugated to PE/Cy7 was incubated with hACE2 coated beads, washed then analyzed with flow cytometry. Figure 3.18 shows specific dose dependent binding of S1 PE/Cy7 to hACE2 beads and not to a-IL1β coated beads.

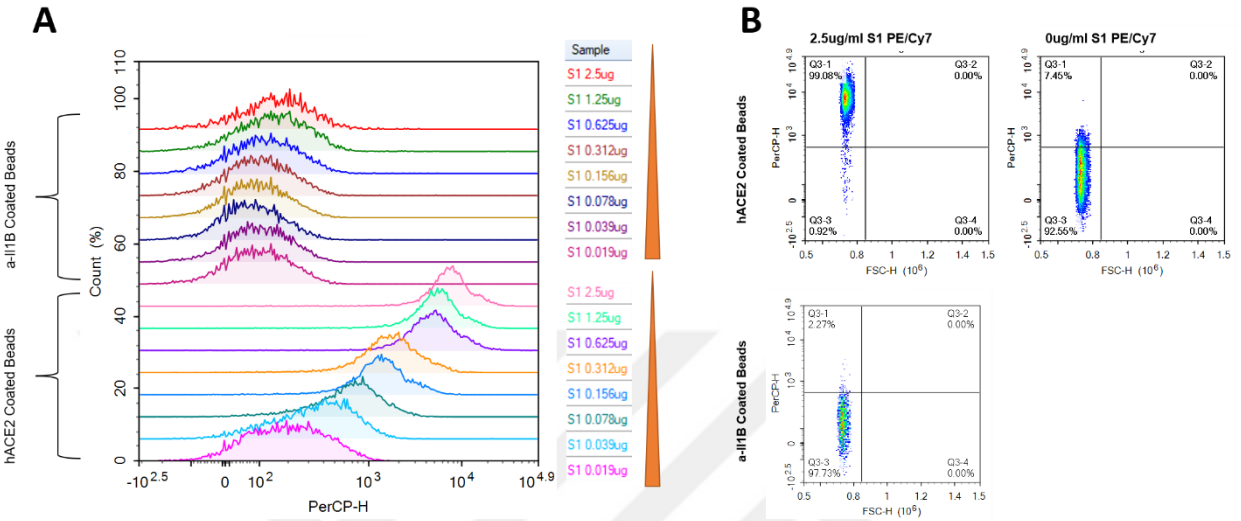

Figure 3.19 Recombinant S1 selectively binds to hACE2 coated carboxy-latex beads. Starting from 2.5ug/ml, S1-PE/Cy7 was serially 2X diluted and binding to hACE2 coated beads and a- IL1β coated beads was measured. **A.** Histograms showing dose dependent binding of S1 to hACE2 but not to a-IL1β. **B.** Binding is specific to hACE2 coated beads as no PE/Cy7 signal is detected with a-IL1β coated beads.

Next, for measuring binding, VLPs were stained with CFDA-SE or CellTracer Violet (Thermo Fischer) as explained in Methods Section 2.2.11, and then separated from excess dye using desalting chromatography. (Figure 3.19) In terms of chemistry, CFDA-SE and CellTracer Violet are the same. These compounds are normally non-fluorescent and cell permeable. Upon entry to a cell or a cell derived vesicle like VLPs, their acetate groups are cleaved by cell derived esterases. Cleavage product is highly reactive and covalently binds proteins via its succinimidyl group. Figure 3.19 shows fluorescent VLPs bind to hACE2 coated beads in a dose dependent manner, similar to S1.

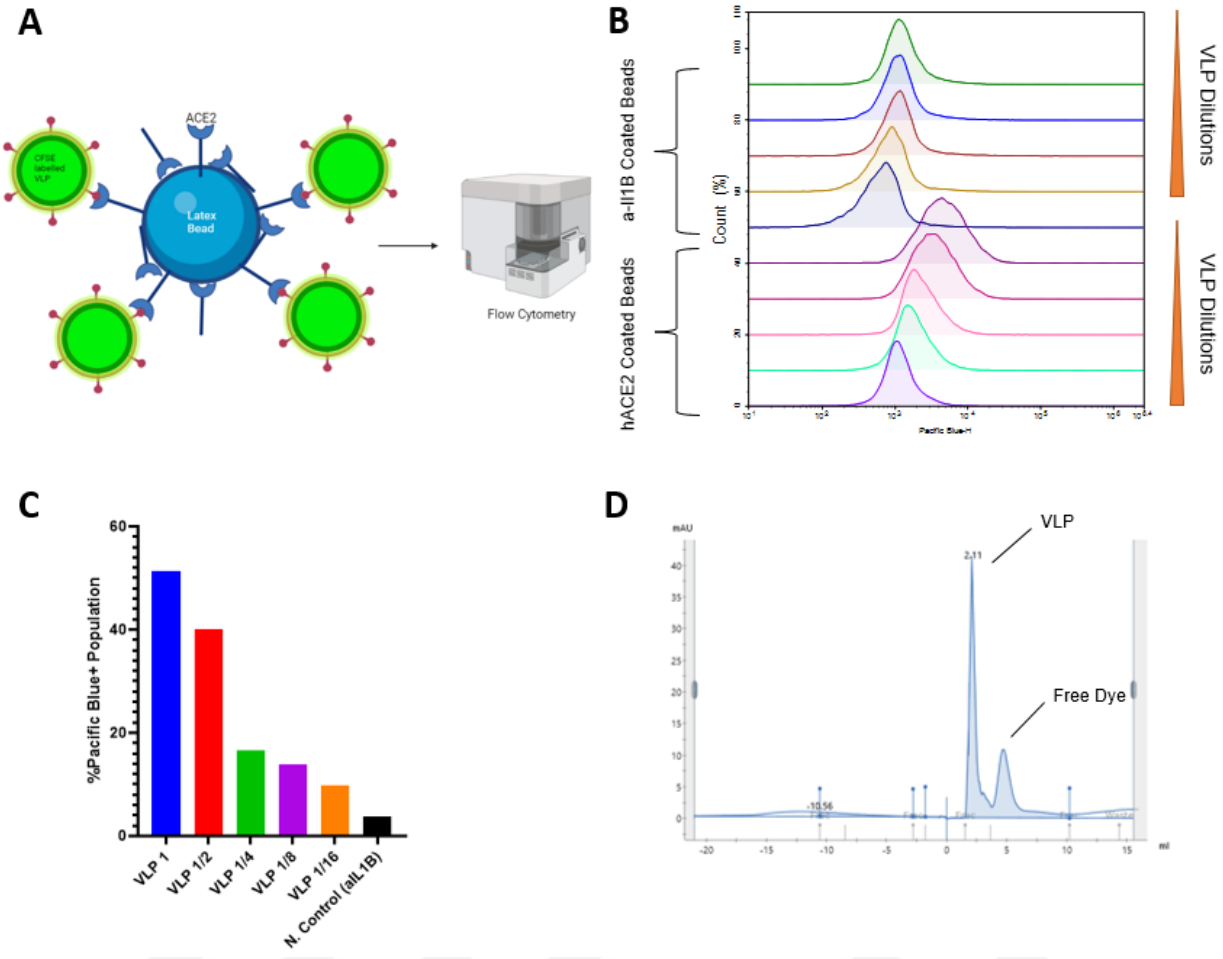

Figure 3.20 Fluorescently labelled VLPs bind to hACE2 coated carboxy-latex beads. A. Principle of the binding assay used for examining VLP binding to hACE2. **B.** Histograms showing dose dependent specific binding of VLPs labelled with CellTracer Violet to hACE2 coated beads. **C.** *Bar graph* showing *percent Pacific Blue positive population for each dilution*. **D.** Chromatogram from desalting chromatography which was used to separate VLPs from free dye.

Because of its mechanism, the CFDA-SE dye also indirectly proves that bead bound particles (VLPs) are cell derived vesicles. Binding is also competitively inhibited by recS1 in a dose dependent manner, further supporting the assay specificity along with the true nature of the Spike protein conformation that would be critical for immunogenicity. (Figure 3.20)

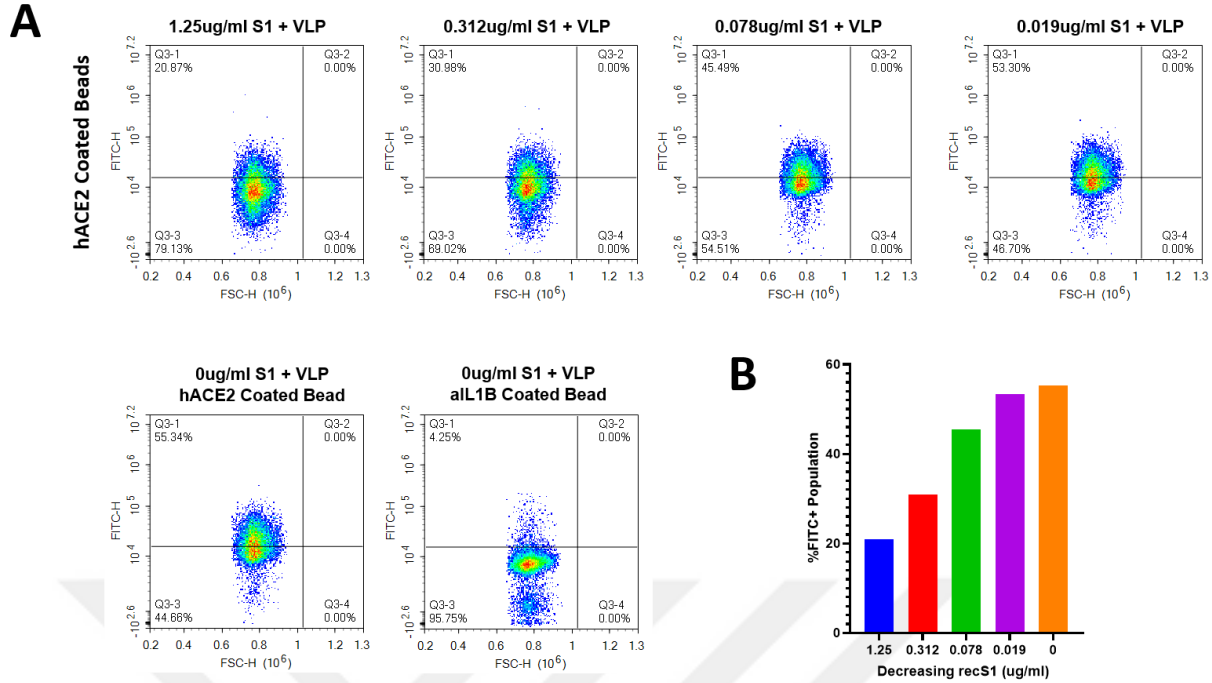

Figure 3.21 VLP binding to hACE2 is competitively inhibited by S1. CFDA-SE labelled VLPs were mixed with hACE2 or a- IL1β coated beads in the presence of serially 4x diluted recombinant S1 (1.25ug/ml) and analyzed with flow cytometer. Density plots **(A.)** shows dose dependent inhibition of VLP binding to hACE2 via recombinant S1, summarized in **(B.)**

3.3.5 Stability of Bulk Antigen

Any vaccine product intended to go for a human testing has to be tested for sentinel features, including but not limited to preclinical immunopotency, identity, being free from contaminating excipients and stability. These tests are conducted to ensure that vaccine which is intended to induce an immune response is stable and its initial state is not altered until the vaccination regimen is fulfilled. To this end, a series of stability tests were conducted and presented in Figure 3.21. Stress test of purified VLPs and further immunoblotting revealed remarkable stability of the VLP antigen even under high temperatures. When incubated at 40 °C for up to three days, no decrease in band intensities for neither of four structural proteins were observed. Similarly, no degradation products, smaller bands near the main protein band, were observed. (Figure 3.21A) Further testing regarding stability of this antigen is being continued in Nobel Pharmaceuticals, Istanbul. Data suggests protein identity of VLPs are stable up to 6 months at room temperature. (Unpublished results.)

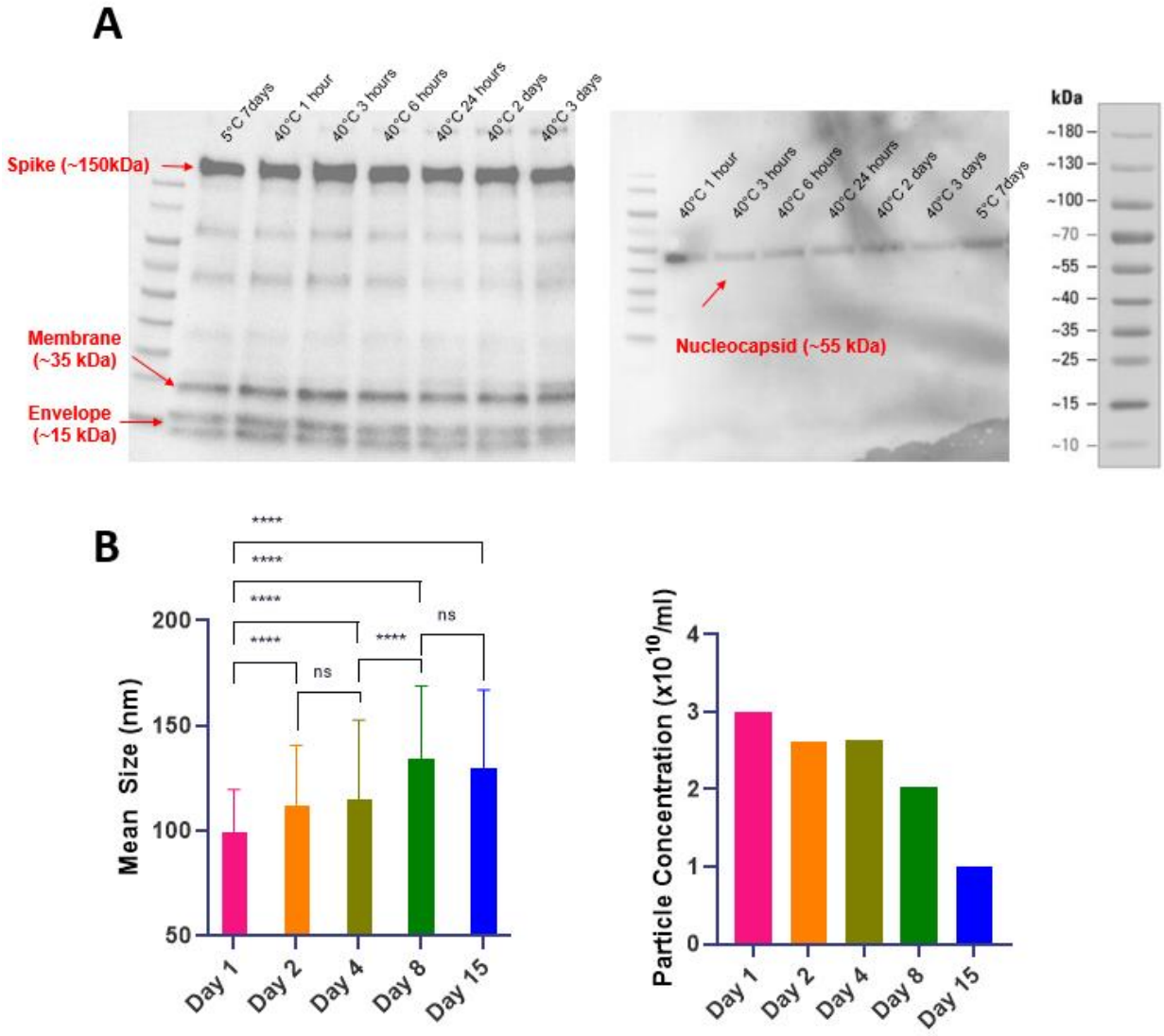

Figure 3.22 Time course stress testing and particulate stability of purified VLP antigen. Stability was assessed with a short-term stress test. **A.** VLPs were kept at 5°C for 7 days or 40°C for 1,3, 6, 24, 48 and 72 hours and analyzed by Western Blotting using antibodies against Histag (left panel) and Nucleocapsid (right panel). Red text and arrows indicate correct band identity. **B.** Exp 18 VLPs stored at 4°C were counted with qNano Gold for the course of 15 days, mean size and concentration was plotted. Statistical testing was done in Graph Pad 7. Groups were compared using one-way ANOVA Sidak's multiple comparison test. (n=500 for each group) ****: $p<0.0001$ and ns: $p>0.05$

Interestingly, longitudinal analysis of Exp 18 VLPs stored at 4°C with nanoparticle tracker qNano Gold suggests that there is some degree of aggregation (Fig. 3.21B left panel). During first 15 days after isolation, the mean size of particles increases from 99±20nm to 130±37nm. Statistical power of this measurement is quite high as the qNano instrument collects at least 500 events. Therefore, there is significant increase in mean size during the storage of purified VLPs in DPBS at 4°C. This is further supported by the decrease in particle concentration (Fig 3.21 right panel).

Durability of the antigen observed in immunoblotting but its tendency towards aggregation suggests that there needs to be experimentation in buffer additives for the purified VLPs. As of now, it isn't clear how time past from isolation to fill and finish might affect immunogenicity of the finished product.

Although finished product keeps its immunogenicity for at least 3 months with no decrease in its potency (see next chapter), aggregation of the purified antigen might cause problems when fill and finish is delayed. This process involves sterile filtration of bulk antigen with a 0.22um microfilter and it is not clear if aggregation at this stage can cause loss of product and therefore immunogenicity. While it is necessary to study the stability of the bulk antigen during a vaccine product development, it is also very important to test stability of the finished product.

3.3.6 Stability of Finished Product

The bulk VLP antigen was first adsorbed onto Alum, and then adjuvanted with K3-CpG ODN as explained in Methods Section 2.2.17.

VLP structure is an important feature of VLP antigen and confers its heightened immunogenicity compared to regular recombinant proteins. To investigate whether Alum absorption disrupts VLP structure, we have analyzed VLP + CpG ODN + Alum formulated vaccine with transmission electron microscopy. Vesicular structures that resemble VLPs in regards to shape and size suggest that Alum absorption does not disrupt VLP structure. As shown in Figure 3.22, there are several vesicular structures scattered around the Alum crystals (arrows and inlet image). The size of these vesicles seems to be uniform following formulation. These data suggest that alum adsorption did not affect vesicular nature of VLPs.

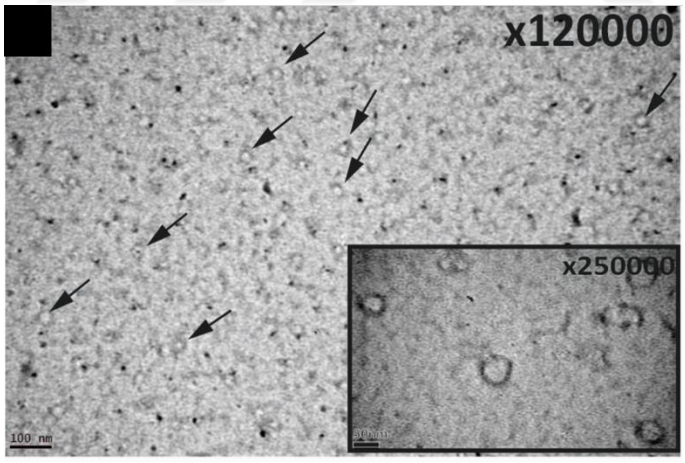

Figure 3.23 Transmission electromicrograph of Alum adsorbed VLPs. Black arrows indicate vesicle structures whose shape and size fits to VLPs, suggesting that Alum adsorption does not disturb structure of VLPs.

Alum formulated vaccines can become more aggregated over time. This can be a sign of freeze-thaw, which is detrimental for Alum formulated vaccines but it can also occur during normal storage. The "shake test" is a simple method to ensure there is no aggregation in a stored Alum adjuvanted vaccine [125].

In Figure 3.23, vials from GMP3, Exp19 and Exp20 were frozen for 24 hours and thawed or stored at 4°C from the time of fill and finish, which corresponds 3 months for GMP3 and 1 week for Exp19 and Exp20. Freeze-thawed vials, which function as a positive control for aggregation, fail the shake test and sediment much faster. This is validated with confocal microscopy. Properly stored vials, on the other hand, do not show this aggregation tendency.

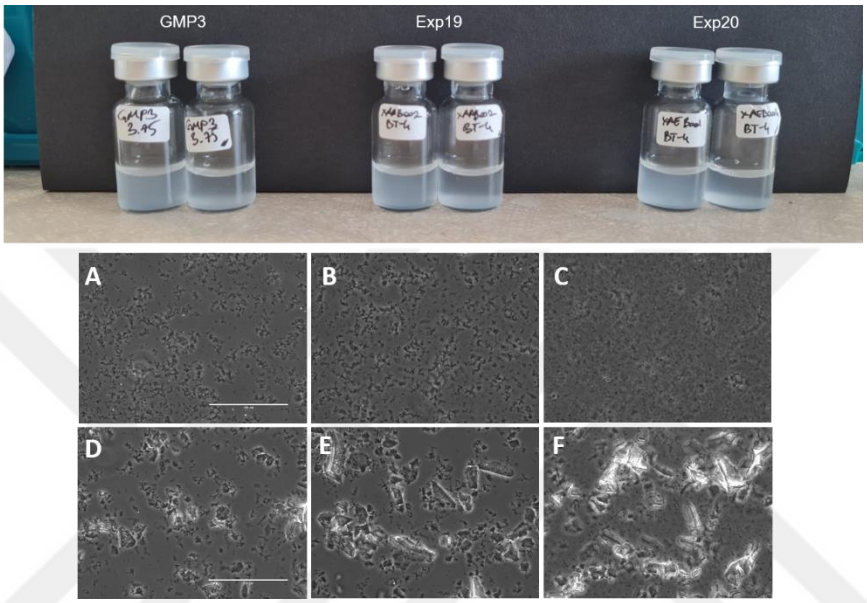

Figure 3.24 Aggregation test of VLP + Alum + CpG ODN formulated vaccine. Finished vials were stored properly or subjected to freeze-thaw. **Upper panel** shows increased speed of sedimentation of Alum particles. **Below panel** shows confocal microscopy images of the vials in the upper panel. **A.D.,** GMP3 vials stored properly or freeze thawed, **B.E.,** Exp19 vials stored properly or freeze thawed and **C.F.,** Exp20 vials stored properly or freeze thawed all respectively.

To test the stability of the finished product in terms of immunogenicity, GMP3 (8 ug/mice) +K3 CpG ODN (60ug/mice) + Alum (120ug/mice) formulated vaccines were used to immunize BALB/c mice (n=12) with a two-weeks apart prime-boost regimen. One group was immunized with freshly formulated vaccine and other group was immunized 3 months later with now 3-month-old vaccine. 2 weeks after second injection, serum was collected and antibody titers (IgG1) against Spike was assessed with ELISA. Antibody titers in mice injected with a freshly formulated or 3-month-old vaccine were indistinguishable, suggesting that the finished product is stable and sustains its immunogenic potential for at least 90 days following filling (Figure 3.24).

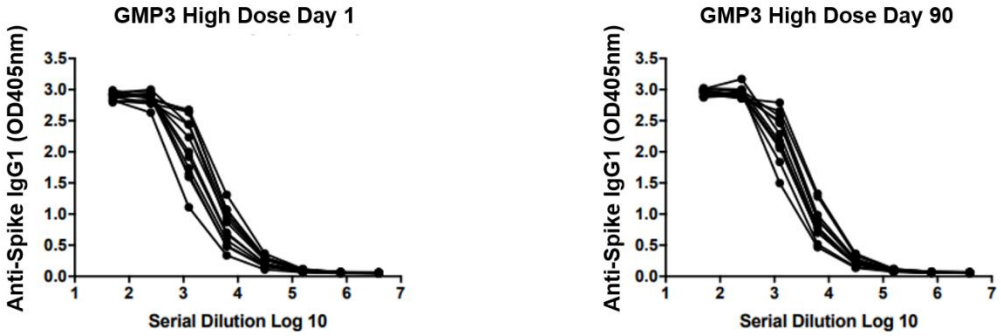

Figure 3.25 Immunogenicity of fresh and 3-month-old fill and finished vaccine. Vaccines formulated GMP3 were used to immunize BALB/c mice (n=12) 3 months apart. Sera from two weeks after booster injection were serially diluted and IgG1 titers against Spike were measured by ELISA.

These studies conducted so far implicate that VLPs are stable either in bulk or even after formulation with Alum and CpG ODN and can be stored at least 3 months at 2-8°C without losing either its original integrity or its immunopotency.

3.3.7 Desorption of VLP Antigen from Alum Adjuvant

In order to validate the fill and finish procedure, it is essential to quantify each ingredient in a vial. Alum ($AlOH_3$) adjuvant is capable of absorbing some substances, which means these become entrapped in Alum gel via electrostatic interactions and released to the formulation solution in time. This is actually needed for some effects of Alum adjuvant in vaccines and a good adsorption efficiency is critical for immunogenicity. [100]. However, this also makes quality control of finished products complicated as Alum, being a particulate material, is not compatible with most common protein detection techniques. The desorption procedure employs several chemical strategies to interfere with the aforementioned electrostatic interactions. To analyze vaccine supernatant and adsorption efficiency via immunoblotting, SDS-citrate-phosphate (SCP) desorption method was used [116] .Details of this procedure is explained in Methods Section 2.2.14.

In an attempt to reveal whether Alum absorbs VLP antigen efficiently, we employed a centrifugation step to sediment the complex first and investigated the vaccine supernatant. Should there be an incomplete adsorption or desorption in time, the supernatant must contain free VLP or its protein-based components.

Figure 3.25 shows that the vaccine supernatant is devoid of any protein that is detectable through immunoblotting using either anti-Histag or by anti-Nucleocapsid antibodies. This suggests 100% adsorption efficiency on to Alum. All four proteins are visible in the desorbed vaccine, validating this method for recovering protein identity. Note that the SCP Buffer used in desorption is extremely high in viscosity and creates problems during gel electrophoresis especially for small proteins (membrane

and envelope). Hence, parts of the blots that correspond to low molecular weight have reduced resolution and appear blurry.

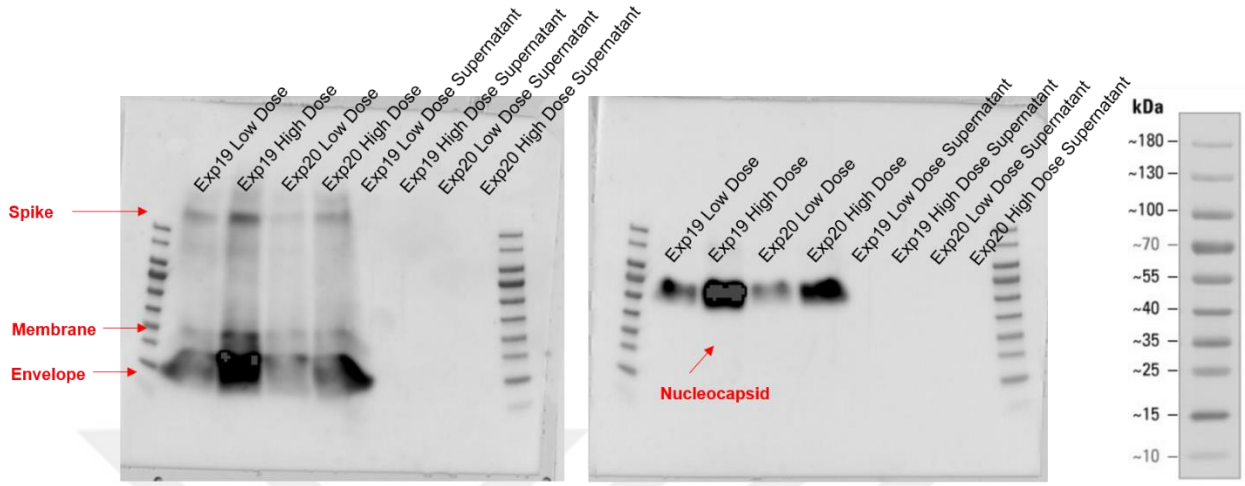

Figure 3.26 Desorption of VLP antigen from formulated vaccine. Finished vials formulated with CpG ODN + Alum + Exp19 or Exp20 VLPs were analyzed with western blot using antibodies against histag (left panel) and nucleocapsid (right panel). Red text and arrows indicate correct band identities. Analyses was done using SCP desorbed vaccine and respective supernatants.

While western blotting provides a suitable qualitative approach to analyze desorbed protein identities from the formulated vaccine, estimating protein quantities deserves additional investigation. To address this issue, the desorbed vaccine was tested in a quantitative dot-blot analysis with bulk antigen serving as a standard. Figure 3.26 shows a linear relationship between adjusted intensity and protein quantity. Using three points for the standard curve, it was possible to calculate the protein concentration in desorbed samples from High Dose and Low Dose GMP3 formulations. Although this proved to be an applicable method to calculate protein concentration in desorbed samples, it slightly overestimates the concentration possibly due to matrix interference from SCP Buffer.

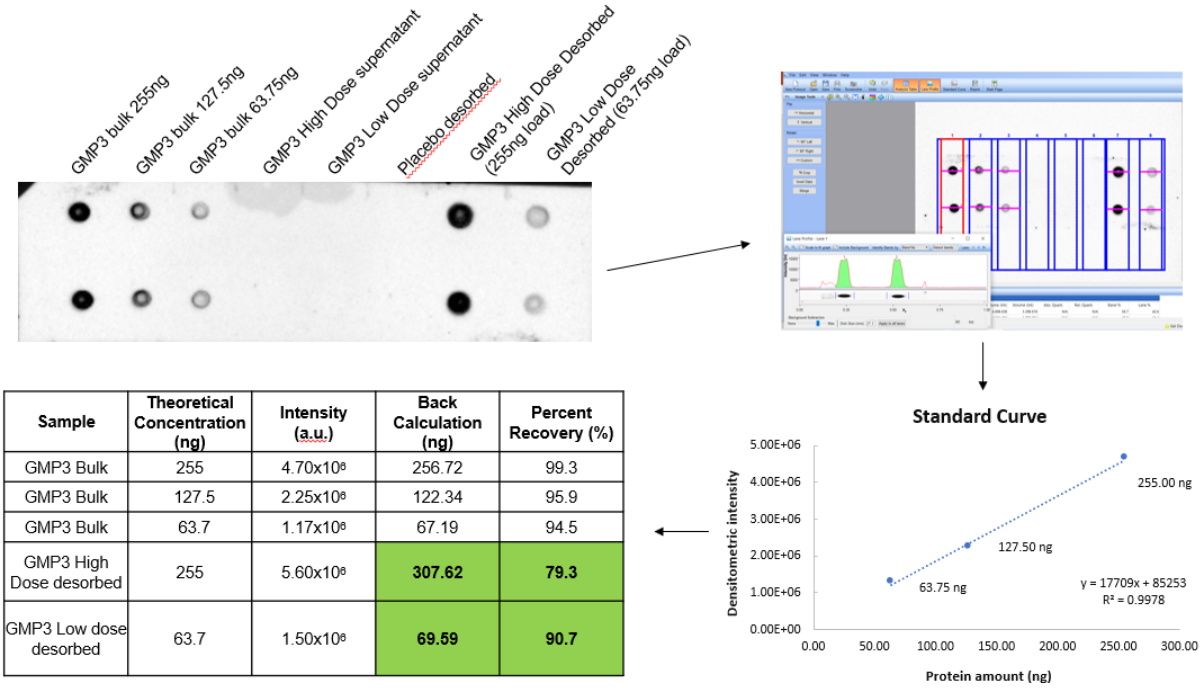

Sample	Theoretical Concentration (ng)	Intensity (a.u.)	Back Calculation (ng)	Percent Recovery (%)
GMP3 Bulk	255	4.70x10⁶	256.72	99.3
GMP3 Bulk	127.5	2.25x10⁶	122.34	95.9
GMP3 Bulk	63.7	1.17x10⁶	67.19	94.5
GMP3 High Dose desorbed	255	5.60x10⁶	**307.62**	**79.3**
GMP3 Low dose desorbed	63.7	1.50x10⁶	**69.59**	**90.7**

Figure 3.27 Quantitative dot blot of desorbed VLP antigen. Desorbed vaccine and its respective supernatant were used for immunoblotting and probed using an antibody against Histag. Purified VLPs were also used for constructing a standard curve. Adjusted intensities were calculated with Image Lab Software. (Bio-Rad), Standard curve was calculated by linear regression and used to back calculate protein amount in desorbed samples. Theoretical protein amount in desorbed samples were calculated assuming 100% adsorption efficiency.

3.3.9 In Vivo Potency of GMP3-Wuhan (Phase-I) and Exp18-Alpha (Phase-II) Vaccine

Before initiating a clinical trial, there are several analytical methods to be executed. Quality assurance teams investigate these findings and based on scientific evidence, approve the release of finished vaccine product to the clinical centers. One of these assays is the vaccine potency. This could be developed either as an in-vitro potency, or as an in vivo potency assay. In our case, and in the lights of COVID-19 pandemic, similar to many vaccine producers whom engaged in developing COVID-19 vaccine employed an in vivo potency assay and tested the immunogenicity of the final vaccine product. Of note, establishing an in-vitro potency assay is preferred but it may take more time to validate it, thus in vivo potency assay is accepted at the early stages of the clinical studies as one of the release criteria. The potency assay is used to ensure that batch to batch variation is minimized. In addition, in our Phase 2 clinical trial, one of the main aims was to compare immunogenicity of VLPs decorated with Alpha variant Spike to VLPs decorated with Spike from the authentic Wuhan strain. However, it is yet unclear if variant specific VLPs are able to drive variant specific RBD antibodies which would be critical to also drive variant specific neutralizing antibodies. To test both general immunogenicity to SARS-CoV-2 antigens and also variant specific RBDs, C57Bl/6 mice (n=10) were vaccinated with 8 µg GMP3 VLP (will be referred to as Wuhan VLP) + 60 µg K3 CpG ODN + 120 µg Alum and 8 µg Exp18 VLP (will

be referred to as Alpha VLP) + 60 µg K3 CpG ODN + 120 µg Alum. As explained in Methods Section 2.2.19, mice were vaccinated with a prime-boost strategy on Days 0 and 14 and blood was collected on Day 28. Below, Figure 2.27 summarizes results of in vivo potency experiments on Alpha and Wuhan strain VLP vaccines.

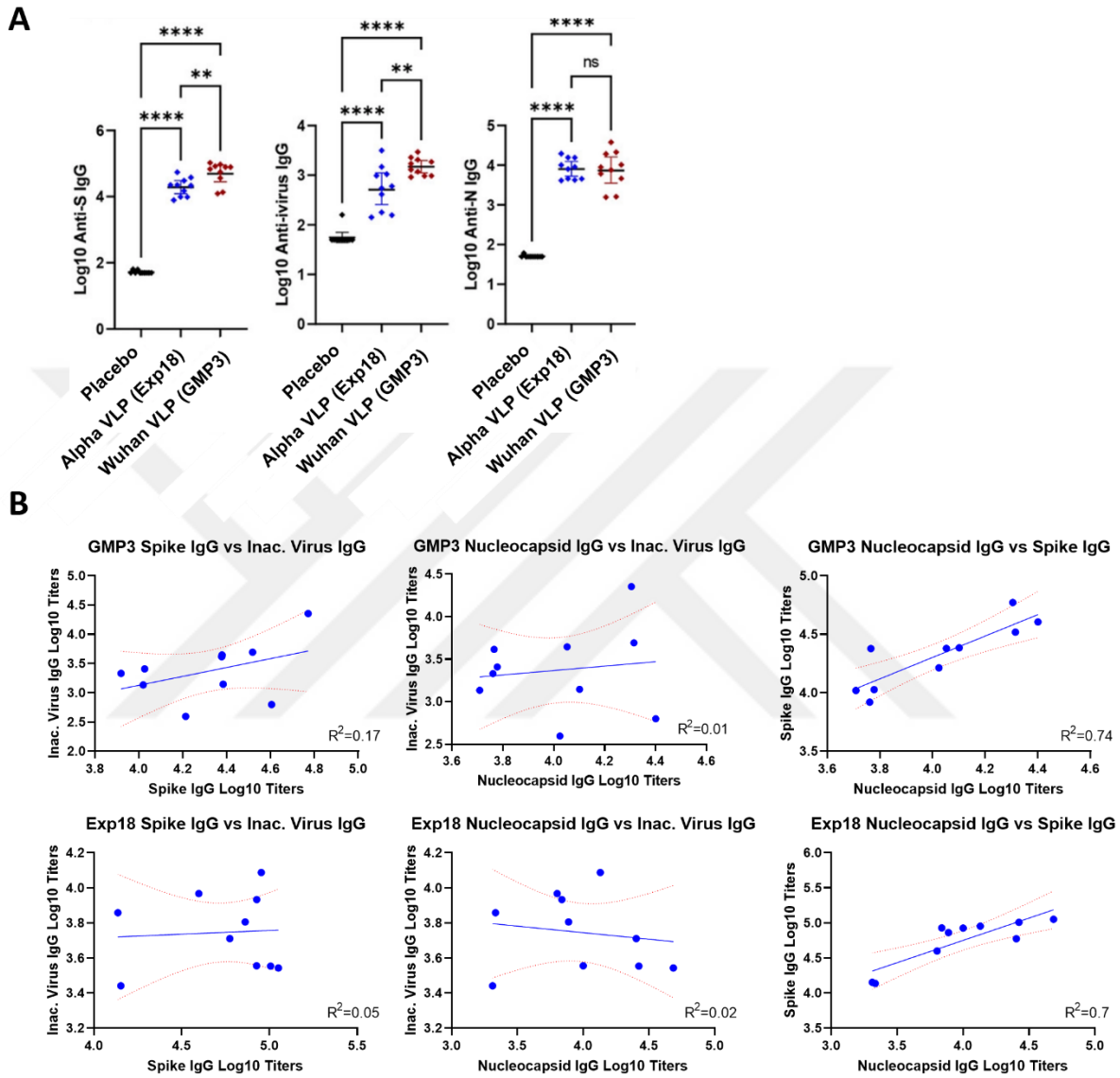

Figure 3.28 In Vivo Potency of GMP3-Wuhan (Phase-I) and Exp18-Alpha Vaccine (Phase-II) A. End point antibody log10 titers (total IgG) elicited by Wuhan and Alpha formulated VLP vaccines against trimeric Spike (left plot), whole inactivated virus (middle plot) and Nucleocapsid (right plot) measured by ELISA. Log10 titers were calculated with nonlinear 4 parametric regression in Graph Pad 9 software. Mean titers were compared with One-way Anova, Dunnett's multiple comparisons test. **B.** Correlation of IgG Log10 antibody titers against different SARS-CoV-2 antigens were calculated by linear regression in Graph Pad 9 software. Red dashed lines indicate 95 percent confidence interval of the regression. (Individual mouse titers are shown in Appendix Figure 5.3.)

Figure 3.27A shows that both antigens, when combined with Alum + K3 CpG ODN are capable of eliciting anti-Spike, anti-Nucleocapsid and anti-whole inactivated virus antibodies. Seroconversion against all tested SARS-CoV-2 antigens as well as inactivated virus were %100 for both VLP vaccines.

Mean IgG titers elicited against Spike and inactivated virus by Alpha VLP antigen (Exp18), as expected, was higher than Wuhan VLP antigen (GMP3). As discussed before, previous work by our group showed that Alpha and Delta variant Spike have enhanced decoration on to the VLPs per microgram. (Güvençli, 2022) Higher titers elicited by Alpha VLP against Spike and inactivated virus can be attributed to this feature of Alpha VLPs. Anti-Nucleocapsid antibody titers, which in theory should not be significantly altered, against these two VLP antigens are indistinguishable, as expected.

Interestingly, correlation analysis for antibody titers elicited in response to different VLPs revealed that anti-Spike and anti-Nucleocapsid titers are highly correlated (Fig 3.27B). This means good responders for Spike antigen are also good responders for Nucleocapsid and vice versa.

However, inactivated virus titers were not correlated with Spike or Nucleocapsid titers. This is quite puzzling as we have confirmed presence of both Nucleocapsid and Spike in these preparations of inactivated virus with immunoblotting (Data not shown.) and difference between Alpha and Wuhan VLPs is also detected by titers against inactivated virus. One possible explanation is the following; inactivated virus is of Wuhan origin, this could lead to different set of antibody response when Alpha Spike decorated VLP is used during vaccination. This should be further analyzed in future. Nevertheless, both antigens are highly immunogenic in mice as evidenced by antibody titers against Spike, Nucleocapsid and inactivated virus. Additionally, it would be interesting to look at how vaccine induced antibody titers and T cell responses against Spike and Nucleocapsid, virus neutralization titers and viral load upon challenge are correlated or not with each other.

3.3.10. Variant Dependent RBD-Specific antibody responses

In an attempt to address the cross-variant antibody levels elicited by the two VLP vaccines, anti-RBD titers of the immunized animals were measured.

Data depicted in Figure 3.29 suggests that variant specific RBD ELISA is a plausible way of assessing variant specific and cross variant antibody levels achieved via either by Wuhan VLP or Alpha VLP vaccination. Differential response against variants were measured with end-point ELISA. Interestingly while GMP3 (Wuhan) elicits RBD antibodies to different variants in the order of Beta > Alpha > Wuhan > Gamma; Exp18 (Alpha) elicits in the order of Alpha > Wuhan > Beta > Gamma. At this time, it is puzzling for us and it is not clear why GMP3 (Wuhan) VLP driven antibodies are not largely Wuhan RBD specific. Alpha VLPs (Exp18) drive significantly higher mean titers against all variant RBDs except Beta, suggesting that variant VLPs may in fact represent a viable way to create variant specific and cross variant immunity. Replicating these results with another method, such as ACE2-Tg mice challenge experiments, might shed more light to this phenomenon since not all variant mutations function through simply evading anti-RBD antibodies. [126] It would be interesting to also assess variant specific vaccination with pseudovirus assay where pseudoviral particles are produced to harbor Spike from specific variants. These steps shall be pursued in future.

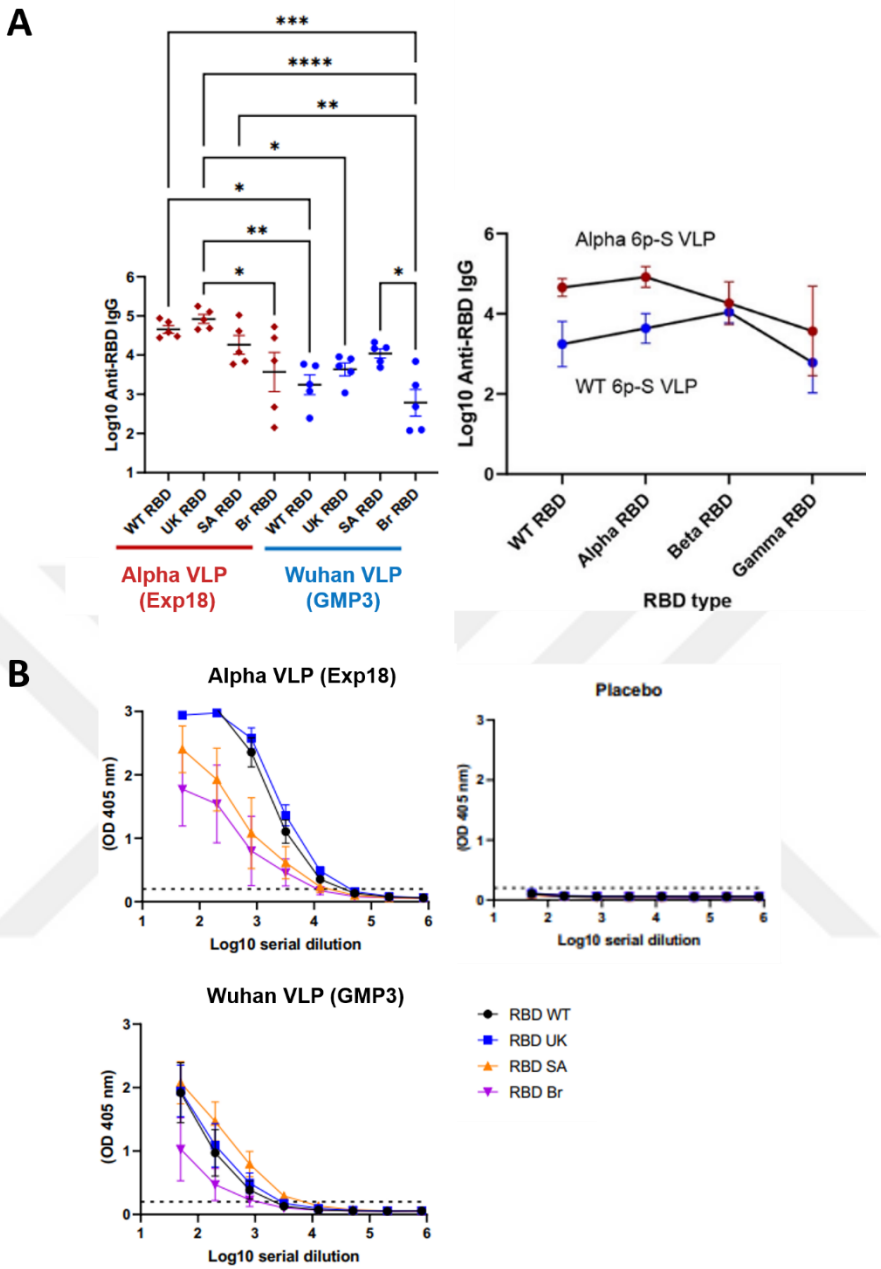

Figure 3.29 Variant RBD Specific Antibodies Elicited by GMP3-Wuhan and Exp19-Alpha Variant VLP Vaccines. (**A)** Mean antibody titers against RBD from the Wuhan, Alpha (British), Beta (South African), Gamma (Brazilian) variants **(B)** Average OD@405nm readings of each dilution from ELISA. Variant specific RBD titers were detected by ELISA coated with commercially available variant specific RBDs. Error bars represent SD and horizontal line represents mean titers. Log10 titers were calculated with nonlinear 4 parametric regression in Graph Pad 9 software. Mean titers were compared with One-way Anova, Dunnett's multiple comparisons test. (Individual mouse titers are shown in Appendix Figure 5.4.)

4. Conclusion and Future Perspectives

Below, Figure 4.1 outlines our devised manufacturing and testing scheme for production of a VLP vaccine targeting SARS-CoV-2.

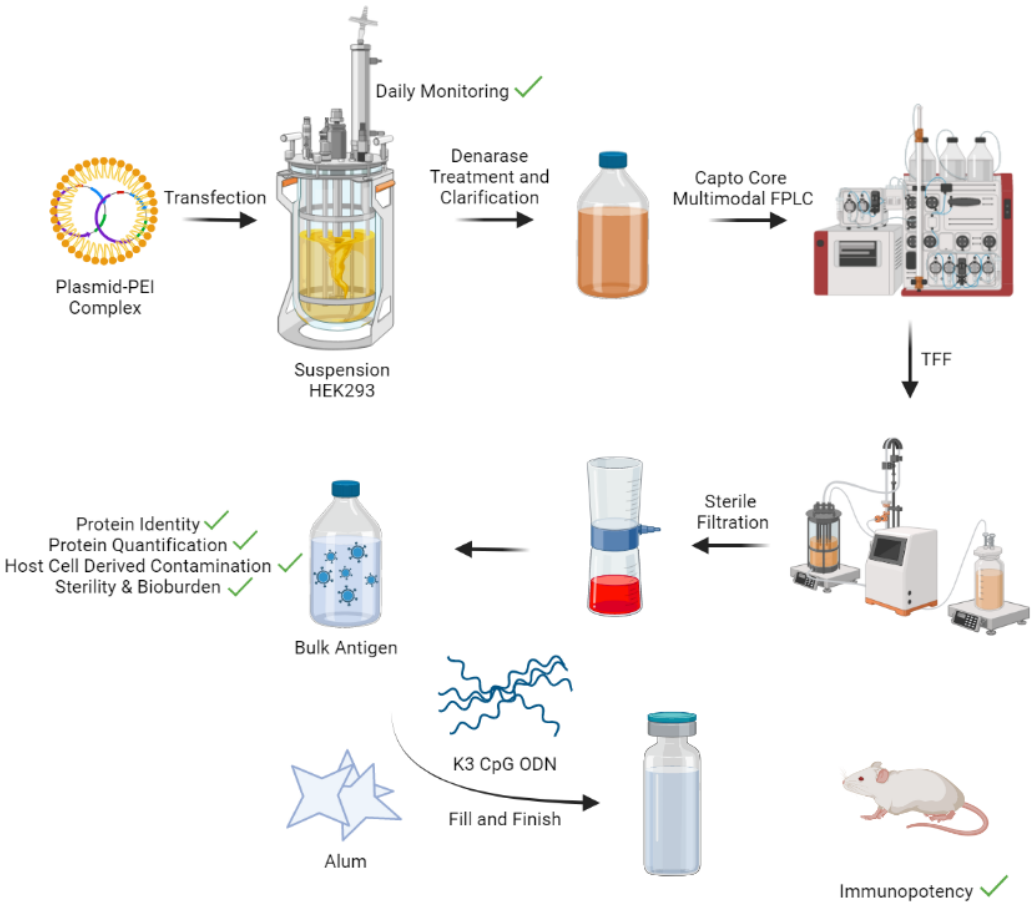

Figure 4.1 Summary of the vaccine manufacturing process.

Our group has previously published numerous studies on a virus like particle vaccine candidate targeting SARS-CoV-2 [112,121]. We have established that SARS-CoV-2 VLPs, when combined with Alum and K3 CpG ODN adjuvants, elicited robust titers of Spike, Nucleocapsid and RBD targeting antibodies, induced Spike and Nucleocapsid specific CD4+ T cells along with Spike specific CD8+ T cells. Usage of Alum + CpG ODN, combined the advantages of both adjuvants. CpG ODNs are Th1 skewing adjuvants but both limited expression of TLR9 in humans and its inefficiency at getting to draining lymph nodes in larger species limit its usage [127] .Combination of CpG with Alum, like in our candidate vaccine or within an emulsion, like GlaxoSmithKline's AS03 can increase ODN amount that drains to the lymph node [128]. CpG ODN is dominant over Th2 skewing mediated by Alum as we have observed that VLP + CpG ODN + Alum formulation induces a Th1 dominant response. This was evidenced by the IgG2a/IgG1 ratio in vaccinated BALB/c mice together with increased secretion of Th1 cytokines from Spike and Nucleocapsid stimulated splenocytes [112]. We have also previously

designed a proof-of-concept production scheme that was scalable. Herein, we have materialized this production scheme to produce a GMP grade VLP based vaccine for use in planned clinical trials.

Production begins with transient transfection of suspension adapted HEK293 cells. Both cells and media were from a biotechnology company based in Turkey — which is an undeniable advantage in a global pandemic. Through optimization of the upstream processing, which encompasses the transfection and consequent 5-day culturing of producer cells, we have achieved yields reaching 40 mg of VLP per Liter of cell culture. A pilot-scale facility with three 50 L bioreactors could produce ~150000 vials (having 40 ug VLP/vial) for human consumption per month. This would equate to nearly 2 million doses per year. Even the modest increase in cell densities achieved here have amplified our yield ~3 folds. Cell culturing is clearly the bottleneck of this process and further development of it remains a great importance. We have used a considerably low cell density ($1.5x10^6$/ml) during transfection, this was because of initial experiments we have conducted in Bilkent University. During this time, both the state of the media and cells were perhaps questionable and doesn't reflect a bioreactor culture. In the literature, starting cell densities of $5x10^6$/ml are common [129] and even densities up to $20x10^6$/ml are reported [130]. This suggests that there is much room to improve for the procedure of initial transfection stage.

Although transient transfection was the only realistic choice during a global pandemic, a stable cell line that produces the four structural proteins would be an exceptional improvement to the procedure. There are however, numerous challenges with this. Firstly, there is evidence for all of these proteins being cytotoxic or cell limiting in different contexts [21,131,132]. Secondly, overexpression of four proteins — three of which are extensively modified post-translationally, will put tremendous burden to growing cells. One simple way to solve all of these problems is to use an inducible system. This would allow for stopping the expression of these proteins during passaging and only turning them on during production. There are several examples for these systems in the literature [133,134] . A stable cell line would both allow for massive increase in yield — since concerns regarding PEI toxicity would be out of the window and also cut production costs.

Although we have achieved continuous increase in concentration of proteins that constitute the VLPs during 5 days of culture, there is still room for improvement. There are many cell culture additives that increase recombinant protein yields. Most of these additives are either epigenetic modifiers or cell cycle arrest agents that slow down proliferation but not protein expression. Some common additives are lithium chloride [135], sodium butyrate [136], valproic acid [137] and sialic acid [138]. Low temperatures are also documented to enhance productivity in recombinant settings [136]. From these, lithium chloride, valproic acid and sialic acid are FDA approved. Nevertheless, downstream processing employed should remove any traces of these agents during purification. Since these are small molecules, this would be easily achievable through tangential flow filtration.

Our downstream processing scheme is composed of fast protein liquid chromatography with Capto Core 400 resin and tangential flow filtration. Data suggests that while Capto Core removes nearly all protein

contaminants, other smaller contaminants including those coming from the cell culture media are not removed completely. Such small contaminants are removed during tangential flow filtration. HPLC-SEC of final purified bulk VLPs and in process samples suggest that our scheme is quite high in effectiveness. However, its efficiency should be questioned. Tangential flow filtration is indispensable as even if yields are increased to a level where there will no more of a need to concentrate VLPs, diafiltration will always be necessary. In theory both FPLC and TFF are scalable to thousands of liters. However, Capto Core is quite problematic in terms of logistics. Huge amounts of resin will be required during initial stages of establishing the dedicated pilot scale GMP facility. Although comparative experimental data about this lacks, tightest column volume per sample volume we have utilized so far was 0.1. This means our exemplary pilot scale laboratory would need at least 1500 L of Capto Core media to simultaneously process 150L of supernatant. This number may be decreased by careful planning to store and separately process cell supernatants but then number of columns needed and process time would increase. To purify a 5 L supernatant through our AxiChrom 70 column, which has a 1 L column volume, 35 L of liquid actually needs to be passed through it. This includes the CIP and washes. Flow rate is slower during CIP and faster during the washes and sample application. This means processing supernatants by doing several runs on the same column — although would require less resin, would increase processing time greatly. TFF on the other hand is much simpler in terms of both scale up and use. Whether it would be possible to replace Capto Core with TFF using perhaps several cassettes with different MWCOs ranging from 500kDa to 100kDa remains a possibility. Our purified VLP antigen is quite pure. However, besides the main peak, there are two other minor peaks apparent in HPLC-SEC. Identity of these peaks remains unelucidated. This might be achieved in the future via HPLC-SEC coupled with mass spectrometry.

As explained above, there is a significant correlation between cell state and total protein. This increase in total protein is also reflected to increase in relative intensity observed in western blots against Spike, Membrane, Envelope and Nucleocapsid. Therefore, increase in total protein also reflects increase in VLP constituents directly. Based on this, we have decided to use total protein measurement for both during release of VLP batches from quality control and also for determining dosage of VLP antigen in the finished vaccine. This was perhaps the simplest solution but total protein amount does not necessarily correspond to immunogen amount. This was for example a major problem for CoronaVac produced by SinoVac Life Sciences as they have observed less immunogenicity of the same inactivated whole virion vaccine during their Phase 1 trial compared to the Phase 2 trial [75]. This was attributed to less Spike decoration on the virions used in two trials. Spike was reported to constitute, in general, around ~15% of the total protein mass in β-propiolactone inactivated virus preparations. [139] Therefore even a two times difference in the amount of Spike in preparations could go unnoticed because it would be indistinguishable from batch-to-batch variation. Therefore, if total protein is used to discriminate between batches and adjust dosage, demonstrating in vivo immunopotency becomes a must. Downside of immunopotency experiments is that it takes at least a month to get a proper reading on vaccine

performance. Instead, implementation of a LC-MS based method to measure levels of all four structural proteins in purified VLPs would solve much of these problems. There are several examples of this application of LC-MS in the literature [139–141]. Even though we have not implemented a LC-MS method because of the time constraints, we have also experimented with several methods regarding quantification of the Spike protein in VLPs with ELISA and quantitative immunoblotting. (Unpublished results.) Although they were successful as a "research" method, because of their intrinsic variation which was especially the case for immunoblotting, they were not validated and weren't used for quality control of VLP antigen.

Denarase treatment was extremely efficient. VLP yield and dsDNA contamination was linearly corelated and but because dsDNA limit is per dose, this should not cause problems in the future. There might be on-limit batches like Exp20, but size of contaminating dsDNA fragments was shown to be <100bp. 10 ng/dose limit might also be increased because VLPs resemble inactivated viruses more than they resemble recombinant proteins. It is also interesting that host cell derived protein contamination (~5 ug/ml) is constant even for batches with different VLP yields. However, this ELISA based method should be interpreted with caution because it is essentially a black box method. To understand more regarding presence of host cell derived factors in VLPs, western blots targeting exosome markers Tsg101 and Alix were performed. Unsurprisingly, these proteins were present in VLP preparations. It is yet unclear if this represents decoration of exosome markers on VLPs (even onto virions during natural course of infection) or whether there is a separate exosome population in our preparations. First option is likely as both exosomes and VLPs bud from ERGIC and over expression of four structural proteins would overwhelm cell's own vesicular trafficking that normally produce exosomes. Although interesting, presence of these proteins should not represent a problem in terms of immunogenicity. Such host derived factors are also present in inactivated virus preparations and also infective viruses. This type of vaccination is much older than our ability to pinpoint what actually is in them [142–144].

Our experiments with VLPs and ACE2 coated carboxy-latex beads show that Spike found on VLPs are functional in terms of binding. ACE2 coated beads were functionally validated first using PE/Cy7 labelled S1 and then CFDA-SE or CellTracer Violet labelled VLPs. Dose dependent binding of labeled VLPs to ACE2 beads but not to a-IL1B coated beads was shown. This binding was also competitively inhibited with recombinant S1. Although these experiments were conclusive for research purposes, implementation of a surface plasmon resonance-based method would greatly benefit our approach. This would not only allow for quantification of binding but would also allow us to compare batches. Only prefusion spikes can bind to ACE2 and this is the most important immunogen in our antigen. Therefore, comparing binding kinetics of different batches with each other would inform us about the relative amount of prefusion-Spikes per ug of VLP antigen for each batch. This has been demonstrated to be an alternative to single-radial immune-diffusion (SRID) assay for influenza vaccines [145].

Our stability testing of VLPs showed that protein content is remarkably stable. Western blot analysis of VLPs stored at 5 °C or at 40 °C for up to three days showed no change in band patterning or relative intensities for all four structural proteins. We have so far extended this study to 6 months at 25 °C with similar findings. (Unpublished results.) However, nanoparticle tracking analysis with TRPS measurements showed slight but obvious increase in mean size of particles and decrease in particle concentration. This shows that when purified antigen is stored at 4 °C as such in DPBS, it has a tendency to aggregate. It is unclear if this is problematic in terms of immunogenicity. One major problem that can be imagined is the following. During fill and finish, VLP antigen is sterile filtered with 0.22 µm microfiltration. It is unclear if this can cause loss of material due to increased average size, which would cause a decrease in immunopotency of finished vials. Another concern is to have heterogeneity in VLP solution which might increase variation in immunopotency of fill and finished vials. Although these are possible scenarios, direct experimental validation for these cases remains absent. To ensure that none of these cases affect our studies, we have generally used any bulk antigen for fill and finish in about a week from purification. In the future, study of buffer additives to ensure aggregation rates are minimal should be conducted. This would also allow us to concentrate VLPs more during TFF. Various additives are described in the literature for inhibiting aggregation of viral particles or proteins in general. These include glycerol, sucrose, amino acids and different salts [146,147].

Stability of Alum + CpG ODN formulated vaccine is arguably more important than bulk antigen as this form will be stored for much longer. To examine this, we firstly looked at sedimentation speed and then particulate characteristics using confocal microscopy. Freeze-thaw induced aggregation served as a positive control. We have detected no signs of aggregation in vials stored at 4 °C for three months. Transmission electron microscopy revealed that Alum absorption preserves membranous structures of VLPs, which is critical for its immunogenecity. Immunopotency experiments with freshly formulated and 3-month-old formulated VLP vaccine revealed vaccine keeps its immunopotency for at least 3 months when stored at 4 °C.

Under GMP regulations, finished products are need to be analyzed to confirm they contain what was intended for them to contain. Vaccine outlined here contains VLP antigen and Alum + CpG ODN adjuvants. Presence of each of these constituents has to be determined in the finished products. Alum was quantified via ICP-MS by a collaborator of ours in Bilkent University. (Data not shown.) CpG ODN was found to be present both as absorbed to Alum and in solution as previously reported [148]. CpG ODN in solution was quantified via A205nm readings of vaccine supernatant and absorbed CpG ODN was attempted to be quantified with a novel Acridine Orange based assay. Although not conclusive (hence not shown in this thesis), data suggests that one third of 300 µg CpG ODN used in formulation is found absorbed to Alum. Both antigen identity and quantity are need to be shown from formulated vials. To achieve this, we have implemented a desorption protocol in which amount of antigen is concentrated such that all four structural proteins can be visualized via immunoblotting. To quantify the antigen, we have experimented with several methods described in the literature including a modified

version of Lowry method and a O-Phthalaldehyde based assay [149,150]. These were unfortunately not successful and therefore abandoned. As an alternative, immunoblotting of desorption samples followed by densitometric analysis was performed. Although there is a slight overestimation, this method proved to be an option. We now have preliminary data that micro-BCA measurement of desorbed samples can also be a viable option. This was achieved by diluting the samples to a degree where SCP buffer constituents do not interfere with the assay but the protein content is still measurable.

VLPs isolated under GMP regulations were used for Phase 1 Clinical Trial (NCT04818281) which explored dose escalation and safety and for Phase 2 Clinical Trial (NCT04962893) which explored humoral and cellular responses elicited by Wuhan and Alpha (British) variant VLP vaccines. Although numerous characterization studies were done to ensure proper immunogenicity, limitations in some of these methods —which were discussed above, made testing immunopotency in vivo a must. Both Wuhan (GMP3) and Alpha VLPs (Exp18) were immunogenic in C57BL/6 mice evidenced by vaccine induced antibody titers against Spike, Nucleocapsid and inactivated whole virus. Our group has showed previously that — possibly due to D614G and other mutations found in several VoCs that cause increased Spike decoration on to live virions — Spike proteins from these strains also allow increased decoration onto VLPs [121]. This allowed Alpha VLPs to elicit more Spike but not Nucleocapsid specific antibodies. Interestingly, robustness of the antibody elicited against Nucleocapsid was lower in Wuhan VLP group, evidenced by increased inter-group variability. Reason for this was not clear. Correlation of antibody titers of individual mice revealed that Spike and Nucleocapsid titers are highly correlated while neither are correlated with inactivated virus titers. Correlation of titers against Nucleocapsid and Spike mimic the case with natural immunity. [89]

We have next wondered about feasibility of our variant specific Spike decorated VLPs in inducing variant RBD specific antibodies. For this, antibodies against RBD from Wuhan, Alpha, Beta, Gamma variants were determined by ELISA. Better Spike targeted immunogenicity of Alpha VLPs were clear, as induced antibody titers against Wuhan RBDs were even higher than Wuhan VLP vaccinated groups. In fact, Alpha VLPs induced more RBD titers against all tested variants. Interestingly, while Alpha VLP elicited RBD antibodies had the most affinity to Alpha specific RBD, Wuhan VLP elicited RBD antibodies had a higher affinity for Beta specific RBD and not Wuhan. Other experiments will be valuable for testing the utility of VLPs decorated with variant specific Spikes. These include virus neutralization using either live SARS-CoV-2 variants or pseudoviral assay with pseudoviruses decorated with variant specific Spike. Of course, vaccinating ferrets or hACE2 transgenic mice with Alpha and Wuhan VLPs and challenging them with either virus will be most conclusive.

Adding to our previous work, we have here experimented with feasibility of our approach for large scale production and also determined some properties of VLP antigen alone or formulated with Alum + CpG ODN. Results of clinical trials will be published in upcoming works by our group. While vaccination rates are approaching 80% for most continents [110], new challenge is to maintain cross protective immunity for masses. It is becoming increasingly clear that SARS-CoV-2 will not magically

go away and will become a common pathogen that continuously evolves like Influenza. In light of this, yearly vaccination schemes will be necessary for especially vulnerable members of the society. Although mRNA vaccines have demonstrated excellent potency in terms of generating Th1 biased Spike specific humoral and cellular immunity, several questions remain regarding their feasibility. First, safety of systematically delivering the same antigen in the form of mRNA repeatedly is not known. So far, platform has been very safe and only extremely rare cases of myocarditis have been reported [40]. But this doesn't mean that it will prove to be safe for annual injections. mRNA vaccines are also harder to store compared to classical vaccines, requiring subzero conditions or even -70 °C cabinets. Most importantly, although Spike is undeniably the most important protein in terms of having an immune response targeting it, it is also the most variable part of SARS-CoV-2 variants. Our vaccine potentially elicits cellular immunity towards Spike, Nucleocapsid and Membrane and humoral immunity towards Spike and Nucleocapsid. Immune response against other proteins than main fusogen (Spike) has proved important for SARS-CoV-2 and also for other viral pathogens [151–154]. Prefusion-stabilized Spike mutant utilized in VLPs also confer high levels of neutralizing antibodies. Therefore, our VLP platform has the potential to be an excellent candidate for inducing a cross variant immunity. Although so far we have utilized subcutaneous injections, intranasal delivery of vaccines is known to induce lung resident memory CD8+ and CD4+ T cells which confer site-specific immunity [155–158]. These so-called tissue resident memory T cells respond faster than central or effector memory T cells to a potential insult [159]. It is clear that VLP + Alum + CpG ODN formulation has the potential to be a near variant-proof vaccine. Even with successful mRNA-based vaccines on the market, VLP formulation can provide a more accessible alternative for protection from emerging variants with subcutaneous/intranasal vaccination administered yearly. In conclusion using our devised procedure, we have manufactured and characterized GMP-grade virus like particles that contain four structural proteins of SARS-CoV-2. VLPs that are decorated with Wuhan or Alpha variant Spike protein were used in Phase 1 (NCT04818281) and Phase 2 (NCT04962893) clinical trials.

5. Appendices

5.1 Supporting Experimental Data

5.1.1 Daily Analysis of Cells Transfected with Different PEI/DNA Ratios

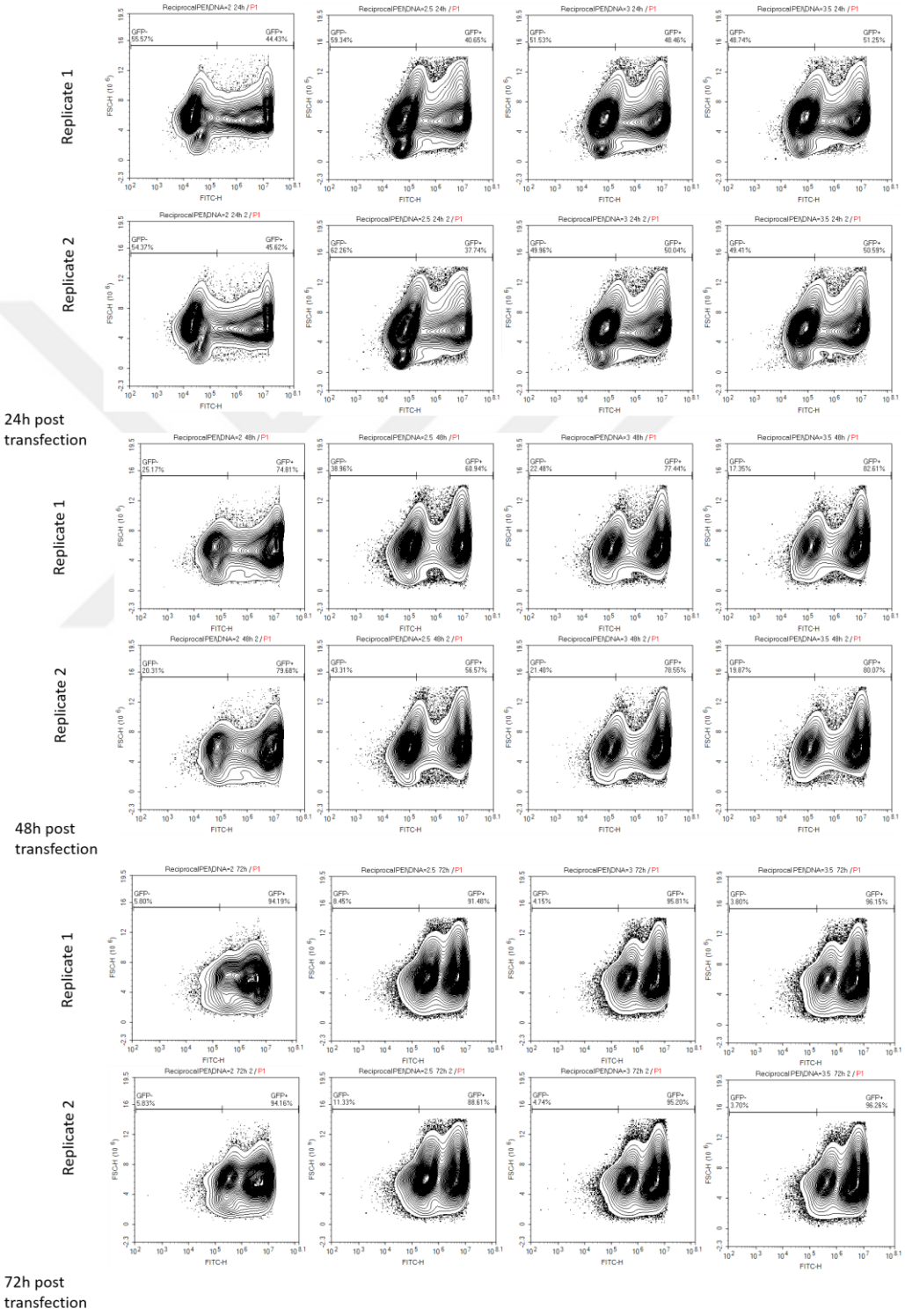

Figure 5.1 Daily flow cytometry analysis of each sample from Section 3.1.2 Optimization of PEIpro/DNA Ratio represented as contour plots. x-axis: FITC-H, y-axis: FSC-H

5.1.2 Daily Analysis of VLP Producing Cells

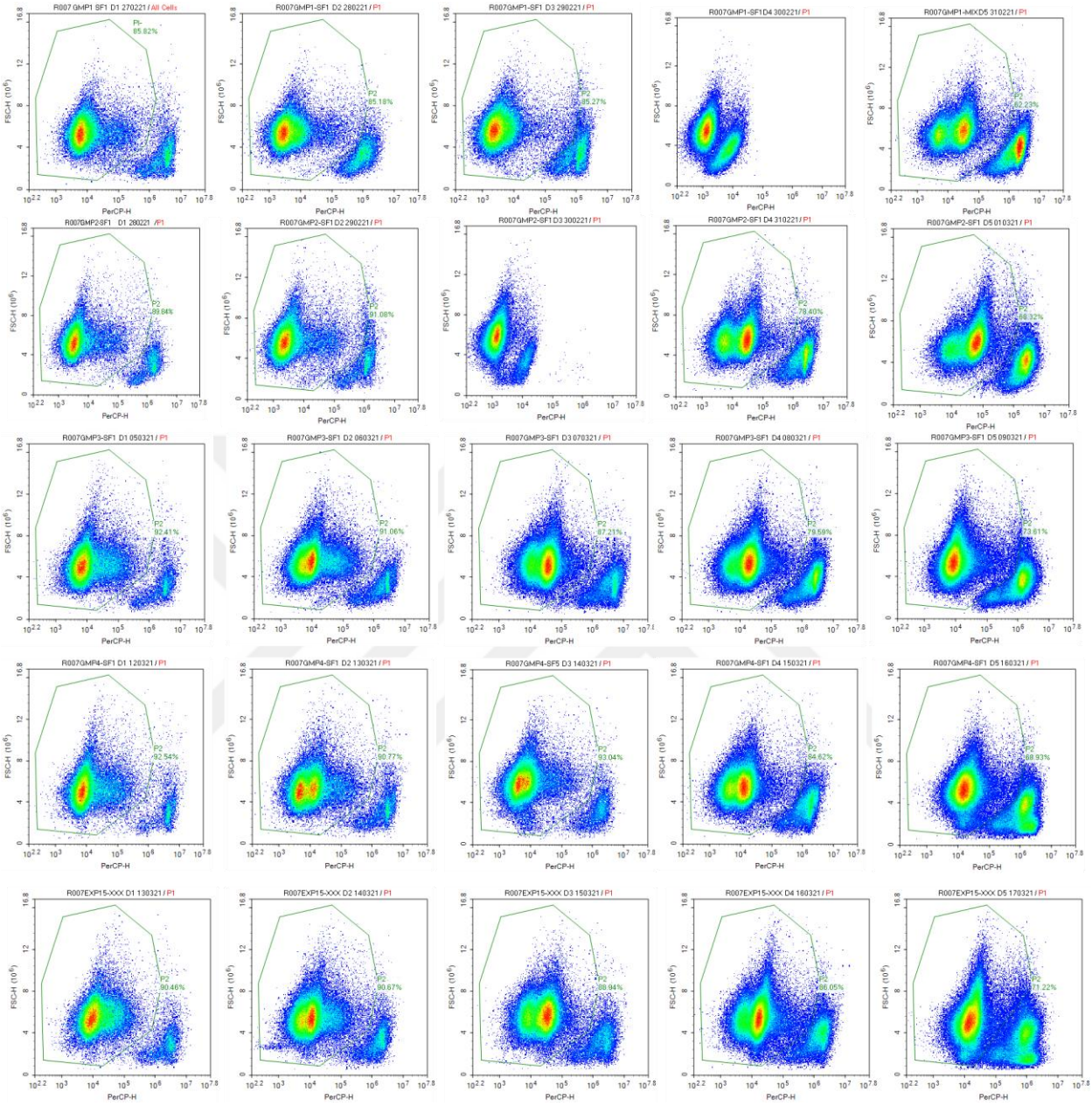

Figure 5.2 Daily flow cytometry analysis of each sample from Section 3.1.5 Cell Culture of Transiently Transfected HEK293 Cells represented as density plots. x-axis: PerCP-H, y-axis: FSC-H. Green gate indicates PI-, viable cells.

5.1.3 OD405 Readings from GMP3 and Exp19 Immunopotency

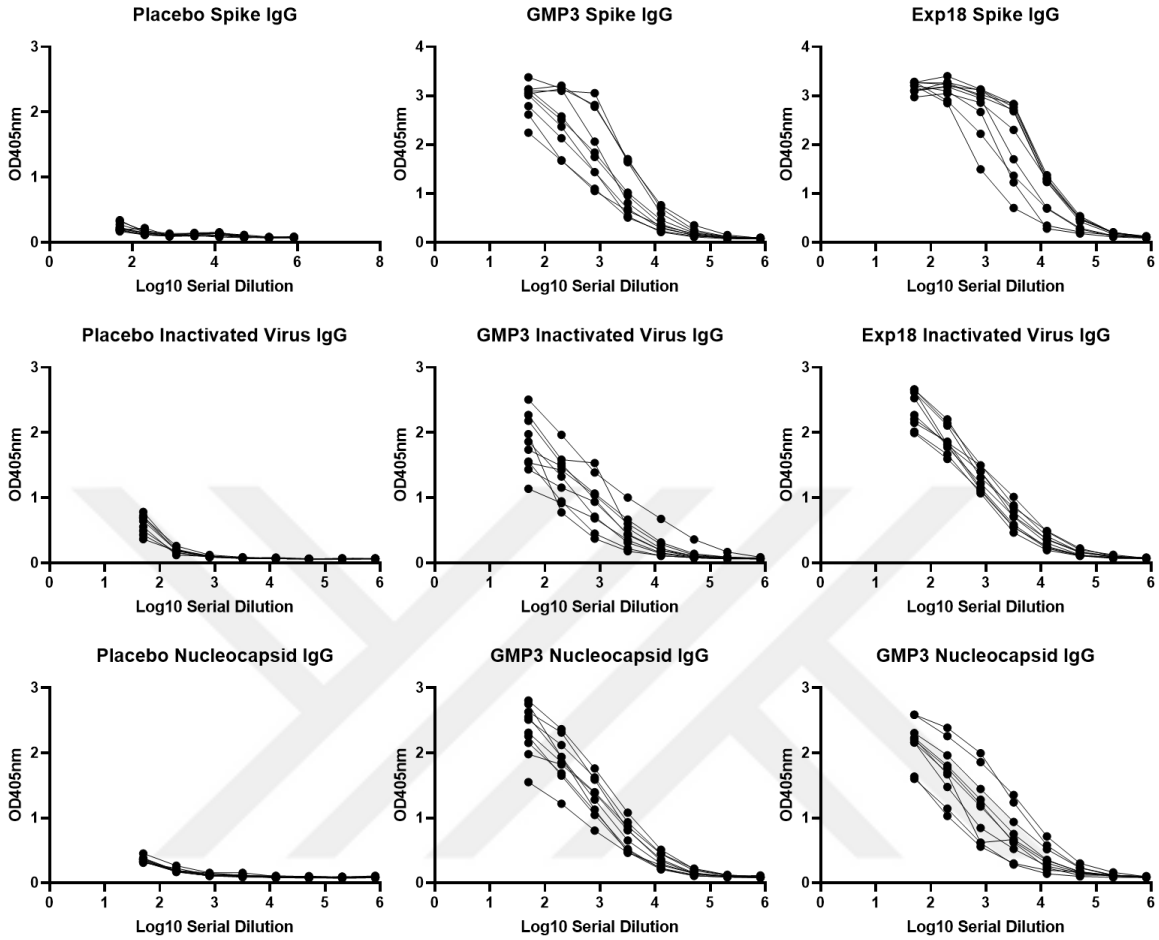

Figure 5.3 Raw OD values of each mouse from Section 3.3.9 In Vivo Potency of GMP3-Wuhan (Phase1) and Exp18-Alpha Vaccine (Phase2) Black dots represent OD values after booster injection. Each line represents values from a single mouse. Plates were coated with Spike, Nucleocapsid or inactivated virus as indicated in graph headers. x-axis: Log10 transformed dilutions. y-axis: OD405nm.

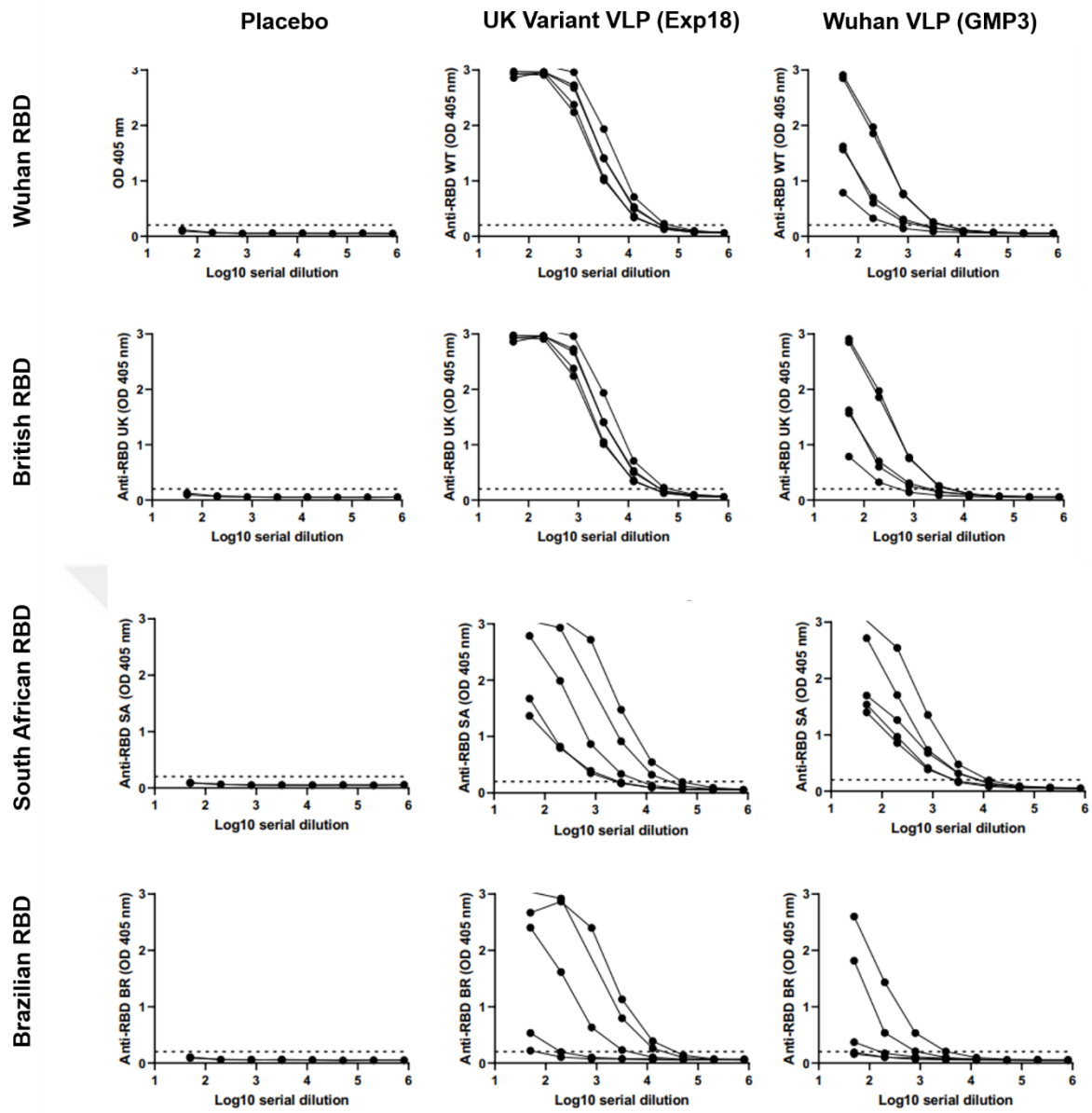

Figure 5.4 Raw OD values of each mouse from Section 3.3.9 In Vivo Potency of GMP3-Wuhan (Phase1) and Exp18-Alpha Vaccine (Phase2) Black dots represent OD values after booster injection. Each line represents values from a single mouse. Plates were coated with RBD from Wuhan, Alpha, beta and Gamma variants as indicated in graph headers. x-axis: Log10 transformed dilutions. y-axis: OD405nm.

5.2 Buffer and Media Ingredients

10X PBS

- 80 g NaCl
- 2 g KCl
- 8.01 g Na2HPO4.2H2O
- 2 g KH2PO4

Finalized to 1L with dH_2O (pH 6.8) and autoclaved. (pH7.4)

Low Salt LB Media

- 10 g Tryptone
- 5 g NaCl
- 5 g Yeast Extract
- 10 g Agar (For Solid Media)

Finalized to 1L with dH_2O and autoclaved. Supplemented with Hygromycin B gold at 100 µg/mL.

50X TAE Buffer

- 242 g Tris free base
- 18.61 g Disodium EDTA
- 57.1 ml Glacial Acetic Acid

Finalized to 1L with dH_2O.

1X DPBS (Capto Core Buffer A, equilibration buffer; TFF Diafiltration buffer)

- 0.2 g KCl
- 0.2 g KH2PO4
- 8 g NaCl
- 1.15 g Na2HPO4

Finalized to 1 L with dH_2O. 0.22 µm filter sterilized. (pH 7.4)

Capto Core Buffer B (Elution Buffer)

- 11.9 g HEPES (50 mM)
- 116.9 g NaCl (2M)

Finalized to 1 L with dH_2O. 0.22 µm filter sterilized. (pH 7.4)

Capto Core Cleaning-In-Place (CIP) Solution

- 40 g NaOH (1M)
- 300 mL isopropanol

Finalized to 1 L with dH_2O. 0.22 µm filter sterilized.

4X Laemmli Buffer

- 4 ml 100% glycerol
- 2.4 ml 1M Tris-HCl (pH=6.8)
- 0.8 g SDS
- 4 mg bromophenol blue
- 0.5 ml β-mercaptoethanol
- 3.1 ml dH_2O

1X PBST

- 100 ml 10X PBS
- 900 ml dH2O
- 1 ml Tween-20

10X Running Buffer

- 30.285 g Tris-Base
- 144.134 g glycine
- 100 ml SDS (10%)

Finalized to 1 L with dH_2O.

10X Transfer Buffer

- 30.285 g Tris-Base
- 144.134 g glycine

Finalized to 1 L with dH_2O.

1X Transfer Buffer

- 100 ml 10X transfer buffer
- 200 ml methanol

Finalized to 1 L with dH_2O.

Blocking Buffer (Immunoblotting)

- 5 g Non-Fat dry milk (5%)
- 100 mL 1X PBST

Blocking Buffer (ELISA)

- 500 ml 1X PBS
- 25 g BSA (bovine serum albumin)
- 250 µl Tween-20

Washing Buffer (ELISA)

- 500 ml 10X PBS

- 2.5 ml Tween-20
- 4.5 L dH_2O

FACS Buffer

- 500 ml 1X PBS
- 5 g BSA
- 125 mg Na-Azide

References

1. Gorbalenya, A. E. *et al.* The species Severe acute respiratory syndrome-related coronavirus: classifying 2019-nCoV and naming it SARS-CoV-2. *Nat. Microbiol.* **5**, 536–544 (2020).

2. Andersen, K. G., Rambaut, A., Lipkin, W. I., Holmes, E. C. & Garry, R. F. The proximal origin of SARS-CoV-2. *Nat. Med. 2020 264* **26**, 450–452 (2020).

3. Zhou, P. *et al.* A pneumonia outbreak associated with a new coronavirus of probable bat origin. *Nat. 2020 5797798* **579**, 270–273 (2020).

4. Zhang, T., Wu, Q. & Zhang, Z. Pangolin homology associated with 2019-nCoV. *bioRxiv* 2020.02.19.950253 (2020) doi:10.1101/2020.02.19.950253.

5. Wan, Y., Shang, J., Graham, R., Baric, R. S. & Li, F. Receptor Recognition by the Novel Coronavirus from Wuhan: an Analysis Based on Decade-Long Structural Studies of SARS Coronavirus. *J. Virol.* **94**, (2020).

6. Xiao, X., Newman, C., Buesching, C. D., Macdonald, D. W. & Zhou, Z. M. Animal sales from Wuhan wet markets immediately prior to the COVID-19 pandemic. *Sci. Reports 2021 111* **11**, 1–7 (2021).

7. Woo, P. C. Y. *et al.* Characterization and Complete Genome Sequence of a Novel Coronavirus, Coronavirus HKU1, from Patients with Pneumonia. *J. Virol.* **79**, 884–895 (2005).

8. Senior, K. Recent Singapore SARS case a laboratory accident. *Lancet. Infect. Dis.* **3**, 679 (2003).

9. Taiwan News. Taiwan confirms researcher infected with COVID in lab. (2021).

10. Ge, X. Y. *et al.* Isolation and characterization of a bat SARS-like coronavirus that uses the ACE2 receptor. *Nat. 2013 5037477* **503**, 535–538 (2013).

11. Menachery, V. D. *et al.* A SARS-like cluster of circulating bat coronaviruses shows potential for human emergence. *Nat. Med. 2015 2112* **21**, 1508–1513 (2015).

12. Jiang, S. *et al.* A distinct name is needed for the new coronavirus. *Lancet* **395**, 949 (2020).

13. Follis, K., York, J., Virology, J. N.- & 2006, U. Furin cleavage of the SARS coronavirus spike glycoprotein enhances cell–cell fusion but does not affect virion entry. *Elsevier* (2006).

14. Alexander, D., Technique, I. B.-R. scientifique et & 2009, U. History of highly pathogenic avian influenza. *europepmc.org* (2009).

15. Menachery, V. D. *et al.* Trypsin Treatment Unlocks Barrier for Zoonotic Bat Coronavirus Infection. *J. Virol.* **94**, (2020).

16. Yogo, Y., Hirano, N., Hino, S., Shibuta, H. & Matumoto, M. Polyadenylate in the Virion RNA of Mouse Hepatitis Virus. *J. Biochem.* **82**, 1103–1108 (1977).

17. Lai, M. M. C. & Stohlman, S. A. Comparative analysis of RNA genomes of mouse hepatitis viruses. *J. Virol.* **38**, 661–670 (1981).

18. Kim, D. *et al.* The Architecture of SARS-CoV-2 Transcriptome. *Cell* **181**, 914-921.e10 (2020).

19. Huang, Y., Yang, C., Xu, X. feng, Xu, W. & Liu, S. wen. Structural and functional properties of SARS-CoV-2 spike protein: potential antivirus drug development for COVID-19. *Acta Pharmacol. Sin. 2020 419* **41**, 1141–1149 (2020).

20. Hoffmann, M., Kleine-Weber, H., Schroeder, S., Cell, N. K.- & 2020, U. SARS-CoV-2 cell entry depends on ACE2 and TMPRSS2 and is blocked by a clinically proven protease inhibitor. *Elsevier* (2020).

21. Savastano, A., Ibáñez de Opakua, A., Rankovic, M. & Zweckstetter, M. Nucleocapsid protein of SARS-CoV-2 phase separates into RNA-rich polymerase-containing condensates. *Nat. Commun. 2020 111* **11**, 1–10 (2020).

22. Narayanan, K., Maeda, A., Maeda, J. & Makino, S. Characterization of the coronavirus M protein and nucleocapsid interaction in infected cells. *J. Virol.* **74**, 8127–8134 (2000).

23. Zúñiga, S. *et al.* Coronavirus Nucleocapsid Protein Facilitates Template Switching and Is Required for Efficient Transcription. *J. Virol.* **84**, 2169–2175 (2010).

24. Neuman, B. W. *et al.* A structural analysis of M protein in coronavirus assembly and morphology. *J. Struct. Biol.* **174**, 11–22 (2011).

25. Nieto-Torres, J. L. *et al.* Severe acute respiratory syndrome coronavirus envelope protein ion channel activity promotes virus fitness and pathogenesis. *PLoS Pathog.* **10**, (2014).

26. Schoeman, D. & Fielding, B. C. Coronavirus envelope protein: current knowledge. *Virol. J.* **16**, (2019).

27. Tseng, Y. T. *et al.* Self-assembly of Severe Acute Respiratory Syndrome Coronavirus MembraneProtein. *J. Biol. Chem.* **285**, 12862 (2010).

28. Ujike, M. & Taguchi, F. Incorporation of Spike and Membrane Glycoproteins into Coronavirus Virions. *Viruses* **7**, 1700 (2015).

29. Cevik, M., Kuppalli, K., Kindrachuk, J. & Peiris, M. Virology, transmission, and pathogenesis of SARS-CoV-2. *BMJ* **371**, (2020).

30. Klemm, T. *et al.* Mechanism and inhibition of the papain-like protease, PLpro, of SARS-CoV-2. *EMBO J.* **39**, (2020).

31. O'Brien, A. *et al.* Detecting SARS-CoV-2 3CLpro expression and activity using a polyclonal antiserum and a luciferase-based biosensor. *Elsevier* (2021).

32. van de Leemput, J. & Han, Z. Understanding Individual SARS-CoV-2 Proteins for Targeted Drug Development against COVID-19. *Mol. Cell. Biol.* **41**, (2021).

33. Hulo, C. *et al.* ViralZone: a knowledge resource to understand virus diversity. *Nucleic Acids Res.* **39**, (2011).

34. CDC. CDC updates COVID-19 transmission webpage to clarify information about types of spread. (2020).

35. Li, Q. *et al.* Early Transmission Dynamics in Wuhan, China, of Novel Coronavirus–Infected Pneumonia. *N. Engl. J. Med.* **382**, 1199–1207 (2020).

36. Harrison, A. G., Lin, T. & Wang, P. Mechanisms of SARS-CoV-2 Transmission and Pathogenesis. *Trends Immunol.* **41**, 1100 (2020).

37. Chen, H. *et al.* SARS-CoV-2 activates lung epithelia cell proinflammatory signaling and leads to immune dysregulation in COVID-19 patients by single-cell sequencing. *medRxiv* 2020.05.08.20096024 (2020) doi:10.1101/2020.05.08.20096024.

38. Moore, J. B. & June, C. H. Cytokine release syndrome in severe COVID-19. *Science (80-.).* **368**, 473–474 (2020).

39. Varga, Z. *et al.* Endothelial cell infection and endotheliitis in COVID-19. *Lancet* **395**, 1417–1418 (2020).

40. Bozkurt, B., Kamat, I. & Hotez, P. J. Myocarditis With COVID-19 mRNA Vaccines. *Circulation* **144**, 471–484 (2021).

41. Tian, F. *et al.* Mutation N501Y in RBD of Spike Protein Strengthens the Interaction between COVID-19 and its Receptor ACE2. *bioRxiv* 2021.02.14.431117 (2021) doi:10.1101/2021.02.14.431117.

42. Zhang, L. *et al.* SARS-CoV-2 spike-protein D614G mutation increases virion spike density and infectivity. *Nat. Commun. 2020 111* **11**, 1–9 (2020).

43. Reincke, S. M. *et al.* SARS-CoV-2 Beta variant infection elicits potent lineage-specific and cross-reactive antibodies. *Science (80-.).* **375**, 782–787 (2022).

44. Wise, J. Covid-19: The E484K mutation and the risks it poses. *BMJ* **372**, n359 (2021).

45. Faria, N. R. *et al.* Genomics and epidemiology of the P.1 SARS-CoV-2 lineage in Manaus, Brazil. *Science* **372**, (2021).

46. Liu, Y. *et al.* Delta spike P681R mutation enhances SARS-CoV-2 fitness over Alpha variant. *bioRxiv Prepr. Serv. Biol.* (2021) doi:10.1101/2021.08.12.456173.

47. Wong, S. C. *et al.* Transmission of Omicron (B.1.1.529) - SARS-CoV-2 Variant of Concern in a designated quarantine hotel for travelers: a challenge of elimination strategy of COVID-19. *Lancet Reg. Heal. - West. Pacific* **18**, (2022).

48. Andrews, N. *et al.* Covid-19 Vaccine Effectiveness against the Omicron (B.1.1.529) Variant. *https://doi.org/10.1056/NEJMoa2119451* (2022) doi:10.1056/NEJMOA2119451.

49. Nealon, J. & Cowling, B. J. Omicron severity: milder but not mild. *Lancet* **399**, 412–413 (2022).

50. Hadfield, J. *et al.* NextStrain: Real-time tracking of pathogen evolution. *Bioinformatics* **34**, 4121–4123 (2018).

51. Medzhitov, R. & Janeway, C. A. How does the immune system distinguish self from nonself? *Semin. Immunol.* **12**, 185–188 (2000).

52. Ayres, J. S. & Schneider, D. S. Two ways to survive an infection: what resistance and tolerance can teach us about treatments for infectious diseases. *Nat. Rev. Immunol.* **8**, 889 (2008).

53. Sperandio, B., Fischer, N. & Sansonetti, P. J. Mucosal physical and chemical innate barriers: Lessons from microbial evasion strategies. *Semin. Immunol.* **27**, 111–118 (2015).

54. Pikaar, J. C. *et al.* Opsonic activities of surfactant proteins A and D in phagocytosis of gram-negative bacteria by alveolar macrophages. *J. Infect. Dis.* **172**, 481–489 (1995).

55. Peschel, A. How do bacteria resist human antimicrobial peptides? *Trends Microbiol.* **10**, 179–186 (2002).

56. Zheng, D., Liwinski, T. & Elinav, E. Interaction between microbiota and immunity in health and disease. *Cell Res. 2020 306* **30**, 492–506 (2020).

57. Akira, S., Uematsu, S. & Takeuchi, O. Pathogen Recognition and Innate Immunity. *Cell* **124**, 783–801 (2006).

58. Takeuchi, O. & Akira, S. Pattern Recognition Receptors and Inflammation. *Cell* **140**, 805–820 (2010).

59. Itano, A. A. & Jenkins, M. K. Antigen presentation to naive CD4 T cells in the lymph node. *Nat. Immunol. 2003 48* **4**, 733–739 (2003).

60. Flajnik, M. F. & Kasahara, M. Origin and evolution of the adaptive immune system: genetic events and selective pressures. *Nat. Rev. Genet. 2010 111* **11**, 47–59 (2009).

61. Iwasaki, A. & Medzhitov, R. Control of adaptive immunity by the innate immune system. *Nat. Immunol. 2015 164* **16**, 343–353 (2015).

62. Medzhitov, R. & Janeway, C. J. Innate Immunity. *http://dx.doi.org/10.1056/NEJM200008033430506* **343**, 338–344 (2009).

63. Papayannopoulos, V. Neutrophil extracellular traps in immunity and disease. *Nat. Rev. Immunol. 2017 182* **18**, 134–147 (2017).

64. Lebegge, E. *et al.* Innate Immune Defense Mechanisms by Myeloid Cells That Hamper Cancer Immunotherapy. *Front. Immunol.* **11**, 1395 (2020).

65. Zheng, M., Karki, R., Williams, E., … D. Y.-N. & 2021, U. TLR2 senses the SARS-CoV-2 envelope protein to produce inflammatory cytokines. *nature.com* (2021).

66. Choudhury, A. & Mukherjee, S. In silico studies on the comparative characterization of the interactions of SARS-CoV-2 spike glycoprotein with ACE-2 receptor homologs and human TLRs. *J. Med. Virol.* **92**, 2105–2113 (2020).

67. Totura, A. L. *et al.* Toll-Like Receptor 3 Signaling via TRIF Contributes to a Protective Innate Immune Response to Severe Acute Respiratory Syndrome Coronavirus Infection. *MBio* **6**, 1–14 (2015).

68. Diamond, M. S. & Kanneganti, T. D. Innate immunity: the first line of defense against SARS-CoV-2. *Nat. Immunol. 2022 232* **23**, 165–176 (2022).

69. Rebendenne, A. *et al.* SARS-CoV-2 Triggers an MDA-5-Dependent Interferon Response Which Is Unable To Control Replication in Lung Epithelial Cells. *J. Virol.* **95**, (2021).

70. Yamada, T. *et al.* RIG-I triggers a signaling-abortive anti-SARS-CoV-2 defense in human lung cells. *Nat. Immunol.* **22**, 820–828 (2021).

71. Pan, P. *et al.* SARS-CoV-2 N protein promotes NLRP3 inflammasome activation to induce hyperinflammation. *Nat. Commun.* **12**, (2021).

72. Xu, H. *et al.* SARS-CoV-2 viroporin triggers the NLRP3 inflammatory pathway. *bioRxiv* 2020.10.27.357731 (2020) doi:10.1101/2020.10.27.357731.

73. Gray, E. E. & Cyster, J. G. Lymph Node Macrophages. *J. Innate Immun.* **4**, 424 (2012).

74. Kumar, B. V., Connors, T. J. & Farber, D. L. Human T Cell Development, Localization, and Function throughout Life. *Immunity* **48**, 202–213 (2018).

75. Zhang, Y. *et al.* Safety, tolerability, and immunogenicity of an inactivated SARS-CoV-2 vaccine in healthy adults aged 18–59 years: a randomised, double-blind, placebo-controlled, phase 1/2 clinical trial. *Lancet Infect. Dis.* **21**, 181–192 (2021).

76. MacLeod, M. K. L. *et al.* Vaccine adjuvants aluminum and monophosphoryl lipid A provide distinct signals to generate protective cytotoxic memory CD8 T cells. *Proc. Natl. Acad. Sci. U. S. A.* **108**, 7914 (2011).

77. Kuchtey, J., Chefalo, P. J., Gray, R. C., Ramachandra, L. & Harding, C. V. Enhancement of Dendritic Cell Antigen Cross-Presentation by CpG DNA Involves Type I IFN and Stabilization of Class I MHC mRNA. *J. Immunol.* **175**, 2244–2251 (2005).

78. Schneider, W. M., Chevillotte, M. D. & Rice, C. M. Interferon-Stimulated Genes: A Complex Web of Host Defenses. *Annu. Rev. Immunol.* **32**, 513 (2014).

79. Matthew, W., AJ, T. & MJ, B. Interleukin-2 signals during priming are required for secondary expansion of CD8+ memory T cells. *Nature* **441**, 890–893 (2006).

80. Klaus, G. G., Pepys, M. B., Kitajima, K. & Askonas, B. A. Activation of mouse complement by different classes of mouse antibody. *Immunology* **38**, 687 (1979).

81. Kipps, T., P, P., J, P. & LA, H. Importance of immunoglobulin isotype in human antibody-

dependent, cell-mediated cytotoxicity directed by murine monoclonal antibodies. *J. Exp. Med.* **161**, 1–17 (1985).

82. Walker, J. A. & McKenzie, A. N. J. TH2 cell development and function. *Nat. Rev. Immunol. 2017 182* **18**, 121–133 (2017).

83. Peeples, L. News Feature: Avoiding pitfalls in the pursuit of a COVID-19 vaccine. *Proc. Natl. Acad. Sci.* **117**, 8218–8221 (2020).

84. Schijns, V. *et al.* Rational vaccine design in times of emerging diseases: The critical choices of immunological correlates of protection, vaccine antigen and immunomodulation. *Pharmaceutics* **13**, (2021).

85. Sette, A. & Crotty, S. Leading Edge Adaptive immunity to SARS-CoV-2 and COVID-19. (2021) doi:10.1016/j.cell.2021.01.007.

86. Grifoni, A. *et al.* Targets of T Cell Responses to SARS-CoV-2 Coronavirus in Humans with COVID-19 Disease and Unexposed Individuals. *Cell* **181**, 1489-1501.e15 (2020).

87. Le Bert, N. *et al.* SARS-CoV-2-specific T cell immunity in cases of COVID-19 and SARS, and uninfected controls. *Nat. 2020 5847821* **584**, 457–462 (2020).

88. Schulien, I. *et al.* Characterization of pre-existing and induced SARS-CoV-2-specific CD8+ T cells. *Nat. Med. 2020 271* **27**, 78–85 (2020).

89. Rydyznski Moderbacher, C. *et al.* Antigen-Specific Adaptive Immunity to SARS-CoV-2 in Acute COVID-19 and Associations with Age and Disease Severity. *Cell* **183**, 996-1012.e19 (2020).

90. Piccoli, L. *et al.* Mapping Neutralizing and Immunodominant Sites on the SARS-CoV-2 Spike Receptor-Binding Domain by Structure-Guided High-Resolution Serology. *Cell* **183**, 1024-1042.e21 (2020).

91. Dan, J. M. *et al.* Immunological memory to SARS-CoV-2 assessed for up to 8 months after infection. *Science (80-.).* **371**, (2021).

92. van Riel, D. & de Wit, E. Next-generation vaccine platforms for COVID-19. *Nat. Mater. 2020 198* **19**, 810–812 (2020).

93. CDC. Birth-18 Years Immunization Schedule. https://www.cdc.gov/vaccines/schedules/hcp/imz/child-adolescent.html (2022).

94. Boylston, A. The origins of inoculation. *J. R. Soc. Med.* **105**, 309 (2012).

95. Jenner, E. An inquiry into the causes and effects of the variolae vaccinae: a disease discovered in some of the western counties of England, particularly Gloucestershire, and known by the name of the cow pox - Digital Collections - National Library of Medicine. *Springfield [Mass.] : Re-printed for Dr. Samuel Cooley, by Ashley & Brewer, 1802* https://collections.nlm.nih.gov/catalog/nlm:nlmuid-2559001R-bk (1802).

96. Hopkins, D. R. The greatest killer: smallpox in history, with a new introduction. 420 (1983).

97. Barranco, C. The first live attenuated vaccines. *Nat. Res. 2021* (2020).

98. Pasteur, L., Chamberland & Roux. Summary report of the experiments conducted at Pouilly-le-Fort, near Melun, on the anthrax vaccination, 1881. *Yale J. Biol. Med.* **75**, 59 (2002).

99. Pasquale, A. Di *et al.* Vaccine Adjuvants: from 1920 to 2015 and Beyond. **3**, 320–343 (2015).

100. Hogenesch, H. & Ghosh, S. K. Mechanism of immunopotentiation and safety of aluminum adjuvants. (2013) doi:10.3389/fimmu.2012.00406.

101. SC, E., OR, C., W, O., FS, S. & RA, F. Crucial role for the Nalp3 inflammasome in the immunostimulatory properties of aluminium adjuvants. *Nature* **453**, 1122–1126 (2008).

102. Franchi, L. & Núñez, G. The NLRP3 Inflammasome is Critical for Alum-Mediated IL-1β Secretion but Dispensable for Adjuvant Activity. *Eur. J. Immunol.* **38**, 2085 (2008).

103. Common Ingredients in U.S. Licensed Vaccines | FDA. https://www.fda.gov/vaccines-blood-biologics/safety-availability-biologics/common-ingredients-us-licensed-vaccines.

104. Verthelyi, D., Ishii, K. J., Gursel, M., Takeshita, F. & Klinman, D. M. Human Peripheral Blood Cells Differentially Recognize and Respond to Two Distinct CpG Motifs. *J. Immunol.* **166**, 2372–2377 (2001).

105. Verthelyi, D. *et al.* CpG Oligodeoxynucleotides as Vaccine Adjuvants in Primates. *J. Immunol.* **168**, 1659–1663 (2002).

106. Kerkmann, M. *et al.* Spontaneous Formation of Nucleic Acid-based Nanoparticles Is Responsible for High Interferon-α Induction by CpG-A in Plasmacytoid Dendritic Cells *. *J. Biol. Chem.* **280**, 8086–8093 (2005).

107. Lee, G. H. & Lim, S. G. CpG-Adjuvanted Hepatitis B Vaccine (HEPLISAV-B®) Update. *https://doi.org/10.1080/14760584.2021.1908133* **20**, 487–495 (2021).

108. Krammer, F. SARS-CoV-2 vaccines in development. *Nat. 2020 5867830* **586**, 516–527 (2020).

109. Yadav, R. *et al.* Role of structural and non-structural proteins and therapeutic targets of SARS-CoV-2 for COVID-19. *Cells* **10**, (2021).

110. Mathieu, E. *et al.* A global database of COVID-19 vaccinations. *Nat. Hum. Behav.* **5**, 947–953 (2021).

111. Nooraei, S. *et al.* Virus-like particles: preparation, immunogenicity and their roles as nanovaccines and drug nanocarriers. *J. Nanobiotechnology 2021 191* **19**, 1–27 (2021).

112. Yilmaz, I. C. *et al.* Development and preclinical evaluation of virus-like particle vaccine against COVID-19 infection. *Allergy* **77**, 258–270 (2022).

113. Medicago. Medicago and GSK announce the approval by Health Canada of COVIFENZ®, an Adjuvanted Plant-Based COVID-19 Vaccine | Medicago. https://medicago.com/en/press-release/covifenz/ (2022).

114. Pillet, S. *et al.* Safety, immunogenicity, and protection provided by unadjuvanted and adjuvanted formulations of a recombinant plant-derived virus-like particle vaccine candidate for COVID-19 in nonhuman primates. *Cell. Mol. Immunol. 2021 192* **19**, 222–233 (2022).

115. Hsieh, C. L. *et al.* Structure-based design of prefusion-stabilized SARS-CoV-2 spikes. *Science (80-.).* **369**, 1501–1505 (2020).

116. Zhu, D. *et al.* Efficient extraction of vaccines formulated in aluminum hydroxide gel by including surfactants in the extraction buffer. *Vaccine* **30**, 189 (2012).

117. Shin, J., Wood, D., Robertson, J., Minor, P. & Peden, K. WHO informal consultation on the application of molecular methods to assure the quality, safety and efficacy of vaccines, Geneva, Switzerland, 7-8 April 2005. *Biologicals* **35**, 63–71 (2007).

118. Hagel, L., Jagschies, G. & Sofer, G. *Handbook of Process Chromatography*. *Handbook of Process Chromatography* (Elsevier Ltd, 2008).

119. Cytiva. Column efficiency testing. (2020).

120. Loewe, D. *et al.* Tangential Flow Filtration for the Concentration of Oncolytic Measles Virus: The Influence of Filter Properties and the Cell Culture Medium. *Membranes (Basel).* **9**, (2019).

121. Güvençli, N. PRODUCTION OF VIRUS LIKE PARTICLES EXPRESSING ALPHA (B.1.1.7) OR DELTA PLUS (B.1.617.2.1) SPIKE VARIANTS AND DEVELOPMENT OF A PSEUDOTYPED VIRUS NEUTRALIZATION ASSAYtle. (2022).

122. Yang, T. J., Yu, P. Y., Chang, Y. C. & Danny Hsu, S. Te. D614G mutation in the SARS-CoV-2 spike protein enhances viral fitness by desensitizing it to temperature-dependent denaturation. *J. Biol. Chem.* **297**, 101238 (2021).

123. Zhou, B. *et al.* SARS-CoV-2 spike D614G change enhances replication and transmission. *Nat. 2021 5927852* **592**, 122–127 (2021).

124. Yáñez-Mó, M. *et al.* Biological properties of extracellular vesicles and their physiological functions. *J. Extracell. vesicles* **4**, 1–60 (2015).

125. Kartoglu, Ü., Özgüler, N. K., Wolfson, L. J. & Kurzatkowski, W. Validation of the shake test for detecting freeze damage to adsorbed vaccines. *Bull. World Health Organ.* **88**, 624–631 (2010).

126. Harvey, W. T. *et al.* SARS-CoV-2 variants, spike mutations and immune escape. *Nat. Rev. Microbiol. 2021 197* **19**, 409–424 (2021).

127. Davis, H. L. Novel vaccines and adjuvant systems: the utility of animal models for predicting immunogenicity in humans. *Hum. Vaccin.* **4**, 246–250 (2008).

128. Lopez, A. M. *et al.* Formulation with CpG ODN enhances antibody responses to an equine influenza virus vaccine. *Vet. Immunol. Immunopathol.* **114**, 103–110 (2006).

129. Swiech, K. *et al.* Transient transfection of serum-free suspension HEK 293 cell culture for efficient production of human rFVIII. *BMC Biotechnol.* **11**, 1–10 (2011).

130. Backliwal, G., Hildinger, M., Hasija, V. & Wurm, F. M. High-density transfection with HEK-293 cells allows doubling of transient titers and removes need for a priori DNA complex formation with PEI. *Biotechnol. Bioeng.* **99**, 721–727 (2008).

131. Lee, J. G. *et al.* Characterization of SARS-CoV-2 proteins reveals Orf6 pathogenicity, subcellular localization, host interactions and attenuation by Selinexor. *Cell Biosci.* **11**, 1–12 (2021).

132. Xia, B. *et al.* SARS-CoV-2 envelope protein causes acute respiratory distress syndrome (ARDS)-like pathological damages and constitutes an antiviral target. *Cell Res. 2021 318* **31**, 847–860 (2021).

133. Kallunki, T., Barisic, M., Jäättelä, M. & Liu, B. How to Choose the Right Inducible Gene Expression System for Mammalian Studies? *Cells* **8**, (2019).

134. Mullick, A. *et al.* The cumate gene-switch: A system for regulated expression in mammalian cells. *BMC Biotechnol.* **6**, 1–18 (2006).

135. Kim, C. L., Ha, T. K. & Lee, G. M. Combinatorial treatment with lithium chloride enhances recombinant antibody production in transiently transfected CHO and HEK293E cells. *Biotechnol. Bioprocess Eng. 2016 215* **21**, 667–675 (2016).

136. Chen, F. *et al.* The combined effect of sodium butyrate and low culture temperature on the production, sialylation, and biological activity of an antibody produced in CHO cells. *Biotechnol. Bioprocess Eng.* **16**, 1157–1165 (2011).

137. Backliwal, G. *et al.* Valproic acid: a viable alternative to sodium butyrate for enhancing protein expression in mammalian cell cultures. *Biotechnol. Bioeng.* **101**, 182–189 (2008).

138. Chen, X., Xiao, S., Wu, J. & Yao, J. Effect of sialic acid on mammalian cell culture and protein expression: A potential productivity enhancer for biopharmaceutical cell culture processes.

Processes **8**, 1–13 (2020).

139. Long, Z. *et al.* Simultaneous quantification of spike and nucleocapsid protein in inactivated COVID-19 vaccine bulk by liquid chromatography-tandem mass spectrometry. *J. Chromatogr. B* **1181**, 122884 (2021).

140. Getie-Kebtie, M., Sultana, I., Eichelberger, M. & Alterman, M. Label-free mass spectrometry-based quantification of hemagglutinin and neuraminidase in influenza virus preparations and vaccines. *Influenza Other Respi. Viruses* **7**, 521 (2013).

141. Sharma, V. K., Sharma, I. & Glick, J. The expanding role of mass spectrometry in the field of vaccine development. *Mass Spectrom. Rev.* **39**, 83–104 (2020).

142. Jia, X., Yin, Y., Chen, Y. & Mao, L. The Role of Viral Proteins in the Regulation of Exosomes Biogenesis. *Front. Cell. Infect. Microbiol.* **11**, 422 (2021).

143. Turner, D. L., Korneev, D. V., Purdy, J. G., de Marco, A. & Mathias, R. A. The host exosome pathway underpins biogenesis of the human cytomegalovirus virion. *Elife* **9**, 1–29 (2020).

144. Kalamvoki, M. & Deschamps, T. Extracellular vesicles during Herpes Simplex Virus type 1 infection: an inquire. *Virol. J. 2016 131* **13**, 1–12 (2016).

145. Estmer Nilsson, C. *et al.* A novel assay for influenza virus quantification using surface plasmon resonance. *Vaccine* **28**, 759–766 (2010).

146. Pelliccia, M. *et al.* Additives for vaccine storage to improve thermal stability of adenoviruses from hours to months. *Nat. Commun. 2016 71* **7**, 1–7 (2016).

147. Vagenende, V., Yap, M. G. S. & Trout, B. L. Mechanisms of protein stabilization and prevention of protein aggregation by glycerol. *Biochemistry* **48**, 11084–11096 (2009).

148. Lu, F., Mosley, Y. Y. C., Carmichael, B., Brown, D. D. & HogenEsch, H. Formulation of aluminum hydroxide adjuvant with TLR agonists poly(I:C) and CpG enhances the magnitude and avidity of the humoral immune response. *Vaccine* **37**, 1945–1953 (2019).

149. Lee, N. *et al.* Improved quantification of protein in vaccines containing aluminum hydroxide by simple modification of the Lowry method. *Vaccine* **33**, 5031–5034 (2015).

150. Rausch, K. M. & Zhu, D. Determination of Protein Content in Alhydrogel ®-Based Vaccines by O-Phthalaldehyde Assay. *Methods Mol. Biol.* **1494**, 263–271 (2017).

151. Matchett, W. E. *et al.* Nucleocapsid Vaccine Elicits Spike-Independent SARS-CoV-2 Protective Immunity. *J. Immunol.* **207**, 376–379 (2021).

152. Dangi, T., Class, J., Palacio, N., Richner, J. M. & Penaloza MacMaster, P. Combining spike- and nucleocapsid-based vaccines improves distal control of SARS-CoV-2. *Cell Rep.* **36**, 109664 (2021).

153. Kalkan-Yazıcı, M. *et al.* Cross-Reactive Anti-Nucleocapsid Protein Immunity against Crimean-Congo Hemorrhagic Fever Virus and Hazara Virus in Multiple Species. *J. Virol.* **95**, (2021).

154. Kohler, P. *et al.* Impact of baseline SARS-CoV-2 antibody status on syndromic surveillance and the risk of subsequent COVID-19—a prospective multicenter cohort study. *BMC Med.* **19**, 1–10 (2021).

155. Zhou, R. *et al.* Nasal prevention of SARS-CoV-2 infection by intranasal influenza-based boost vaccination in mouse models. *eBioMedicine* **75**, (2022).

156. Wu, Q. *et al.* Antigen-specific tissue-resident memory T cells in the respiratory system were generated following intranasal vaccination of mice with BCG. *J. Immunol. Res.* **2021**, (2021).

157. Bedford, J. G., Caminschi, I. & Wakim, L. M. Intranasal Delivery of a Chitosan-Hydrogel

Vaccine Generates Nasal Tissue Resident Memory CD8+ T Cells That Are Protective against Influenza Virus Infection. *Vaccines 2020, Vol. 8, Page 572* **8**, 572 (2020).

158. Morabito, K. M. *et al.* Intranasal administration of RSV antigen-expressing MCMV elicits robust tissue-resident effector and effector memory CD8+ T cells in the lung. *Mucosal Immunol. 2017 102* **10**, 545–554 (2016).

159. Collins, D. R., Gaiha, G. D. & Walker, B. D. CD8+ T cells in HIV control, cure and prevention. *Nat. Rev. Immunol. 2020 208* **20**, 471–482 (2020).

BMJ PUBLISHING GROUP LTD. LICENSE
TERMS AND CONDITIONS

Apr 28, 2022

This Agreement between Mr. Artun Bülbül ("You") and BMJ Publishing Group Ltd. ("BMJ Publishing Group Ltd.") consists of your license details and the terms and conditions provided by BMJ Publishing Group Ltd. and Copyright Clearance Center.

License Number	5297650924283
License date	Apr 28, 2022
Licensed Content Publisher	BMJ Publishing Group Ltd.
Licensed Content Publication	The BMJ
Licensed Content Title	Virology, transmission, and pathogenesis of SARS-CoV-2
Licensed Content Author	Muge Cevik, Krutika Kuppalli, Jason Kindrachuk, Malik Peiris
Licensed Content Date	Oct 23, 2020
Licensed Content Volume	371
Type of Use	Dissertation/Thesis
Requestor type	Individual
Format	Electronic
Portion	Figure/table/extract

SPRINGER NATURE LICENSE
TERMS AND CONDITIONS

Apr 28, 2022

This Agreement between Mr. Artun Bülbül ("You") and Springer Nature ("Springer Nature") consists of your license details and the terms and conditions provided by Springer Nature and Copyright Clearance Center.

License Number	5297651297986
License date	Apr 28, 2022
Licensed Content Publisher	Springer Nature
Licensed Content Publication	Nature Immunology
Licensed Content Title	Innate immunity: the first line of defense against SARS-CoV-2
Licensed Content Author	Michael S. Diamond et al
Licensed Content Date	Feb 1, 2022
Type of Use	Thesis/Dissertation
Requestor type	academic/university or research institute
Format	print
Portion	figures/tables/illustrations
Number of figures/tables/illustrations	1

SPRINGER NATURE LICENSE
TERMS AND CONDITIONS

Apr 28, 2022

This Agreement between Mr. Artun Bülbül ("You") and Springer Nature ("Springer Nature") consists of your license details and the terms and conditions provided by Springer Nature and Copyright Clearance Center.

License Number	5297660059483
License date	Apr 28, 2022
Licensed Content Publisher	Springer Nature
Licensed Content Publication	Nature
Licensed Content Title	SARS-CoV-2 vaccines in development
Licensed Content Author	Florian Krammer
Licensed Content Date	Sep 23, 2020
Type of Use	Thesis/Dissertation
Requestor type	academic/university or research institute
Format	print
Portion	figures/tables/illustrations
Number of figures/tables/illustrations	1